Laboratory Characterization of Mars In-Situ Resource Utilization (ISRU) using the Mars Oxygen ISRU Experiment (MOXIE) FlatSat Testbed

by

Shravan Hariharan
B.S. Aerospace Engineering
Georgia Institute of Technology, 2020

Submitted to the Department of Aeronautics and Astronautics
in partial fulfillment of the requirements for the degree of
Master of Science in Aeronautics and Astronautics
at the
MASSACHUSETTS INSTITUTE OF TECHNOLOGY
May 2023

Author .....
Shravan Hariharan
Department of Aeronautics and Astronautics
May 12, 2023

Certified by .....
Jeffrey A. Hoffman
Professor of the Practice, Aeronautics and Astronautics
Thesis Supervisor

Accepted by .....
Jonathan P. How
R. C. Maclaurin Professor of Aeronautics and Astronautics
Chair, Graduate Program Committee

Laboratory Characterization of Mars In-Situ Resource Utilization (ISRU) using the Mars Oxygen ISRU Experiment (MOXIE) FlatSat Testbed

by

Shravan Hariharan

Submitted to the Department of Aeronautics and Astronautics
on May 12, 2023, in partial fulfillment of the
requirements for the degree of
Master of Science in Aeronautics and Astronautics

Abstract

The Mars Oxygen In-Situ Resource Utilization Experiment (MOXIE) is a payload onboard NASA's Perseverance Rover demonstrating the production of oxygen through solid oxide electrolysis of carbon dioxide in the Martian atmosphere. MOXIE has successfully generated oxygen on Mars 14 times since landing in February 2021 and will continue to demonstrate oxygen production during night and day throughout all Martian seasons.

As opportunities to run MOXIE on Mars are limited due to mission constraints such as energy usage and a fixed instrument configuration, the MOXIE team at the Massachusetts Institute of Technology (MIT), MIT Haystack Observatory, and NASA Jet Propulsion Laboratory (JPL) developed the MOXIE FlatSat as a ground-based operational testbed to further characterize the MOXIE system, evaluate and validate planned MOXIE operations on Mars, and demonstrate potential operating modes and configurations for a next-generation Mars in-situ resource utilization (ISRU) system.

The research presented in this thesis involves a series of experiments conducted on the FlatSat testbed to inform design and operation of a next-generation Martian ISRU system. Specifically, this thesis discusses the capabilities of the FlatSat system, and how experiments analyzing the FlatSat compressor and FlatSat operations at low pressures inform optimal operating conditions for a future full-scale Martian ISRU system that minimize energy usage and maximize oxygen production. In addition, qualitative and quantitative differences between the FlatSat and MOXIE Flight Model are discussed to examine the extensibility of FlatSat data to MOXIE's operations on Mars.

Thesis Supervisor: Jeffrey A. Hoffman
Title: Professor of the Practice, Aeronautics and Astronautics

Acknowledgments

This research would not have been possible without the continued guidance, support, and mentorship of many people throughout the last two years. MOXIE is demonstrating the technology that may one day sustain a village on Mars, and it certainly took a village to enable the research I have conducted throughout my graduate career.

First and foremost, I would like to thank my graduate advisor and MOXIE Deputy Principal Investigator, Professor Jeffrey Hoffman. You have continued to challenge me to think critically and communicate my opinions with confidence, while still demonstrating the importance of humility. Thank you for always prioritizing my interests, advocating for me personally and professionally, and never making me feel like a question is a bad one, irrespective of its relevance to my research or coursework.

I would also like to thank the MOXIE Principal Investigator, Michael Hecht, for teaching me to never leave a stone unturned and that the importance of diligence can never be overstated. Thank you to the rest of the MOXIE team at the MIT Haystack Observatory, NASA Jet Propulsion Laboratory, and OxEon Energy, particularly Donald Rapp, Andy Liu, and Joe Hartvigsen, for continuously providing insights into my experimental methods and results. I would also like to thank former MOXIE students, especially Eric Hinterman and Maya Nasr, for guiding me through my transition to MIT and for establishing a research foundation for me to build upon.

Thank you to Parker Steen for partnering with me every step of the way in designing and conducting my experiments. I would also like to thank Kyle Horn for your support and camaraderie throughout this degree.

Lastly, I would like to thank my parents, brother, sister, roommates, friends, and partner Shreenu for your unwavering emotional support and votes of confidence. I know that I have leaned on all of you more than you have asked for, and your love has continuously reminded me that I have never been alone in this journey.

My research was supported by the National Science Foundation Graduate Research Fellowship Program, MOXIE contracts awarded by NASA, and the MIT Department of Aeronautics and Astronautics.

Contents

List of Figures

List of Tables

Chapter 1

Introduction

1.1 Mars ISRU Overview

Since Mars was first observed through a telescope by Galileo Galilei in 1610, it has long held the fascination of scientists studying the evolution of our solar system, as well as the interest of the general public. Humans have been characterizing Mars using spacecraft since the Mariner 4 mission first reached the red planet in 1965, and have made tremendous strides in the decades since, including several orbiters to image the planet and characterize its atmosphere, landers to conduct measurements and experiments on the Martian surface, and rovers with increased mobility to build upon past work and search for evidence of past life (Masson, 2005). However, humans have not yet successfully landed on Mars due to the challenges associated with landing large masses on the Martian surface, maintaining crew health during the extended duration transit and surface mission stages, and producing the significant resources such as oxygen for propellant and crew use that would be needed for such a mission (Drake and Watts, 2009).

Teams at the National Aeronautics and Space Administration (NASA) have developed several potential architectures for crewed missions to Mars, the most prevalent of which is the Design Reference Architecture (DRA), currently in its fifth iteration (Drake and Watts, 2009). The DRA quantifies resources needed for a crewed mission to Mars and identifies critical technology areas and current gaps preventing the im-

plementation of such architectures. One such enabling technology to sustain a crew on Mars is In-Situ Resource Utilization, or ISRU. ISRU is the use of resources present on another planetary body for the production of materials and consumables to aid exploration of these bodies. ISRU can essentially be likened to "living off the land" - by processing resources found at destination sites, missions to other planets do not need to bring all of the required materials from Earth, which reduces launch mass, mission preparation time, and cost.

The benefits of ISRU, specifically related to Mars exploration, can be observed using the "gear ratio" methodology used by (Rapp, 2013). A mission to and from Mars consists of several stages, including launch from Earth, transit to Mars, landing on Mars, ascent from the Martian surface, and the return to Earth. For each of these stages, the gear ratio is the ratio of initial mass to the final delivered mass at the end of that stage. The gear ratio for delivering cryogenic propellant from Low Earth Orbit (LEO) to the Martian surface is approximately 16:1, which means that for every ton of propellant delivered to Mars, 16 tons would be required to transfer this propellant from Earth orbit (Rapp, 2013). Therefore, minimizing the amount of payload brought from Earth to Mars is critical for reducing mission mass, size, and cost. For a crew of four, approximately 24 metric tons of O_2 would be required just for use as oxidizer for a Mars ascent vehicle, in addition to the oxygen that would be required for crew use on the Martian surface (Hecht et al., 2021). As the gear ratios suggest, the supporting mass from LEO of such a large quantity of oxygen would be on the order of 400 tons - this oxygen would have to be stored without boiloff during the several months of cruise between the Earth and Mars as well as during surface operations on Mars, which would require additional technological development and increase cost further. Therefore, producing this oxygen in-situ is critical for a crewed Mars mission, and this is a key assumption of the current DRA for Mars exploration.

However, while there has been significant progress towards developing ISRU methods and validating them on Earth, prior to 2021 there were no successful demonstrations of ISRU on another planetary body. The Mars ISRU Precursor (MIP), which was designed to produce oxygen from CO_2 in the Martian atmosphere, was devel-

oped in the late 1990s for inclusion on the 2001 Mars Surveyor Lander.(Kaplan et al., 2001). MIP was tested extensively in the laboratory - however, with the cancellation of the Mars Surveyor Lander mission, this payload never flew to Mars. Therefore, demonstrating the production of oxygen on Mars is a key step towards crewed Mars missions, and is a gating factor for the development of sustained human activities on the Martian surface. In 2021, the Perseverance rover landed on Mars hosting several payloads designed to search for evidence of past life on Mars as well as demonstrate key technologies for future human exploration of Mars. Among these payloads, which together comprise the Mars 2020 mission, is the Mars Oxygen ISRU Experiment, or MOXIE; MOXIE is the first demonstration of ISRU on another planetary body, and is furthering ISRU research to enable human exploration of the solar system.

1.2 Mars Oxygen ISRU Experiment (MOXIE)

MOXIE is a technology demonstration focused on the production of oxygen from the Martian atmosphere, with the goal of validating Mars-based ISRU and informing the design of a future full-scale Mars ISRU oxygen production system. MOXIE has three mission-level requirements, listed below:

1. Be capable of producing at least 6 g/hr of oxygen in the context of the Mars 2020 mission (with the environmental conditions at Jezero Crater and within the Perseverance rover).

2. Produce oxygen with $> 98\%$ purity.

3. Meet the above requirements for at least 10 operational cycles after delivery.

In addition to the above requirements, MOXIE was also designed to demonstrate oxygen production during day and night throughout all Martian seasons, showing robustness to variations in atmospheric pressure and temperature (Hoffman et al., 2022). An image of the MOXIE system is shown below, as well as its location within the Perseverance rover.

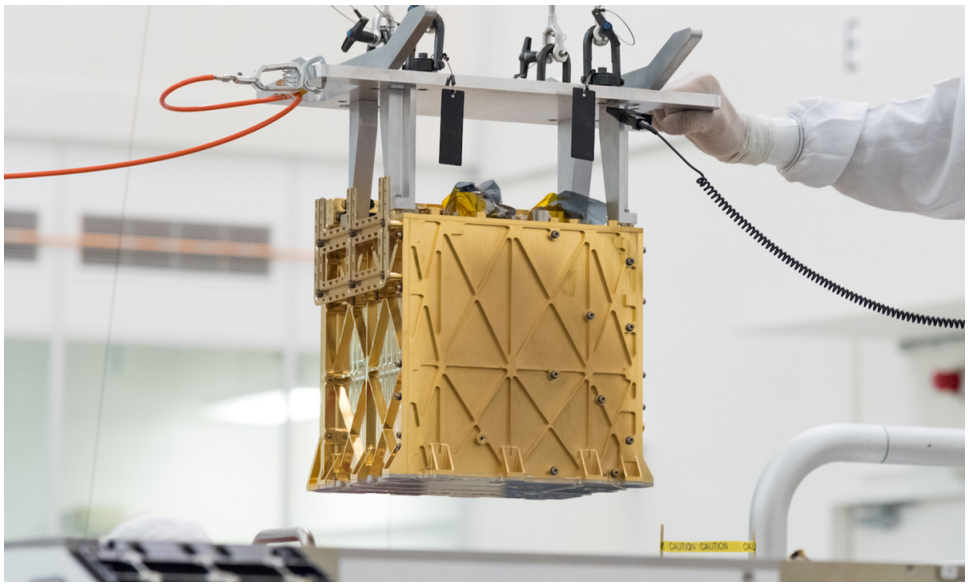

Figure 1-1: MOXIE being lowered into the Perseverance rover prior to launch (National Aeronautics and Space Administration (NASA), 2020).

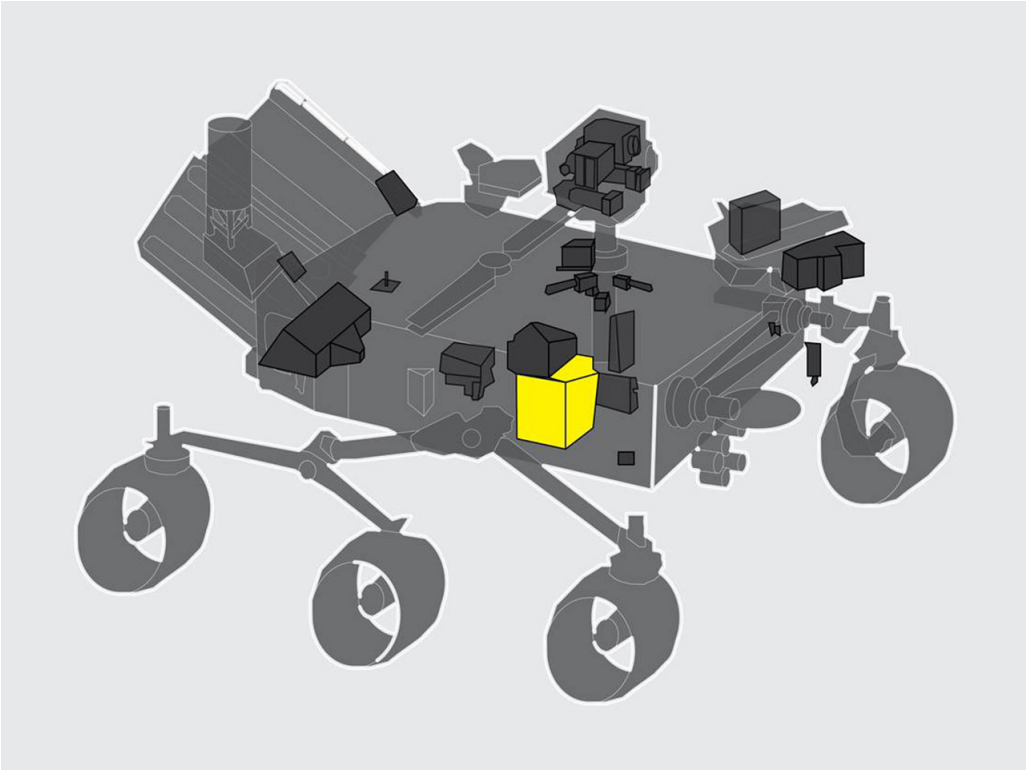

Figure 1-2: The location of MOXIE, shown in yellow, within the Perseverance rover (National Aeronautics and Space Administration (NASA), 2020).

MOXIE operates using a process called electrolysis, which separates CO_2, which constitutes approximately 95.5% of the Martian atmosphere, into CO and O_2 through the reaction in Equation (1.1) (Hecht et al., 2021).

$$2CO_2 \rightarrow 2CO + O_2 \tag{1.1}$$

During a MOXIE operational cycle, or run, gas from the Mars atmosphere is drawn into the system using a mechanical scroll compressor, which takes in a fixed volume of gas with each rotation and compress it to a smaller fixed volume. The rotational speed of the compressor can be commanded directly, or can be controlled through a control loop to match a downstream pressure setpoint. The MOXIE scroll compressor is shown below in a disassembled configuration in Figure 1-3.

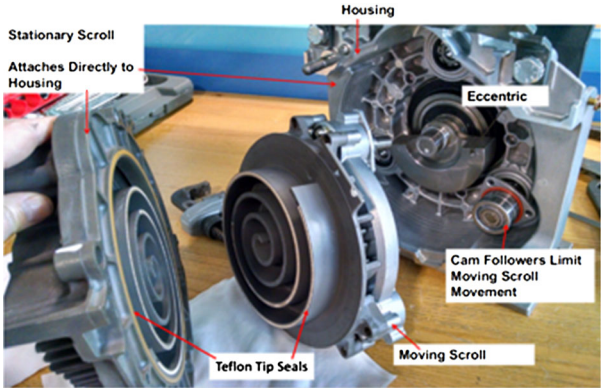

Figure 1-3: The MOXIE scroll compressor, disassembled (Hecht et al., 2021).

The compressed gas is then fed into a downstream plenum of a fixed size. The air is passed to the compressor inlet through a HEPA (High Efficiency Particulate Air) filter to prevent any dust from the Martian environment from entering the system. The pressurized gas from the compressor is preheated in an Inconel heat exchanger, and is then flowed into a Solid OXide Electrolysis reactor (SOXE), which consists of ten electrolysis cells arranged in two groups of five cells each. The SOXE stack is heated to approximately 800 °C through heaters on both ends of the stack, which are controlled through a control loop to match temperature setpoints for the top and bottom heaters. The electrolysis cells consist of an electrolyte with porous electrodes on either side - the

solid oxide electrolyte is made of Scandia-stabilized Zirconia (ScSZ), which contains vacancies in its crystal lattice structure. The vacancies in the crystal structure allow the passage of oxygen ions but not electrons; therefore, the oxygen ions carry the current in the electrolysis cell and recombine at the anode to form O_2, resulting in pure oxygen on the anode side of the cell. Specifically, when an electric potential is applied to heated CO_2 flowing over the nickel felt-covered cathode surface, it is decomposed to form CO and O^{2-} ions. The oxygen ions are then electrochemically driven through the electrolyte, filling the vacancies in the ScSZ structure. As the plenums on the cathode and anode sides of the electrolysis cells are separated by the non-porous ScSZ electrolyte, the produced oxygen is physically separated from the CO and unreacted CO_2 (and inert gases in the Martian atmosphere). This prevents contamination of the O_2 gas that is produced within the SOXE, maintaining purity. The electric potential across the SOXE can be controlled through either a direct voltage setpoint or a current setpoint, which utilizes a control loop to increase the voltage until the measured current matches the setpoint. A diagram illustrating the flow of the gases and ions through the SOXE is shown in Figure 1-4.

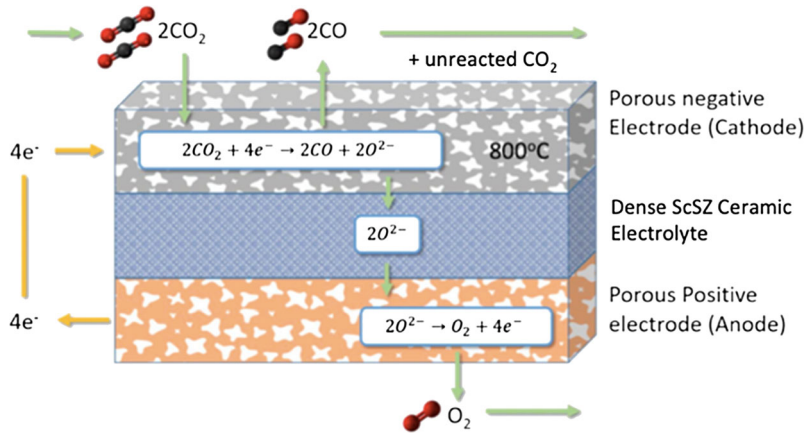

Figure 1-4: A cross-sectional view of a single SOXE cell layer, showing the transport of molecules within the system (Hecht et al., 2021).

The distinct cathode and anode outlet streams then pass through additional filters and heat exchangers prior to passing through composition sensors to verify the purity of the produced oxygen. The cathode and anode gases are then exhausted to

the Martian atmosphere through fixed flow resistance Viscous Flow Control Devices (VFCDs), which are temperature-compensated precision apertures. As the VFCDs are of a fixed flow resistance, cathode and anode pressures are directly dependent on the inlet gas density and compressor rotational speed, and cannot be controlled independently in the MOXIE configuration. VFCDs were included rather than pressure regulators to minimize mass and volume of the system - this is discussed further in later sections of this thesis. Lastly, a few percent of the exhaust gas in the cathode line is recirculated back to the compressor inlet through another VFCD - CO_2 is a mildly oxidizing gas, so including the reducing CO from the cathode in the SOXE inlet stream prevents oxidation of the nickel in the cathode. A schematic of the MOXIE gas flow system is shown in Figure 1-5, with additional details in (Hecht et al., 2021).

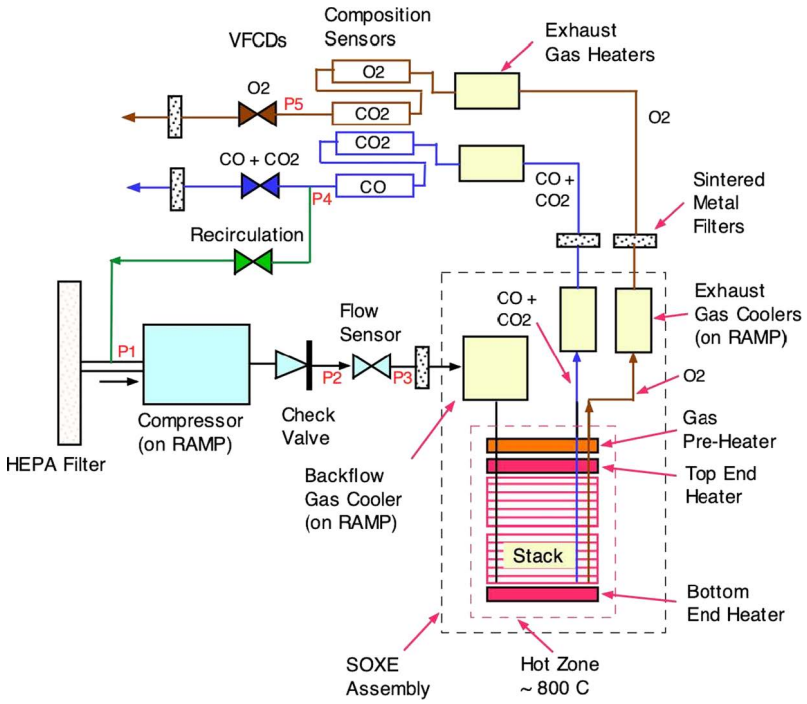

Figure 1-5: Schematic layout of gas flow through MOXIE (Hecht et al., 2021).

Various temperature and pressure sensors throughout the MOXIE flow path measure gas properties during operations, and collect data at 1 Hz. These sensors are shown in Figure 1-6. Of note are the P4 and P5 pressure sensors, which measure pressure at the cathode and anode exhausts respectively, TT and TB, which mea-

sure the heater temperatures, and M1 which measures the compressor motor speed. The remaining sensors are discussed in great detail in the MOXIE Command and Telemetry Dictionary (Morris, 2018).

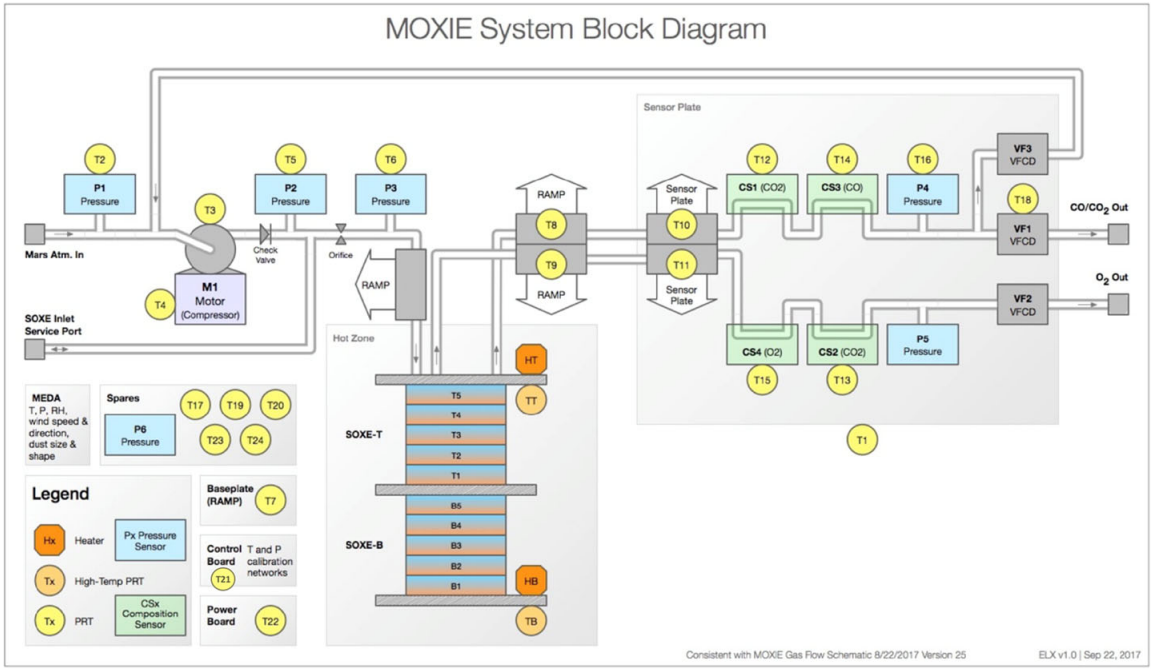

Figure 1-6: MOXIE system block diagram showing sensor locations and types (Hecht et al., 2021).

As of February 2023, MOXIE has completed 13 oxygen-producing operational cycles since landing on Mars in February 2021. These runs, which have demonstrated oxygen production at day and night across an entire Martian year, have also allowed for characterization of different system operating modes (controlling SOXE voltage vs. current), performance of the SOXE at different temperatures, and demonstrations of extended run segments (Hoffman et al., 2022). Therefore, MOXIE has achieved all of its mission-level requirements, and further studies are focused on expanding the performance envelope of the system and evaluating further operating modes to better inform design of a full-scale Martian oxygen production system. The MOXIE team has also focused on conducting laboratory efforts in parallel to MOXIE's operations on Mars, which provides complimentary data and additional flexibility that is not

possible on a Mars flight mission. By operating on Mars and on Earth in parallel, the MOXIE team is seeking to further characterize ISRU technology for applications on the Moon, Mars, and beyond. This thesis is focused mainly on these laboratory activities, specifically relating to the MOXIE FlatSat testbed.

1.3 MOXIE Laboratory Testbed: The FlatSat

1.3.1 Limitations with the MOXIE System

Opportunities to characterize the MOXIE system are limited due to several factors. First, as an active payload on the Mars 2020 mission, MOXIE is operated conservatively - all planned runs for the MOXIE Flight Model (FM) on Mars are reviewed and modeled thoroughly, and any run steps and formats that have not yet been demonstrated on Mars must first be demonstrated on the MOXIE Engineering Model (EM), which is a component-by-component replica of the MOXIE system hosted in a laboratory at the MIT Haystack Observatory. This increases the time and effort required for each run, and also limits the scope of each run, as the MOXIE system cannot be accessed to replace components in the case of degradation or failure. Therefore, runs are designed to operate within the confines of the MOXIE operating envelope rather than push the limits of the system. Although the EM is used as a platform for proving new run techniques, it is also a mission-critical article of hardware, so EM runs are only conducted after the run has been analyzed using dynamic and steady-state modeling techniques (Hecht et al., 2021). This prohibits the use of the EM and FM for experimentally characterizing operating regimes that are not well understood and have not yet been modeled extensively.

In addition, the FM is limited to usage in its as-launched configuration, as making modifications to the system on Mars is not possible. As the EM is intended to replicate the FM system, it is also in a fixed configuration. This prevents the MOXIE team from making modifications to either system to fit evolving mission needs and characterization efforts. For example, the amount of sensors that could be included

on the FM was limited due to volume and areal constraints when designing and packaging the system and its electronics board (Hecht et al., 2021). Therefore, there are no sensors to measure temperature within the SOXE stack or voltages of individual SOXE cells. As the SOXE performance is temperature-dependent due to the relationship between temperature and the resistance of each cell, estimation techniques must be used when analyzing the performance without data for stack temperatures. Likewise, the voltage across each cell, which would indicate degradation on a cell-by-cell basis, cannot be measured. In addition to the sensors, the FM and EM also have fixed flow paths, discussed previously in Section 1.2. The inclusion of VFCDs with fixed flow resistances on the cathode and anode exhausts result in cathode and anode pressures directly dependent on the flow rate through the system - this prohibits certain characterization efforts that are dependent on controlling the cathode pressure, which are discussed later in this thesis. Flow through the FM and EM is also fixed through the compressor without an option to exhaust compressor-driven flow (for independent compressor characterization).

Lastly, the FM is directly constrained by its environmental and mission context. As MOXIE is just one of several payloads on the Perseverance rover, it cannot be operated whenever the team desires. There must be sufficient time and energy to operate MOXIE in place of other rover and payload operations, which often results in significant delays between the planning and execution of a run. The atmospheric environment during MOXIE runs can also not be controlled - while the MOXIE team can request runs at different times of day and year to capture changes in Martian atmospheric density, the composition of this atmosphere is fixed, and the aforementioned delays in run execution may result in MOXIE operations at atmospheric conditions other than those that were planned for. Therefore, while the FM is an incredible platform for demonstrating and understanding ISRU in a space context, it is limited in its operations, specifically with respect to characterizing components of the system and operating modes for a next-generation Martian oxygen production system.

Therefore, the MOXIE team at the Massachusetts Institute of Technology (MIT), MIT Haystack Observatory, and NASA Jet Propulsion Laboratory (JPL) developed

the MOXIE FlatSat as a ground-based operational testbed to further characterize the MOXIE system, evaluate and validate planned MOXIE operations on Mars, and demonstrate potential operating modes and configurations for a next-generation Mars in-situ resource utilization (ISRU) system.

1.3.2 MOXIE FlatSat Overview

The FlatSat consists of the main MOXIE subsystems and components arranged in a spread-out configuration within a laboratory, allowing for additional instrumentation, environmental control, and flow path modifications. This allows for more aggressive and flexible experimentation than is possible on Mars, furthering knowledge of and experience with ISRU systems and their operation without the risk and cost of a flight mission. The FlatSat is shown below in Figure 1-7.

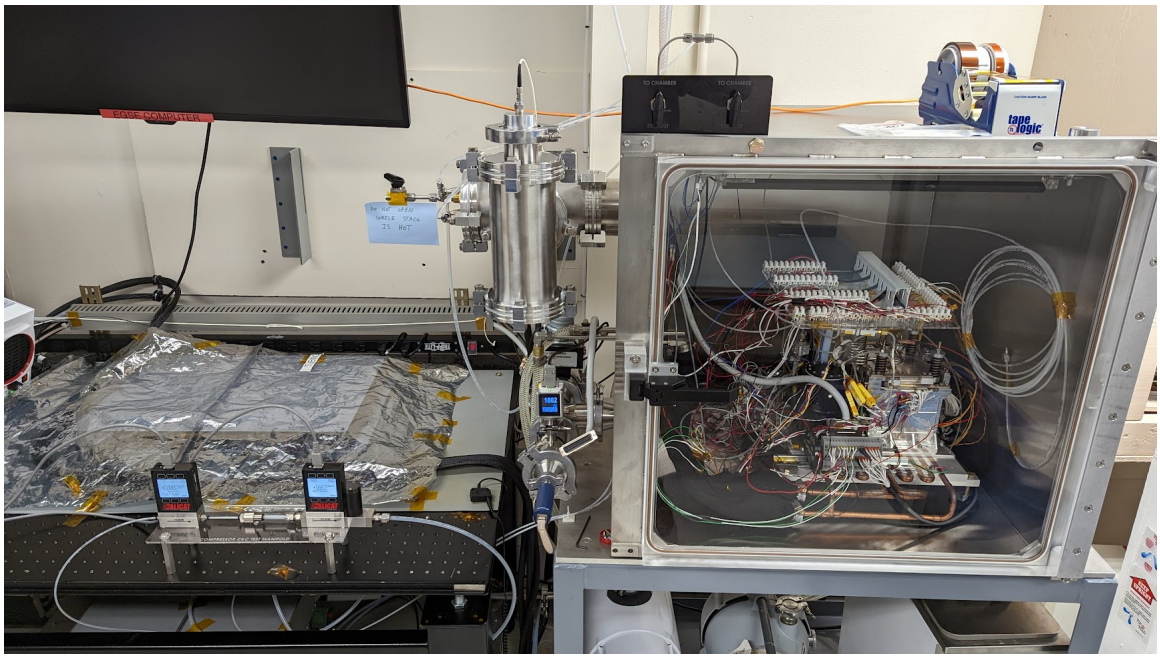

Figure 1-7: The MOXIE FlatSat in November 2022, configured for a compressor characterization experiment.

The FlatSat includes the same hardware components and sensors as the FM and EM, but allows the MOXIE team to replace these components, add new sensors,

and independently control the environmental composition of the vacuum chamber the FlatSat is hosted in. For example, the FlatSat includes voltage sense leads on each of the 10 cells within the SOXE, allowing for the logging of cell voltage data during each run to track cell performance and degradation. In addition, the FlatSat includes additional auxiliary thermocouples to measure stack temperature at the top, bottom, and midplates, which better informs the temperature distribution within the stack during an oxygen production run. As the open layout of the FlatSat allows access to the internal hardware of the system, it is also possible to make changes to the flow path within the FlatSat that would not be possible on the FM or EM. For example, the compressor outlet can be disconnected to perform standalone compressor characterization tests without flowing gas through the remainder of the MOXIE flow path, and the VFCDs on the cathode and anode outlets can be replaced with pressure regulators to independently control the pressures in each plenum. The compressor can also be bypassed entirely, which allows for the direct feed of mixed CO_2 and CO gas into the SOXE at a fixed mass flow rate for independent SOXE characterization.

The environment within the FlatSat chamber can also be controlled, as the composition of gas within the chamber, chamber pressure, and chamber temperature can all be controlled using supporting laboratory hardware. This allows the MOXIE team to replicate any desired Martian atmospheric conditions and change these conditions at a much more rapid rate than on Mars. Additional external components such as mass flow meters, pressure gauges, and three-way valves to direct flow also enable finer measurement and control of flow through the FlatSat system. In addition to the increased flexibility with hardware configuration and data collection, the FlatSat can also be operated and monitored directly, unlike the FM. Both the standard MOXIE telemetry as well as auxiliary sensors and atmospheric conditions are displayed in real-time during FlatSat operations, which allows the operators to abort a run if any off-nominal behaviors are observed. This allows for the validation and characterization of operating modes that would be considered too high-risk to run on the FM, as a run can be aborted immediately if real-time data indicates any damage to the FlatSat system. All runs are also commanded using a rover emulator, which stores

and relays data in the same format as the Perseverance rover, allowing for redundant use of the FlatSat as a verification platform for planned FM runs. As the software governing FlatSat operations is the same as the flight software used on the FM, the FlatSat can also be used to verify software updates prior to uploading them to the FM on Mars. Lastly, the FlatSat can be operated continuously for extended periods of time, as it is not constrained by the limited battery energy available to the FM from the Perseverance rover. This enables the completion of longer duration experiments, such as component lifetime degradation tests, which cannot be run on the FM due to the aforementioned energy constraints. With this increased flexibility, as well as the ability to operate the FlatSat on a daily basis as opposed to the limited opportunities to run the FM, this testbed enables the completion of MOXIE and broader ISRU-related characterization activities to understand the limitations of the MOXIE system, how it can be improved and optimized for a larger-scale Martian ISRU system, and how performance of the MOXIE system may change over time.

The FlatSat system was fully commissioned in February 2022 after thorough tests to verify the entire system on a subsystem and system-level basis. This included calibration of sensors within the system, modifications to the rover emulator software to include additional telemetry streams, and oxygen-producing runs to verify that the system operated as intended. While these commissioning activities are not the focus of this thesis, of note is the second oxygen-producing run on the FlatSat, FS OC03. After the first oxygen-producing run, FS OC02, it was discovered that oxygen from the anode was mistakenly recirculated to the cathode due to a plumbing error. This led to oxidation of the Ni felt within the cathode, which decreased system performance. To remediate this, FS OC03 included a run segment where N_2 and H_2 forming gas was flowed through the cathode to reduce the oxidized Ni felt, as well as a bakeout of the system in ambient air to remove any conductive char from binding agents within the SOXE. Oxygen-producing segments prior to and after these restorative efforts demonstrated a restoration in SOXE performance, therefore demonstrating another key benefit of the FlatSat - the highly configurable flow path and composition enabled the remediation of system health, which would not be possible on the FM or EM.

Specifically, the MOXIE team demonstrated that oxidation within the SOXE could be reversed, and in the case of future FlatSat experiments that cause degradation, that similar efforts could be completed to restore system performance. Through repeated operations on the FlatSat since that run, MOXIE team members have increased their comfort, familiarity, and confidence in this testbed for use as an experimental platform for furthering ISRU research.

1.4 FlatSat Characterization Introduction

After preliminary calibration and commissioning were conducted for the FlatSat, it became available as a testbed for use by the MOXIE team. As discussed in previous sections, the FlatSat is a versatile tool that can be used to inform the operations of the MOXIE FM on Mars, as well as a research platform that can be used to further characterize the performance of the various technologies used for MOXIE and how these may be scaled for use in a full-scale Martian atmospheric oxygen production system. The following chapters detail characterization efforts that were conducted with the following goals in mind:

1. Characterize how the MOXIE system and subsystems can be used to inform design and operations of a full-scale system.

2. Refine methods for predicting MOXIE performance and behavior, and use these improvements to better plan and model FM operations on Mars.

3. Understand how FM performance on Mars as well as performance of a future full-scale system may change over time due to component-level degradation.

4. Qualitatively and quantitatively examine the differences between the FlatSat and FM/EM, to determine the extensibility of FlatSat data to the other models.

Chapter 2

Low Cathode Pressure Operation

2.1 Motivation

Operating the SOXE at a low cathode pressure offers several benefits over operation at the typical MOXIE cathode pressures of approximately 500 to 800 mbar. First, by lowering the cathode pressure, the required compressor outlet pressure is reduced, therefore reducing the compression ratio. As the energy cost of this thermodynamic compression is proportional to the ΔP between the compressor inlet and outlet, decreasing the compressor outlet pressure reduces compressor power, and therefore the energy usage of the compressor. As energy usage is constrained on the MOXIE FM, reducing compressor energy usage through operating at a low cathode pressure enables longer runs. These factors are discussed in further detail in Section 3.1. In addition, minimizing compressor energy usage through a decreased cathode pressure reduces the power required for a future full-scale Martian oxygen production plant or increases available power for electrolysis and thermal control for a fixed-power system, which is advantageous when optimizing the system for maximum oxygen production. (Hinterman, 2022).

In addition to the reduced energy for thermodynamic compression, operating at a low cathode pressure also enables the SOXE to operate at higher voltages and currents when compared to a higher cathode pressure, which enables a higher safe oxygen production rate without increasing the amount of CO_2 flowing into the system.

This is because at lower cathode pressures, the Nernst potential for oxygen production from CO_2 is unaffected, whereas the Nernst potential for carbon production from CO increases. The Nernst potential in this case is the voltage at which the electrochemical reaction can move forward; for the SOXE to produce oxygen, each cell must be operating above the Nernst potential for oxygen production, shown in Equation (2.1). However, the cell must also operate below the Nernst potential for carbon production, shown in Equation (2.2), as exceeding this potential would cause the deposition of carbon on the electrodes, resulting in degradation of the cell and a reduction in performance. In the below equations, V_{rev} is the voltage above which the reaction would proceed in the opposite direction as a fuel cell, T is the temperature in Kelvin, R is the universal gas constant, and F is the Faraday constant. The terms labeled p are the partial pressures of the respective gases, on the cathode side for CO and CO_2 and on the anode side for O_2 (Hecht et al., 2021).

$$V_N(2CO_2 \rightarrow 2CO + O_2) = V_{rev} + \left(\frac{RT}{4F}\right) \ln\left(\frac{pCO^2 pO_2}{pCO_2^2}\right) \tag{2.1}$$

$$V_N(2CO \rightarrow 2C + O_2) = V_{rev} + \left(\frac{RT}{4F}\right) \ln\left(\frac{pO_2}{pCO^2}\right) \tag{2.2}$$

Equation (2.1) and Equation (2.2) can be re-written in terms of the cathode pressure, P_{ca}, and the mole fractions of the cathode gases, x_i, as shown below in Equation (2.3) and Equation (2.4) (Hinterman, 2022).

$$V_N(2CO_2 \rightarrow 2CO + O_2) = V_{rev} + \left(\frac{RT}{4F}\right) \ln\left(\frac{(x_{CO})^2 (pO_2)}{(x_{CO_2})^2}\right) \tag{2.3}$$

$$V_N(2CO \rightarrow 2C + O_2) = V_{rev} + \left(\frac{RT}{4F}\right) \ln\left(\frac{pO_2}{(P_{ca})^2 (x_{CO_2})^2}\right) \tag{2.4}$$

As seen above in Equation (2.3), the Nernst potential for oxygen production through CO_2 is independent of cathode pressure, whereas the Nernst potential for carbon production through CO reduction, shown in Equation (2.4) is inversely proportional to cathode pressure. If the cathode pressure is decreased, the gap between

the two Nernst potentials widens, allowing for a higher voltage to be applied to the stack without exceeding the Nernst potential for carbon formation. Therefore, by decreasing cathode pressure, the SOXE can be operated at a higher voltage without risking carbon deposition, increasing the possible safe oxygen production rate for a given flow rate of CO_2. This is illustrated below in Figure 2-1, which shows the Nernst potentials for both CO_2 reduction and CO reduction as a function of cathode pressure (as indicated by the different colored lines) and CO mole fraction in the cathode exhaust, which is governed by both the gas mixture ratio as well as the voltage applied to the stack, as a higher voltage results in a higher utilization of CO_2 through conversion to CO.

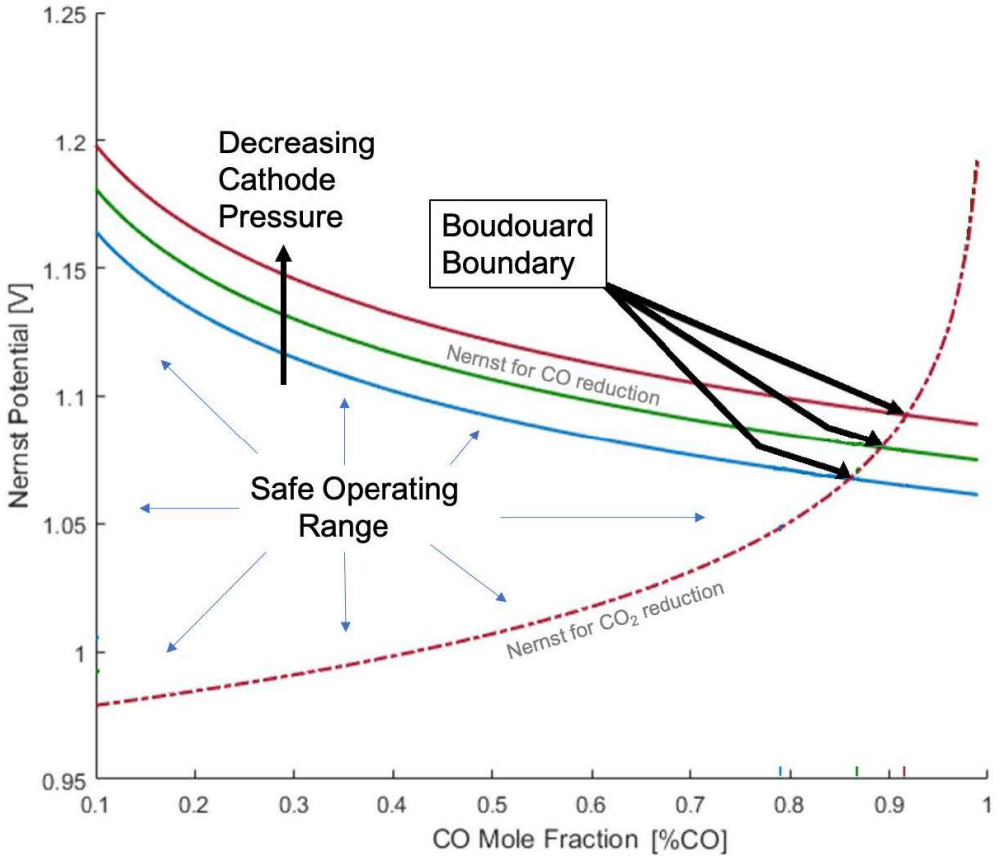

Figure 2-1: Effect of decreased cathode pressure on Nernst potentials for CO_2 reduction and CO reduction (Hinterman, 2022).

Conversely, the higher safe operating voltage at a lower cathode pressure enables an equivalent oxygen production rate with a lower flow rate of CO_2 into the system, which would reduce further reduce compressor energy usage. In addition, for a full-scale Martian oxygen production plant, reducing the flow into the system would reduce the required solid oxide electrolysis (SOE) cell surface area, therefore decreasing system mass - lowering the cathode pressure from 1 bar to 0.1 bar would reduce the number of electrolysis cells by 43% for a system producing 2 kg/hr of O_2 using an active cell area of 100 cm^2 (Hinterman, 2022).

However, there may be a minimum operating pressure for the SOXE. At low pressures, molecular diffusion through the electrode may be limited by the concentration overpotential in the cell, or the physical resistance of molecules diffusing through the electrode. While relatively constant at typical SOXE operating pressures, the concentration potential increases at low pressures due to the transition to Knudsen diffusion in these conditions, which is proportional to pressure (Hinterman, 2022). In this case, the resistance to diffusion would result in a decreased current through the SOXE cells, as the current-carrying oxygen ions would not diffuse through the cell as readily. There are also activation overpotentials, which are due to the chemical resistance of the electrochemical reaction; these overpotentials also increase as cathode pressure decreases. The effect of both the concentration and activation overpotentials are shown in Figure 2-2 for a water SOE system, labeled as "conc" and "act" respectively.

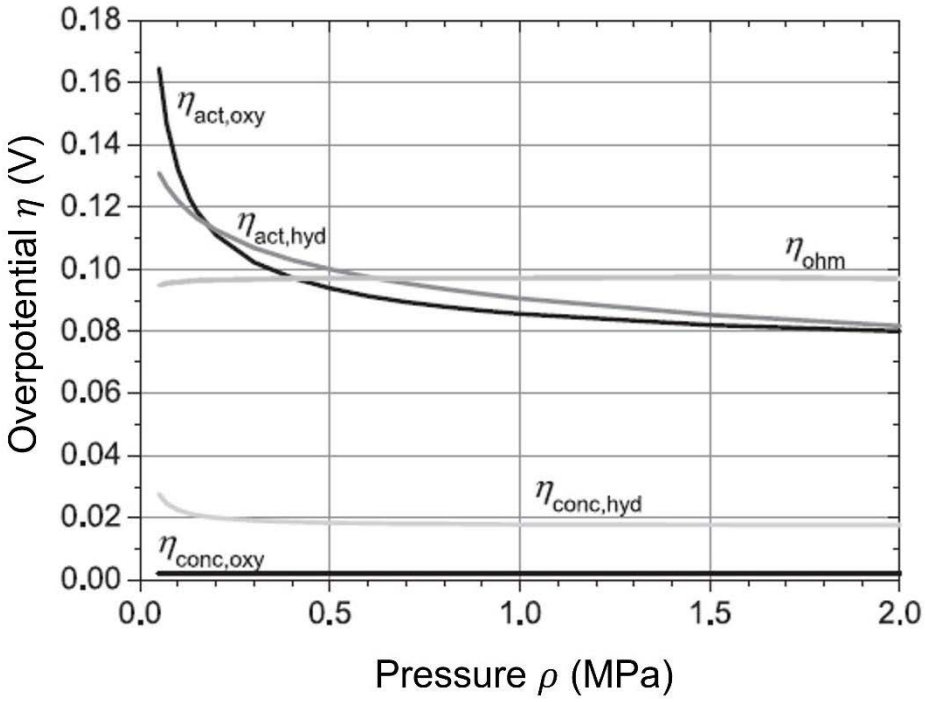

Figure 2-2: Effect of decreased cathode pressure on concentration and activation overpotentials in a water-based SOE system (Hinterman, 2022).

In addition to the above potentials, the minimum operating pressure may also be determined by pressure drops throughout the MOXIE flow path. As per Bernoulli's principle, a decrease in operating pressure with a fixed mass flow rate would result in an increase in the gas velocity. As pressure drops across flow restrictions are proportional to gas velocity, operating at a low pressure would result in larger pressure drops in the flow path - if the operating pressure is too low, pressure drops in the system may reach a level where the system may no longer function as intended (e.g. there is insufficient pressure for downstream flow to continue). For example, a modeled full-scale Martian atmospheric production plant would not be able to operate at a cathode pressure below 83 mbar, as pressure drops throughout the system would prevent operations below this threshold (Hinterman, 2022). Therefore, it is essential to not only demonstrate the benefits of lowering the SOXE cathode pressure, but also identify the minimum operating pressure that is viable for either electrolysis or the MOXIE-specific flow path.

As operating the SOXE at a lower cathode pressure offers benefits in terms of both minimizing energy usage as well as maximizing oxygen production, demonstrating and characterizing oxygen production in this operating regime is essential for the design of a next-generation Martian oxygen production plant. Specifically, it is necessary to quantify the minimum possible operating pressure for the SOXE, and determine if this is due to pressure drops throughout the system or due to the physical and/or chemical resistance within the electrolysis cell, as this would influence flow path design and electrolysis operating assumptions of a next-generation system. In addition, if such a minimum pressure is identified, it is necessary to qualitatively and quantitatively characterize oxygen production both above and below this pressure. For example, if a pressure is reached where molecular diffusion is limited due to the concentration overpotential, the current through the SOXE cells would decrease for a given applied voltage due to the increased cell resistance. However, as a low cathode pressure enables a larger voltage to be applied to the SOXE without risk for carbon deposition, the highest obtainable safe current may be higher than if the SOXE was operating at a higher cathode pressure, even with the increased cell resistance. As the presence of VFCDs on the FM prevents independent control of cathode pressure, this is a characterization effort that is only possible for MOXIE using the FlatSat, where the flow path and hardware can be modified and reconfigured. Therefore, although this characterization activity is not primarily intended to characterize the FlatSat testbed itself, it is a clear demonstration of how the FlatSat can be used to conduct Mars ISRU and SOE research activities not possible on the MOXIE FM alone. Prior work in this area is discussed in the following section.

2.2 Prior Work

A former graduate student working on the MOXIE project, Eric Hinterman, conducted an in-depth experimental study into low pressure SOE operations as a part of his doctoral thesis research on optimizing a full-scale Martian oxygen production plant. The completed research, summarized below, can be examined in greater detail

in his doctoral thesis (Hinterman, 2022).

Prior work was conducted at OxEon Energy in North Salt Lake, Utah, with a stack of SOE cells approximately five times larger than the cells in MOXIE, with the goal of characterizing the performance of the cells themselves at low pressure. Therefore, this experiment specifically targeted analyzing the electrolysis performance at low pressures, and the possible effect of the concentration overpotential as discussed in Section 2.1, rather than limited low pressure operation due to pressure drops across the MOXIE flow path. In this experiment, a mixture of CO_2 and CO was flowed through the stacks at a fixed mass flow rate, with a variable flow restriction on the outlet of the electrolysis cells in order to control the cathode pressure of the cells. The experimental setup is shown below in Figure 2-3.

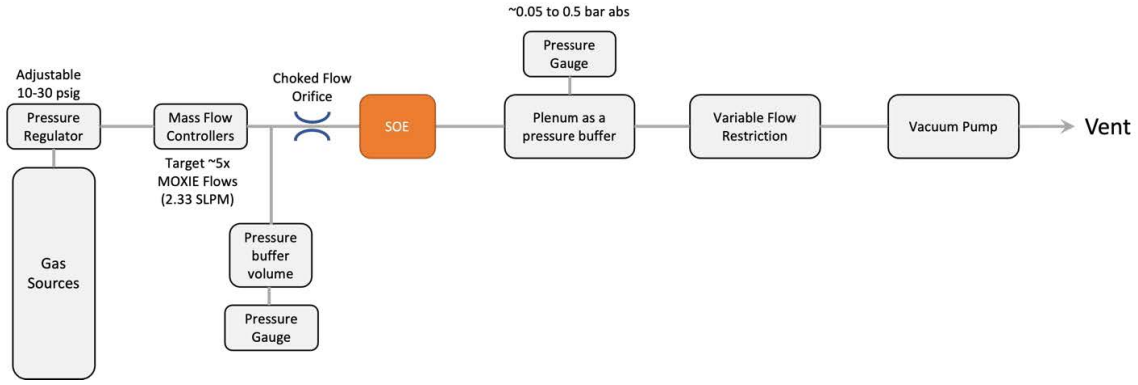

Figure 2-3: Block diagram of experiment conducted at OxEon energy to characterize low pressure SOE operations (Hinterman, 2022).

During this test, the cathode pressure was stepped down from 860 to 150 mbar, and at each pressure setpoint a current-voltage (I-V) sweep was completed to increase the envelope in which the SOE cells' performance could be characterized. The test was initially planned to test cathode pressures as low as 50 mbar, but a leak due to a failed seal in the electrolysis stack prevented the system from reaching pressures below 150 mbar. Because of this leak, ambient air flowed into the cathode, and the vacuum pump was unable to decrease the pressure below 150 mbar.

To analyze the performance of the electrolysis stack at each pressure step, the

average intrinsic area specific resistance (iASR) of each cell was computed. The iASR represents the resistance of flow through the electrolyte, driven by the ohmic resistance of ion conduction and with contributions from electron conduction through the electrical interconnect and from the electrochemical reaction resistance in the anode and cathode (Hecht et al., 2021). The equation for calculating iASR is shown below in Equation (2.5), where V_{op} is the operating voltage of the cell in volts, V_0 is the Nernst potential for CO_2 reduction plus an additional observed empirical voltage offset in volts, I is the current through the cell in amps, and A_{cell} is the cell area in cm^2.

$$iASR(\Omega - cm^2) = \frac{(V_{op} - V_0)(A_{cell})}{I} \tag{2.5}$$

If the concentration overpotential was high enough at a low cathode pressure to cause the increased resistance to current flow discussed in Section 2.1, the iASR of the cell would increase compared to the iASR at a higher cathode pressure where the effect concentration overpotential was negligible. Therefore, by calculating the iASR at each pressure step, the reduction in cell performance due to the concentration overpotential could be quantified and compared to cell performance during standard operations at a higher cathode pressure. The calculated average iASR for the stack at each cathode pressure is shown in Figure 2-4.

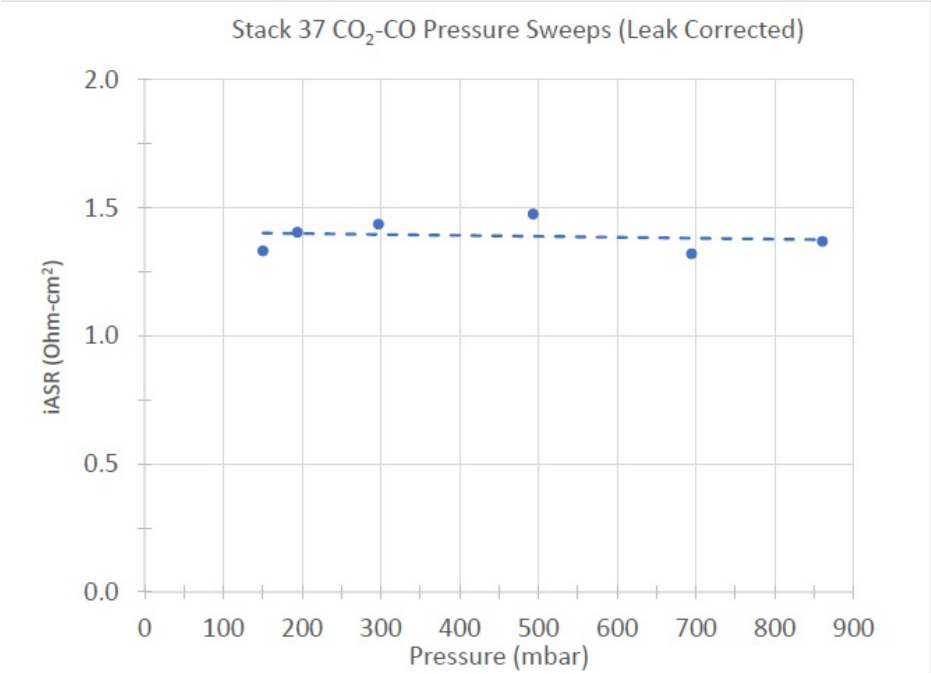

Figure 2-4: iASR as a function of cathode pressure for the low pressure experiments conducted at OxEon energy (Hinterman, 2022).

As seen in Figure 2-4, there was no significant observed increase in iASR as the cathode pressure was decreased. This indicates that the concentration overpotential-driven low pressure limit was not reached, as operating at a cathode pressure below this limit would correspond with a sharp increase in iASR. In addition, these results suggest that the activation overpotential does not have a significant effect on iASR as pressure is decreased. Therefore, this experiment demonstrated that SOE cells can operate as low as 150 mbar without experiencing a reduction in performance. However, as this experiment was unable to verify SOE performance at cathode pressures lower than 150 mbar, further experimentation is necessary to increase the resolution of the cathode pressure steps, quantify the lower limit for operations, and how the iASR of the electrolysis stack changes at this limit. In addition, as this experiment was independent of the MOXIE system, it does not investigate the other possible low limit for operations, where pressure drops throughout the flow path prevent operations below a certain pressure. Therefore, while this experiment certainly demonstrated SOE performance at pressures lower than the typical MOXIE cathode pressures, ad-

ditional work is needed to characterize the low limit for SOE operations, determine the underlying cause of this limit, and characterize SOE performance at or below this limit compared to performance at higher cathode pressures. The FlatSat experiments that were conducted to answer these questions are discussed in the following section.

2.3 Experimental Methods

A single experiment was conducted to characterize low pressure SOXE operations on the FlatSat. This experiment was designed to yield both qualitative and quantitative data to allow for characterization of SOXE performance at various operating pressures, which will inform the optimal operating conditions for a full-scale Martian oxygen production plant.

There were two direct objectives for this experiment:

1. Experimentally determine if there is a minimum cathode operating pressure on the FlatSat, and if so, quantify this lower limit to within 5 mbar.

2. Determine the underlying mechanisms behind the minimum operating pressure, and determine if it is due to pressure drops throughout the system or due to limited diffusion caused by the concentration overpotential.

The indirect objectives of these experiments were as follows:

1. Qualitatively and quantitatively characterize the changes in SOXE performance if a minimum operating pressure is reached, either due to the concentration overpotential or pressure drops across the system.

2. Compare the minimum operating pressure and mechanisms driving this minimum to the modeled pressure drop-limited minimum pressure of 83 mbar on a full-scale system, to determine if the limiting factor in full-scale SOE operation is due to pressure drops or the increased concentration overpotential.

Initially, a second experiment was planned in order to demonstrate the higher utilization that can be achieved with a low cathode pressure, by operating at a high

utilization that would exceed the Nernst potential for carbon deposition at the typical VFCD-driven cathode pressures. However, this second experiment was not conducted due to limitations in how low of a cathode pressure was achievable, which is discussed later in this section.

This experiment was designed to identify the lowest cathode pressure at which the SOXE can operate, and determine the causal mechanism behind the minimum operating pressure. The experiment consisted of repeated I-V sweeps at various cathode pressures, similar to prior work discussed in Section 2.2, which provides a baseline performance across several voltage setpoints for comparison as the cathode pressure is changed. The laboratory configuration and data acquisition methods used in this experiment are summarized below in Table 2.1.

Table 2.1: Low Pressure Tests: FlatSat Configuration

Overview	This test involved repeated I-V sweeps on the FlatSat SOXE while the cathode pressure was changed using a back pressure regulator (BPR) connected to the cathode exhaust. The anode pressure was held constant at 500 mbar using a BPR connected to the anode exhaust. The SOXE voltage setpoints were set via standard MOXIE run control table. The FlatSat was in a direct-feed configuration, where the compressor was bypassed and a mixture of CO_2 and CO was flowed directly into the SOXE at a mass flow rate of 21.9 g/hr.
Environment composition	FlatSat vacuum chamber at vacuum for duration of test, and mixture of 98% CO_2 and 2% CO by mole fraction flowed directly at 21.9 g/hr to SOXE upstream of check valve (see Figure 2-5). Mass flow rate of gas controlled by Alicat 2 SLPM Mass Flow Controller and measured by Alicat Whisper MW–Series Low Pressure Drop 2 SLPM Flow Meter upstream of SOXE entry.
Compressor configuration	Compressor bypassed by direct feed line to SOXE assembly.

Vacuum pump configuration	**Before/after applying voltage**: Cathode and anode exhausts connected to independent vacuum pumps, and direct gas feed line directed to auxiliary pump upstream of SOXE. **While voltage applied to SOXE**: Cathode and anode exhausts connected to independent vacuum pumps.
SOXE configuration	**Inlet**: Gas flowed directly to check valve upstream of SOXE (bypassing compressor) and through the SOXE cathode. **Outlet**: VFCDs on cathode and anode exhausts bypassed. Cathode and anode exhausts instead connected to BPRs to control cathode and anode pressures. Cathode and anode exhaust pumps connected downstream of BPRs. **SOXE Temperature**: Top stack temperature was set to 838.8 K through ZTT_SP in the run control table, and bottom stack temperature was be set to 836.9 K through ZTB_SP in the run control table. Stack temperatures were maintained through a control loop (Morris, 2018).
Temperature Measurements	Standard FlatSat temperature measurements taken (Morris, 2018). SOXE stack temperatures was monitored using additional auxiliary thermocouples to measure stack top, bottom, and mid-plate temperatures.
Pressure Control and Measurements	Standard FlatSat pressure measurements were (P2, P3, P4, P5 in telemetry data). P4 and P5 sensors removed from VFCD manifold and installed in-line with BPRs. **Cathode outlet**: Pressure measured and controlled by Alicat PC-Series Pressure Controller (BPR), with redundant measurement through P4 sensor. **Anode outlet**: Pressure measured and controlled by Alicat PC-Series Pressure Controller (BPR), with redundant measurement through P5 sensor.

Data acquisition	All non-standard MOXIE measurements (mass flow meter, BPR measurements, SOXE auxiliary thermocouples, cell voltage measurements) were made with 16bit 0-5 VDC analog inputs read via a LabJack T7. Mass flow into the SOXE was measured using an Alicat Whisper MW–Series Low Pressure Drop 2 SLPM Flow Meter. Cathode and anode exhaust pressures were measured using Alicat PC-Series Pressure Controllers with redundant measurement through P4 and P5 in the MOXIE FlatSat electronics and rover emulator data module. Stack temperatures (TT, TB), voltages (VT, VB, VT_OUT, VB_OUT), and currents (IT, IB) were observed by MOXIE FlatSat electronics and rover emulator data module. Stack iASR was calculated using IT, IB, VT, and VB readings from the FlatSat telemetry.
Data format	All data was saved in a .xlsx file in calibrated units.

The experimental setup is shown below in Figure 2-5.

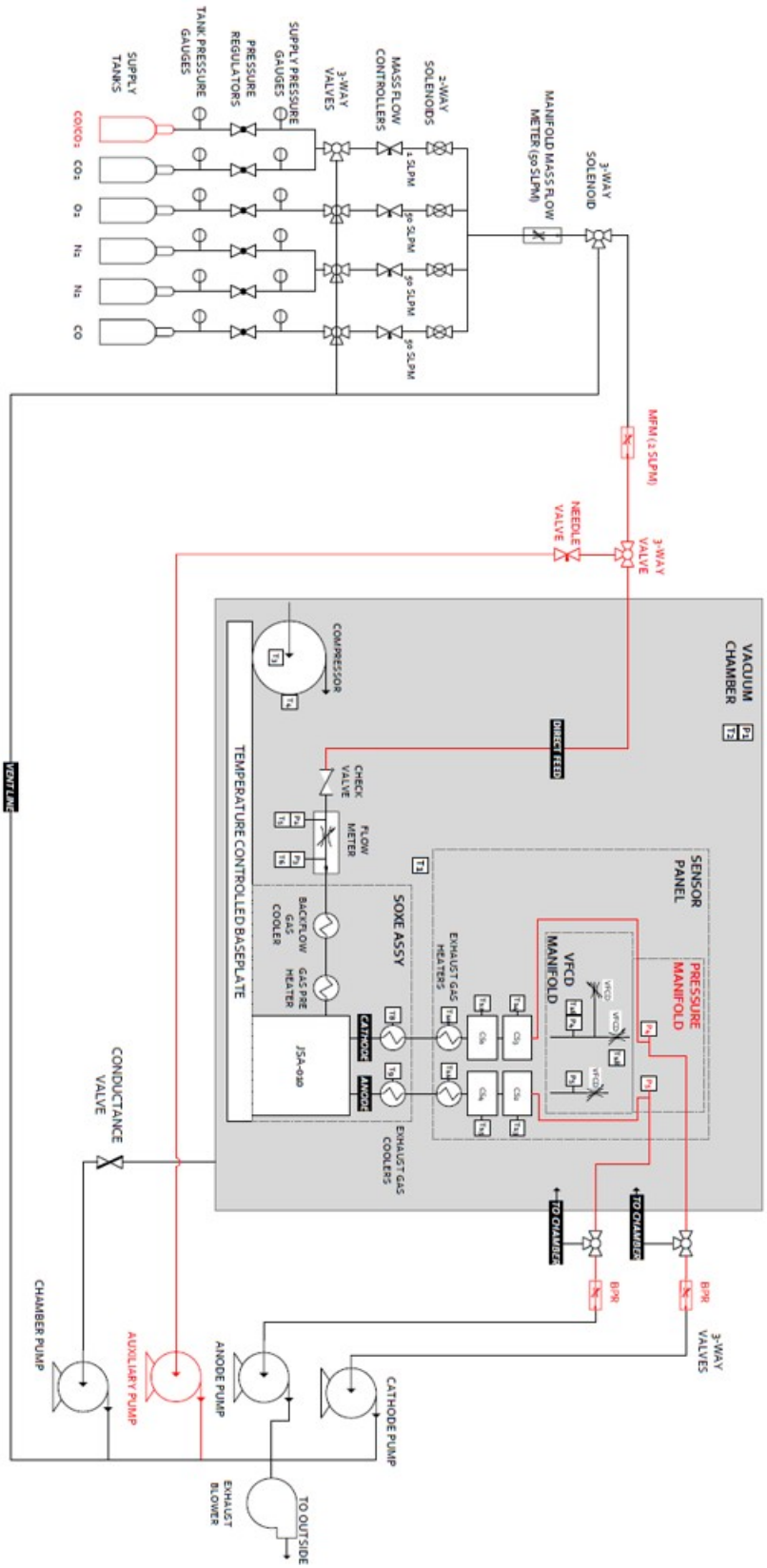

Figure 2-5: FlatSat low pressure operations experimental setup.

The configuration shown in Figure 2-5 and discussed in Table 2.1 involves several modifications to the standard FlatSat flow path. First, the compressor was bypassed, and gas flow into the SOXE wa instead controlled directly using a mass flow controller. This ensured a constant mass flow rate of 21.9 g/hr through the system, as flow from the compressor is dependent on the compressor volumetric efficiency, which is directly affected by the compressor outlet pressure. As the pressure was constantly changing in this experiment, the compressor-driven mass flow rate would also change for a given rotational speed setpoint for each pressure step. This is discussed in further detail in Chapter 4. As the Nernst potentials are affected by the partial pressures of each gas, changes in mass flow rate would result in changing Nernst potentials for a fixed oxygen production rate. Therefore, the direct-feed configuration was implemented to ensure that mass flow rate remained a controlled parameter.

This experiment was initially designed with a flow rate of 75 g/hr, as a higher flow rate is beneficial to the goals of this experiment. A higher flow rate enables a higher operating voltage; the SOXE must operate below a utilization of 0.90 to prevent the generation of carbon through the Boudouard reaction, which is when a gas rich in CO disproportionates into C and CO_2 (Hecht et al., 2021). At higher flow rates, a higher voltage can be applied without increasing the utilization, therefore increasing oxygen production. Due to this advantage, a full-scale system will likely operate at both high throughput and high voltage, so this experiment was initially designed to operate under the same conditions. However, when conducting commissioning tests for this experiment, it was discovered that even with the cathode exhaust pressure (P4) being brought down to near-vacuum conditions at 75 g/hr, the pressure immediately upstream of the cathode (P3) remained well above 100 mbar. As the cathode flow field pressure is closer to P3 than P4, this indicates that the true cathode pressure was not controllable down to near-vacuum conditions at high flow rates. This is due to the small geometry of flow channels within the SOXE stack, heat exchangers, and inlet and exit plenums, which function as flow restrictions preventing the further decrease of cathode pressure without decreasing the flow rate. With the cathode BPR commanded to 0 mbar (fully open position), the flow rate through the system was

repeatedly stepped down to measure the effect of flow rate on pressures throughout the system. This is shown below in Table 2.2.

Table 2.2: Low Pressure Flow Rate Sweep

Flow Rate (g/hr)	**P2 (mbar)**	**P3 (mbar)**	**P4 (mbar)**	**BPR reading (mbar)**
78.7	356	311	52.4	24.7
69.9	328	289	48.3	22.3
62.5	302	268	43.7	20.2
53.9	272	244	39	17.7
46.4	244	221	35.5	15.2
38.9	215	198	31.3	13.3
30.2	181	169	26.2	10.8
21.9	149	141	22.1	8.6
15.1	114	109	16.9	6.3
6.4	64.5	64.5	11.3	3.6

As seen above, decreased flow rates correspond to decreased pressures throughout the flow path, as expected. Based on these results, a flow rate of 21.9 g/hr was chosen as it was sufficiently high to ensure that the system can operate at current densities and utilization factors typical of both MOXIE and planned future systems. In addition, it is sufficiently low that the lowest achievable pressure is not as constrained as it would be at higher flow rates. At this low flow rate, the difference between the controllable cathode pressure and what would be observed using the VFCDs was only about 150 mbar, which led to an increase in the Nernst potential for carbon deposition by about 40 mV. As this is within the range of uncertainty in the stack cell voltages, it was determined that the planned second experiment to operate at a high utilization would introduce more risk than reward. At such high utilizations, this uncertainty may have resulted in accidental carbon deposition, which would increase degradation in the stack and affect further experiments. Therefore, no test was conducted to demonstrate the higher utilization, and the results of the conducted experiment

were instead used to analytically predict the additional safe utilization that could be achieved at low cathode pressures. This is discussed in further detail in Section 2.4.2.

As listed in Table 2.1, the direct-feed gas includes CO in the mixture to prevent oxidation of the cathode, as there is no recirculation flow as discussed in Section 1.2 with the compressor disconnected from the flow path. In addition, the VFCDs on the cathode and anode outlets were replaced with back pressure regulators to provide direct control of the cathode and anode outlet pressures, and therefore the pressures within the cathode and anode plenums themselves. As the VFCDs have a fixed flow resistance, cathode and anode pressures in the standard FlatSat configuration are dependent on the flow rates through each plenum. As this experiment was designed to control the cathode and anode pressures, replacing the VFCDs with back pressure regulators allowed independent pressure control.

Figure 2-6 and Figure 2-7 show the cathode pressure and voltage setpoints for this test. The initial segment of the run (until approximately 120 minutes) was when the SOXE is heating to the commanded setpoints of 838.8 K and 836.9 K for the top and bottom stacks respectively. The cathode pressures were chosen to cover both the range of standard MOXIE operating pressures as well as a range of low pressures so that SOXE performance can be compared across a wide range of pressures. In addition, these steps provide redundancy for prior experiments in this area as well as provide data points at a fine resolution at pressures below what was reached in prior experimentation. The voltage setpoints for the top and bottom stacks were calculated using a "target current" methodology: voltages were selected for planned currents of 0.7, 0.8, 0.9, 1.0, 1.1, and 1.2A for each respective step in the I-V sweep. These steps correspond to utilizations of 0.30 to 0.50, which is the typical utilization range for MOXIE. This ensures that the main variable in these tests is the cathode pressure, rather than the cathode pressure as well as utilization and current density. The 0.7A steps were 3 minutes long to allow the new cathode pressure to stabilize, and the remaining steps were all 1 minute long. The first 0.7A step was 20 minutes long to allow for thermal equilibration in the SOXE. By having an estimated current for each voltage setpoint, changes in current due to increases in iASR could be easily

observed during the test. The experiment was designed to command voltages rather than currents as a commanded current may increase the risk for carbon deposition if there was an iASR increase during the run. For example, if a current of 1.2A was commanded, and the stack iASR increased due to the concentration overpotential, the current through the stack would decrease. The voltage would then be increased through the control loop in the FlatSat electronics to try to reach the commanded current, which may then result in a commanded voltage higher than the Nernst potential for CO reduction. If the voltage was commanded, however, an increase in iASR would then result in a decrease in current for a fixed voltage, which would not endanger the stack as the Nernst potential for CO reduction would increase due to the decreased partial pressure of CO at a lower current (see Equation (2.2)). Several additional I-V sweeps were included for margin in the run, to enable fine-resolution bracketing of the minimum operating pressure. For example, if this limit was identified at an operating pressure of 50 mbar, but was not reached at an operating pressure of 60 mbar, the cathode pressure could be set to various pressures between 50 and 60 mbar in order to identify the actual pressure at which the limit was reached.

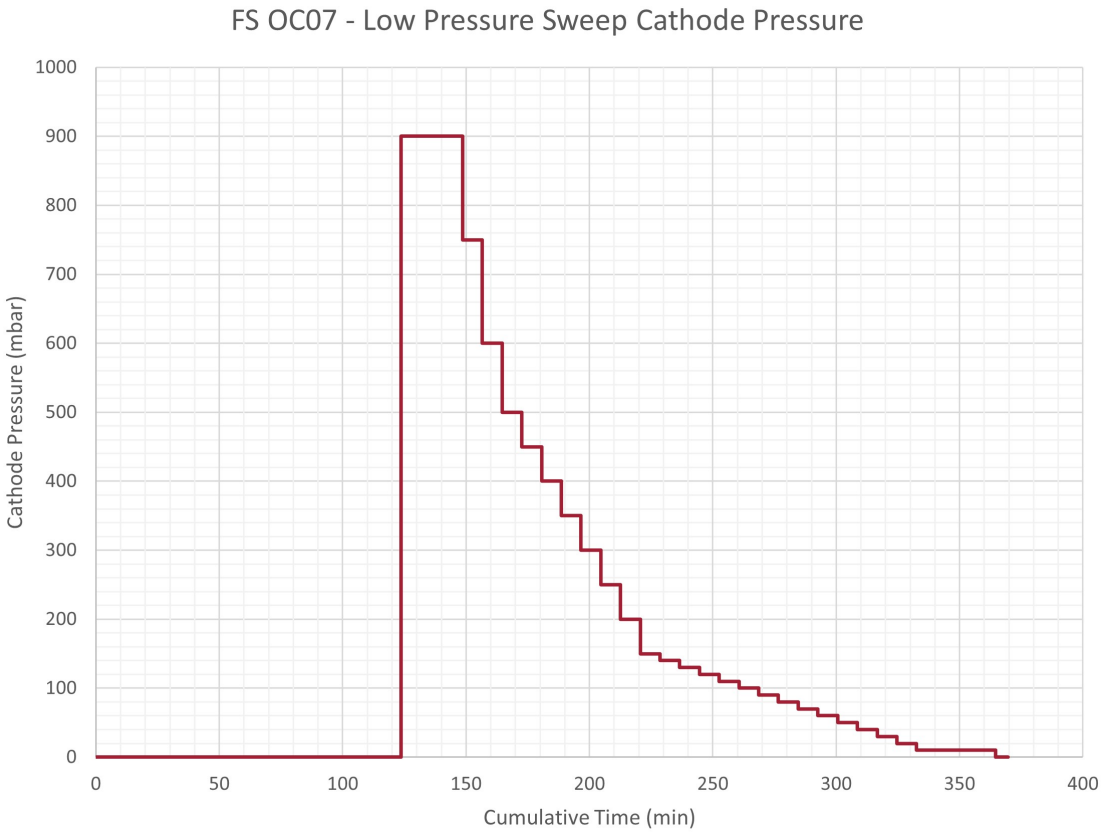

Figure 2-6: Planned cathode pressures for repeated I-V sweeps at low pressures.

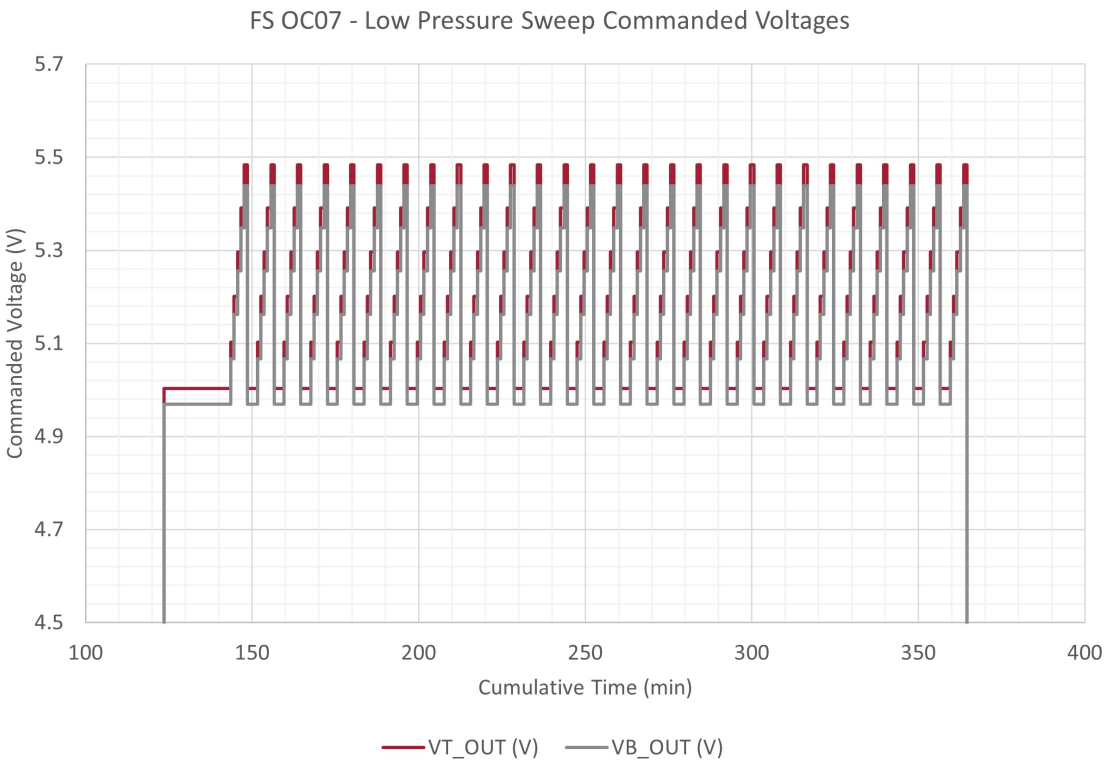

Figure 2-7: Commanded voltages for repeated I-V sweeps at low pressures.

The following run procedure was developed to identify the minimum operating pressure while maintaining SOXE safety.

1. During the 3 minute 0.7A target current step at the beginning of each pressure setpoint, monitor and make note of the stack currents (IT and IB).

2. Compare the measured currents to the measured currents at the previous cathode pressure setpoint.

3. If both currents are within 0.1 A of the previously measured current, allow the I-V sweep to proceed. Previous FlatSat experiments have showed changes in current up to 0.1A for identical voltage setpoints due to thermal equilibration in the stack, so this amount of change is within standard operating parameters.

4. If either current is lower than the previously measured current by more than

0.1 A, or if the current decreases by more than 0.1A during the 3 minute dwell, increase the pressure setpoint back to the previous setpoint after the I-V sweep has completed. This indicates an increase in iASR due to a rising concentration overpotential.

5. Compare measured currents at this setpoint to previous measurements taken at same setpoint, to ensure that no permanent damage has occurred to stack. If current is lower than previously measured current by more than 0.1 A, abort the run as this indicates a permanent increase in iASR.

6. If no change seen in current compared to previous step at same pressure, decrease cathode pressure by 1 mbar and repeat steps 1 through 5 until the minimum pressure has been identified.

7. If time allows, decrease the cathode pressure below the identified minimum operating pressure in steps of 5-10 mbar, completing the I-V sweep at each step. This allows for qualitative and quantitative characterization of how the concentration overpotential affects iASR beyond the "minimum" operating pressure threshold.

Through this experiment, the minimum operating pressure of the FlatSat could be characterized. The results and conclusions from the above experiment are discussed in the following section.

2.4 Results and Conclusions

2.4.1 Low Pressure Experimental Results

The above experiment was conducted on the FlatSat in February 2023; as it was the seventh cycle on the FlatSat SOXE, this run was labeled FS OC07. Using the hardware described in Table 2.1, the cathode BPR was set to the setpoints shown in Figure 2-6. While the BPR controlled pressure downstream of the cathode exhaust, the actual pressure in the cathode flow field is higher than this controlled value due

to pressure drops across the SOXE and other flow restrictions between the cathode and cathode exhaust, including heat exchangers and small-diameter exit plenums. Therefore, the readings of the P3 and P4 sensors, shown in Figure 1-5 and Figure 1-6, were averaged to estimate the actual pressure in the cathode flow field. The calculated cathode pressure is shown below in Figure 2-8.

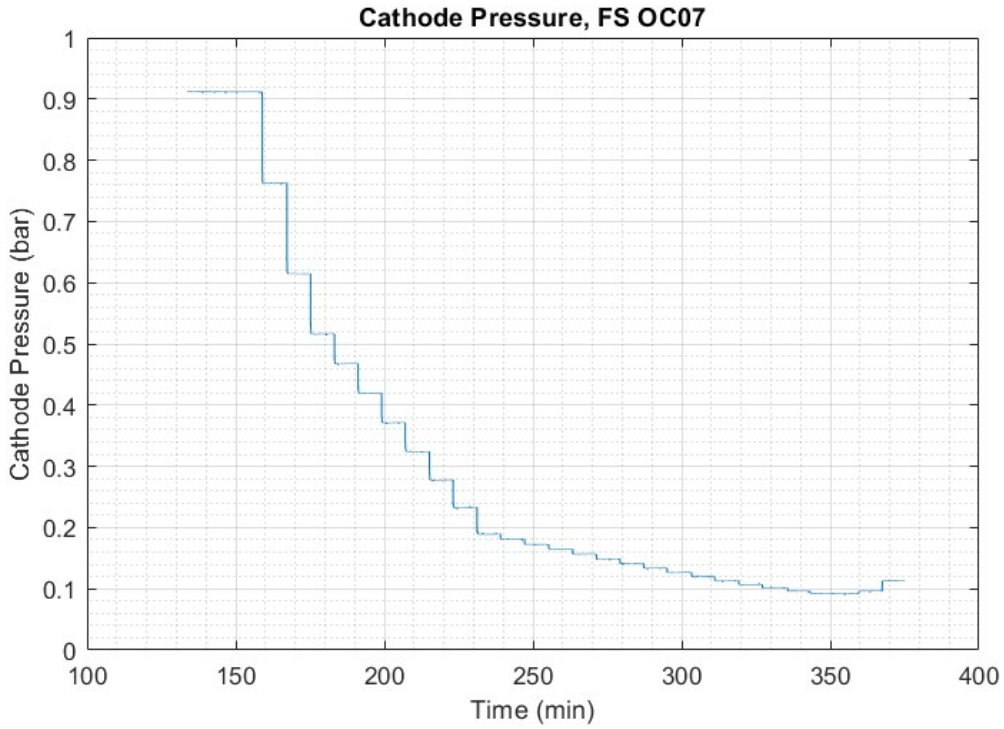

Figure 2-8: Estimated FSOC07 cathode pressures.

As seen in Figure 2-8, the achievable cathode pressure was higher than the BPR steps due to the limitations in P3 reduction seen in Table 2.2; for a BPR setpoint of 10 mbar, a cathode pressure of approximately 90 mbar was reached. The stack currents corresponding to the voltage setpoints shown in Figure 2-7 are shown below in Figure 2-9.

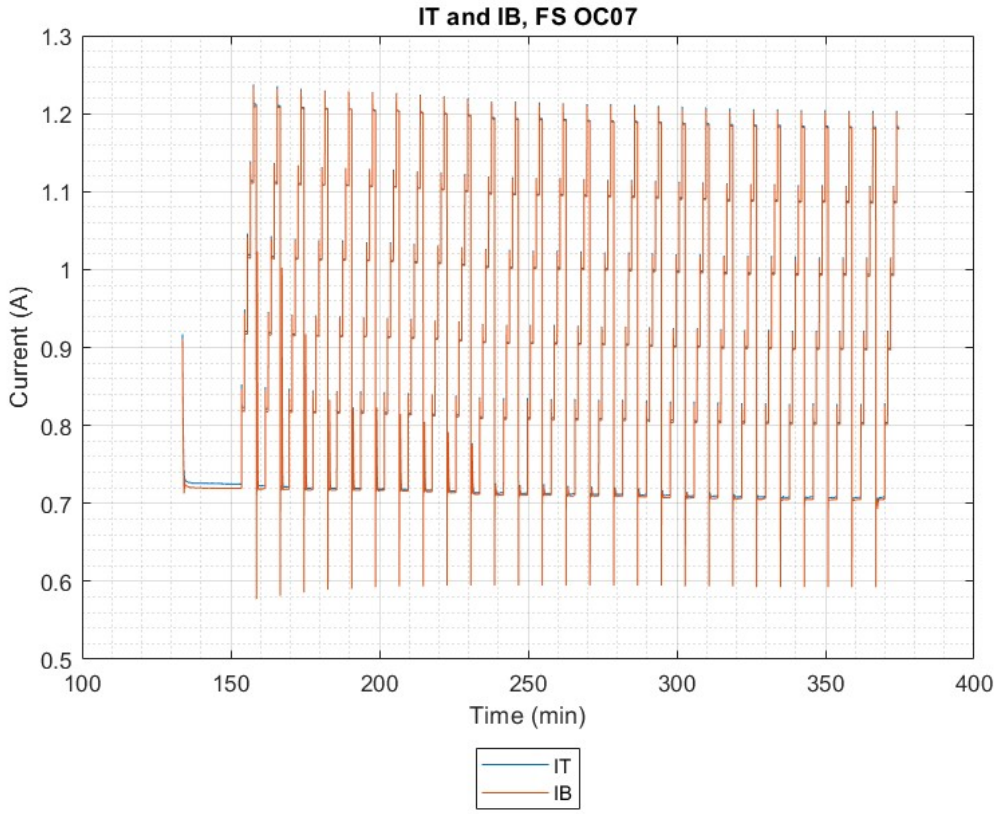

Figure 2-9: Measured top and bottom stack currents for FS OC07. The voltage setpoints were designed with target currents of 0.7, 0.8, 0.9, 1.0, 1.1, and 1.2 A.

As seen in Figure 2-9, both the top and bottom stack currents were within 5% of the target currents for all run segments. However, it is clear when examining both the top and bottom stack currents that they decrease steadily over the course of the run for an identical series of voltage setpoints, by about 2% over the course of the 4 hours of oxygen production. When examining the data, it was observed that the decrease in current did not occur during the high voltage setpoints, which would indicate carbon deposition due to high cell voltages exceeding the Nernst potential for CO reduction, but rather at the low voltage steps where the cathode pressure was changed. However, to ensure that the decrease in current was not due to an increase in cell iASR due to carbon deposition, the Nernst potential for CO reduction was

calculated for each step in the run and compared to the average cell voltage for both the top and bottom stacks. This is shown in Figure 2-10.

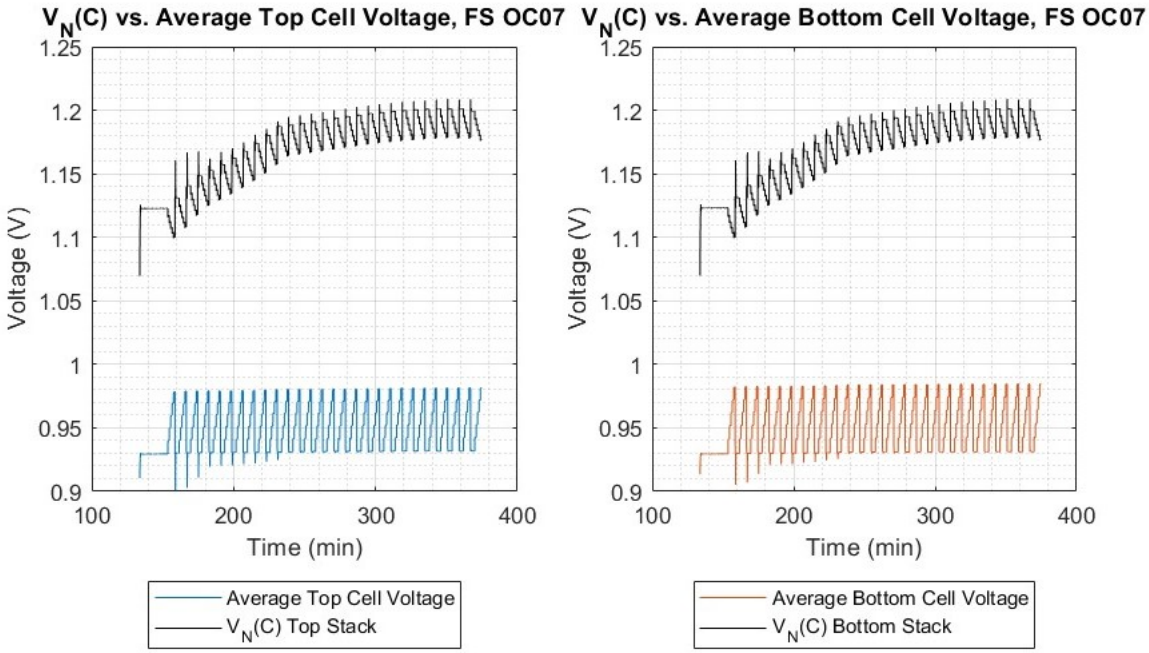

Figure 2-10: Measured top and bottom stack currents for FS OC07. The voltage setpoints were designed with target currents of 0.7, 0.8, 0.9, 1.0, 1.1, and 1.2 A.

As seen in Figure 2-10, there was significant margin between the average cell voltage and the Nernst potential for CO reduction for both stacks throughout FS OC07, ranging from over 120 mV at the highest cathode pressure and voltage setpoint to approximately 200 mV at the highest voltage at the lowest cathode pressure. As the voltage spread among the cells in the stack has been measured to be less than 50 mV, which is significantly lower than the Nernst potential margin in this run, it is extremely unlikely that the Nernst potential for CO reduction was exceeded and that carbon deposition was the underlying cause behind the decrease in current (Hecht et al., 2021). Therefore, especially because the decrease in current was observed when the cathode pressure was decreased, this data suggests that the decrease in current was due to an increase in iASR as the cathode pressure was lowered.

The iASR was then calculated for both the top and bottom stacks using Equa-

tion (2.5). The iASR is plotted below as a function of time in Figure 2-11 and as a function of cathode pressure in Figure 2-12. As the iASR varies slightly at different voltage setpoints due to changes in the concentrations of the component gases in Equation (2.1) and changes in the stack temperature, the median iASR value at each pressure step was used in Figure 2-12.

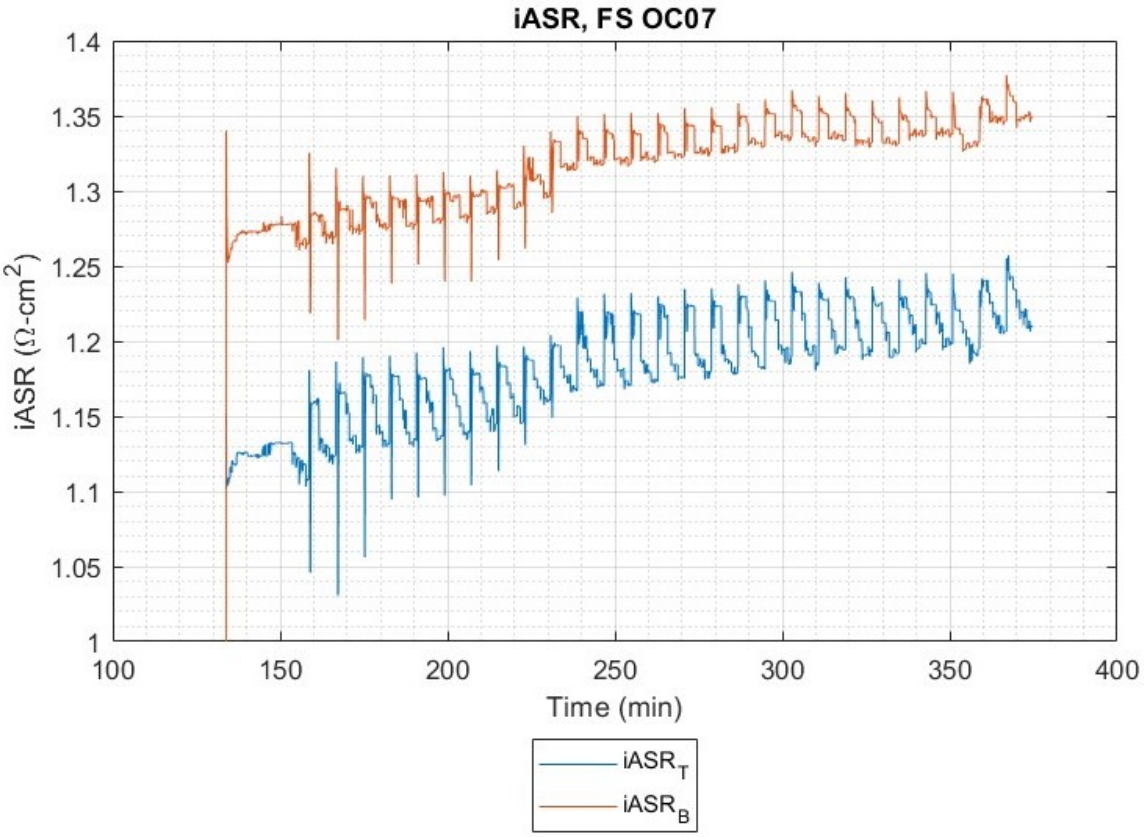

Figure 2-11: Top and bottom stack iASR for the duration of oxygen production in FS OC07.

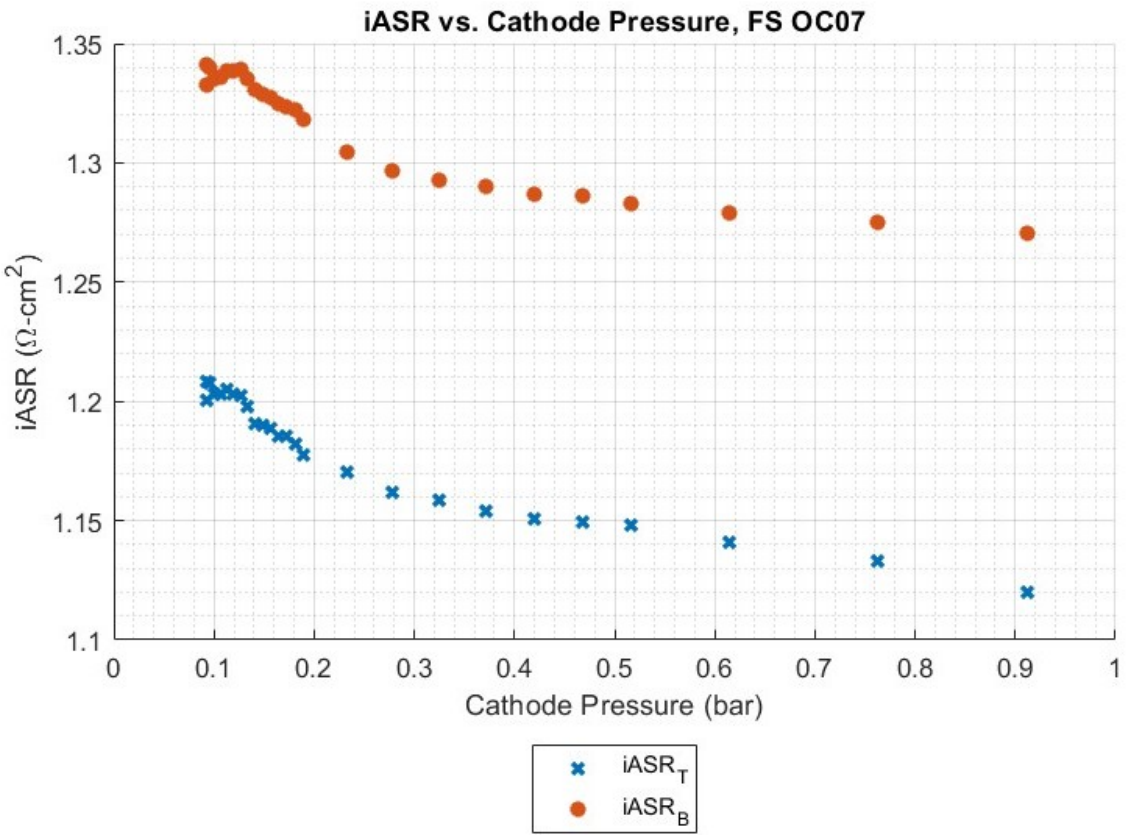

Figure 2-12: Top and bottom stack iASR plotted as a function of cathode pressure for FS OC07.

The trends in iASR seen in Figure 2-12 show a small initial increase in iASR as pressure is decreased, followed by a sharper rise in iASR below cathode pressures of approximately 250 mbar. The general trend of this curve is similar to the influence of the activation and concentration overpotentials seen in Figure 2-2. This suggests that as the cathode pressure is decreased, the physical resistance to diffusion across the electrolyte (e.g. the concentration overpotential) as well as the chemical resistance to the electrolysis reaction at the anode and cathode (e.g. the activation overpotential) both increase, resulting in a higher overall cell resistance. However, the rise in iASR appears to plateau at cathode pressures of approximately 120 mbar. While an interesting observation, this may be due to the large concentration of data points near this cathode pressure, which may give the impression of a leveling off in iASR because

there are many points around this pressure and no data at low pressures. Regardless, it can be seen that decreasing the cathode pressure for a fixed I-V sweep increases the SOXE iASR, resulting in a decrease in current and therefore oxygen production for a fixed voltage. The iASR increases by approximately 7% as the cathode pressure is decreased from 900 mbar to 100 mbar; this shows that a pressure at which the rising concentration overpotential would prevent or severely inhibit oxygen production was not reached. In other words, this study demonstrated that oxygen production is possible at cathode pressures as low as 92 mbar, which was the minimum pressure reached in this test. However, the increase in iASR shows that as the cathode pressure is decreased, the resulting current for a fixed voltage step decreases. Therefore, to reach the same current (and therefore utilization) at that cathode pressure, the voltage must be increased, which would bring the cell voltages closer to the Nernst potential for CO reduction. Therefore, while operating at lower cathode pressures does increase the operating voltage and therefore utilization that is possible without carbon deposition, the required voltage to reach that utilization would increase as cathode pressure decreases. This indicates that there may be an optimal cathode pressure for maximum oxygen production, where the effects of the increase in achievable utilization and increase in required voltage to reach that utilization for a fixed voltage reach a local maximum for oxygen production. The optimization study conducted to identify if such a local maximum exists is discussed in the following section.

2.4.2 Optimization for Ideal Operating Pressure

After FS OC07 was run in the laboratory, it became necessary determine if an optimal operating pressure exists to maximize oxygen production accounting for the effect of cathode pressure on both iASR and the Nernst potential for CO reduction. As discussed in Section 2.1, operating at as low of a pressure as possible is advantageous for compressor power. However, as seen in the FS OC07 results, decreasing the cathode pressure increases the SOXE iASR, which adversely impacts oxygen production as more power is needed to reach a certain utilization and the voltage margin at that uti-

lization decreases. That being said, decreasing the cathode pressure inherently raises the Nernst potential for CO reduction, increasing the voltage margin. Therefore, a study was conducted to identify if an operating pressure exists where the possible oxygen production without carbon deposition reaches a local maximum.

In this study, a flow rate of 55 g/hr was assumed, as this is a flow rate typical of the MOXIE FM reference segment. However, this study assumed an independently controllable cathode pressure, which was implemented on the FlatSat for FS OC07 and will likely be a feature of next-generation Mars-based oxygen production systems, even though it is not possible on the MOXIE FM. In addition, while FS OC07 used a direct feed of mixed CO and CO_2, this study assumed that the incoming flow has the composition of the Martian atmosphere, which is approximately 95.5% CO_2 by mole fraction. In addition, this study assumed recirculation from the cathode exhaust back to the compressor of 5.83% of the cathode exhaust gas, which is how the FM flow path is configured (Hecht et al., 2021). The anode pressure was held fixed at 0.5 bar, which is the same configuration used in FS OC07, and the cathode pressure was stepped down following the steps in FS OC07. The SOXE temperature was set to 811.4 °C, which was the temperature read by the SOXE mid-plate auxiliary thermocouple during FS OC07. The assumption of SOXE temperature is key because stack iASR is temperature-dependent, so keeping the same temperature as FS OC07 allows the calculated iASR values from the run to be used in the study.

The optimization study used the top and bottom stack currents as the objectives to be maximized, as oxygen production is directly proportional to current. A constraint was imposed to limit the average cell voltage to values more than 0.05 V below the Nernst potential for CO reduction, as this 50 mV margin is greater than the spread of cell voltages on all SOXE assemblies used in the MOXIE program. By limiting the average cell voltage, CO_2 utilization was limited to only values that would not introduce a risk of carbon deposition, therefore bounding the optimization within the constraints used when designing MOXIE runs.

At each cathode pressure from FS OC07, the stack iASRs were assumed equal to the FS OC07 values at those pressures. Then, using Equation (2.2), Equation (2.1),

and Equation (2.5), along with the relationship between current, O_2 production, and the resulting CO production rates discussed in Section 1.2, the maximum current that could be achieved with the constraints discussed earlier was calculated for each pressure step. The resulting currents are shown below in Figure 2-13, along with the corresponding utilization at those currents and the selected flow rate in Figure 2-14.

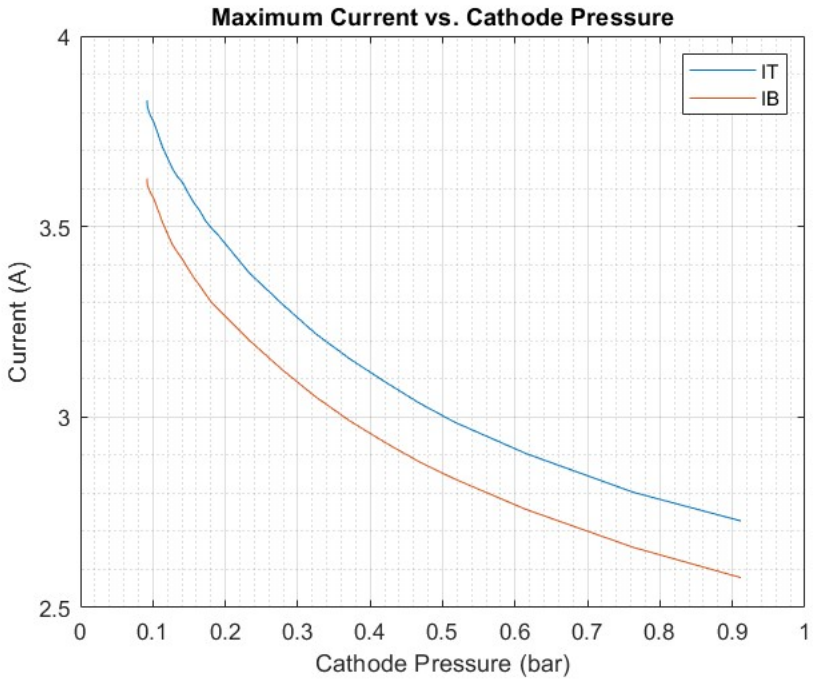

Figure 2-13: Maximum safe current as a function of cathode pressure.

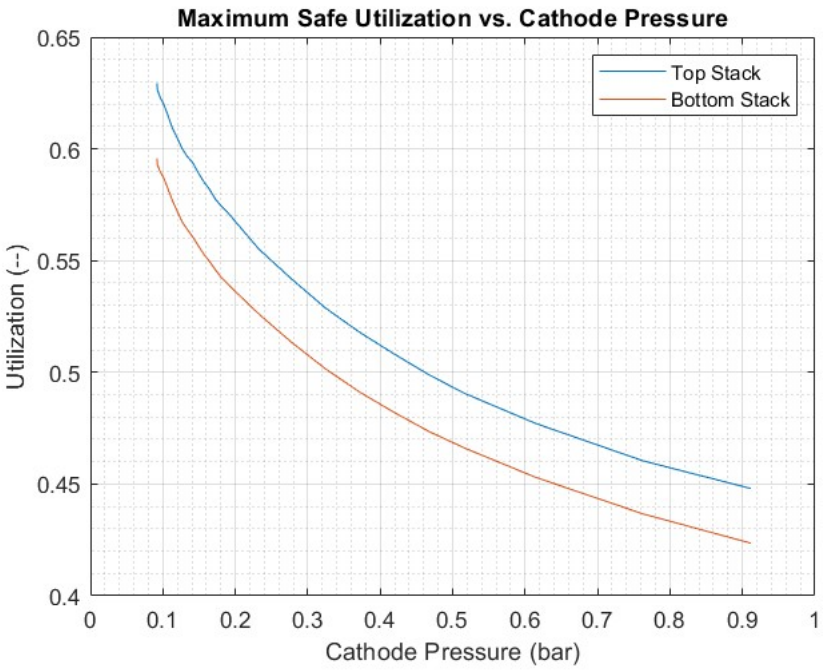

Figure 2-14: Utilizations corresponding to maximum safe currents as cathode pressure is decreased.

As seen in Figure 2-13, there is no local maximum current as cathode pressure decreases - this shows that the higher safe utilizations at decreased cathode pressures due to the increase in the Nernst potential for CO reduction have a greater effect on achievable current than the increase in stack iASR. Therefore, even though iASR increases due to the activation and concentration overpotentials as cathode pressure is decreased, minimizing the cathode pressure still maximizes safe utilization and therefore oxygen production in MOXIE-derived systems.

To quantify the effect of the iASR increase on the utilization, the oxygen production rate at the above currents was plotted against the achievable oxygen production rates if the iASR remained fixed as a function of cathode pressure. This is shown in Figure 2-15.

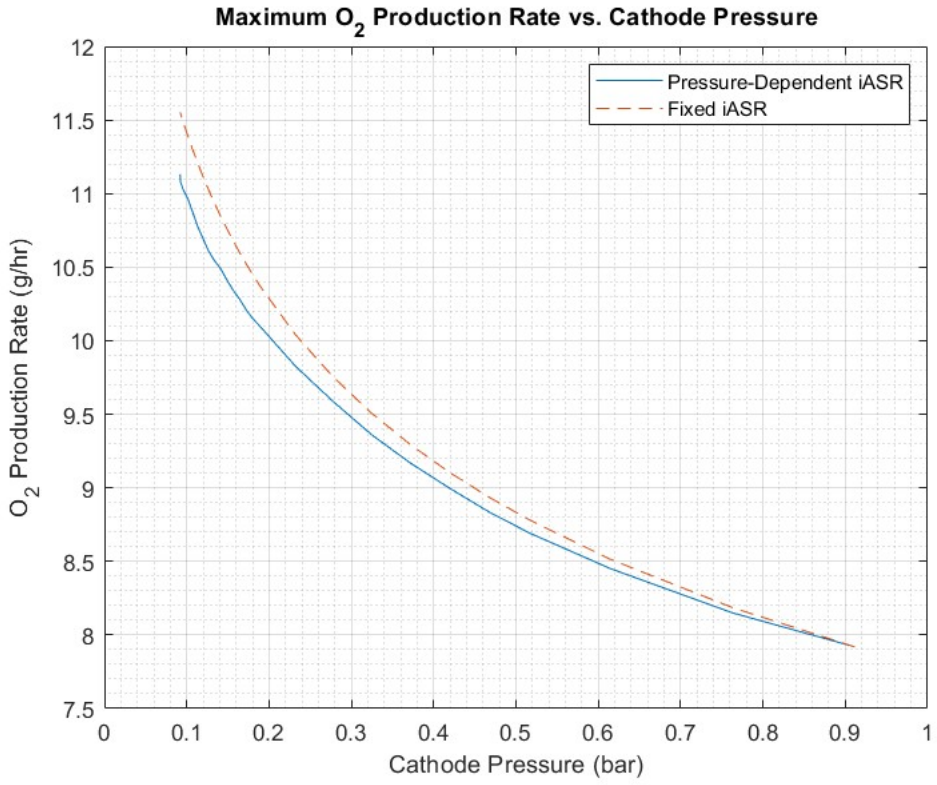

Figure 2-15: Achievable oxygen production rate accounting for iASR increase compared to oxygen production rate at a fixed iASR.

As seen in Figure 2-15, the increase in iASR as cathode pressure is decreased does have an observable effect on the achievable O_2 production rate. Specifically, the change in iASR from cathode pressures of 900 to 92 mbar caused a decrease in the achievable O_2 production rate by approximately 4%, whereas the increase in iASR itself over this cathode pressure range seen in Figure 2-12 was approximately 8%. This indicates that while the increase in iASR did decrease the achievable O_2 production, the increase in V_N (C) over this same range has a greater net effect on oxygen production. However, if the iASR were to increase by a greater amount, this would not be the case, and a local optimum would exist. This would be the case if the concentration overpotential became the limiting factor to operations at lower pressures than those achieved in this test. Under those conditions, the iASR would likely increase exponentially, and the achievable O_2 production would decrease as

pressure was decreased. However, this experiment demonstrated that decreasing the cathode pressure as low as 92 mbar has a net positive benefit on the achievable oxygen production without carbon deposition.

2.4.3 Low Pressure Operations Conclusions

Operating a Mars-based SOE system at low pressure offers several advantages. First, operating at a lower cathode pressure reduces power and energy consumption by the the compressor, therefore reducing the total energy usage of the system. In addition, reducing the cathode pressure increases the Nernst potential for CO reduction without changing the Nernst potential for CO_2 reduction. This increases the utilization that the system can operate at, as it can run at higher voltages and currents (and therefore produce more oxygen) without increasing the risk of degradative carbon deposition. However, the increase in concentration and activation overpotentials at low pressures may place a limit on how low of a pressure such systems can operate at; as there is little prior work focused on characterizing SOE oxygen production systems at low pressures, additional experimentation in this area was necessary.

The FlatSat, which allows the replacement of VFCDs on the cathode and anode exhausts with back pressure regulators, was a testbed suited for these characterization efforts, as it allowed for independent control of cathode pressure that was not possible on the MOXIE FM. The results of this experiment, which consisted of repeated I-V sweeps at decreasing cathode pressures, demonstrated that the MOXIE system and its underlying electrolysis technology can be operated at pressures as low as 92 mbar to produce oxygen. This investigation found that in the MOXIE system, the limiting factor for how low of a cathode pressure could be achieved was flow restrictions within the internal flow path of the system. Namely, small-diameter flow restrictions within the SOXE channels, heat exchangers before and after the SOXE, and exit plenum prevented a decrease in cathode pressure without also decreasing the flow rate of the system. This indicates that for a full-scale system, the flow path must be carefully designed to limit areas of flow restriction so that the cathode pressure can be independently controlled.

At a flow rate of 21.9 g/hr, oxygen production was demonstrated from cathode pressures of 900 mbar down to 92 mbar. As the cathode pressure was decreased, a decrease in current was observed, corresponding to an increase in iASR within the SOXE. Due to the large margin between the SOXE cell voltages and the Nernst potential for CO reduction, this increase in iASR is unlikely to have been caused by carbon deposition, and is therefore likely related to the cathode pressure, specifically the rising overpotentials as the pressure was decreased. The system iASR increased by about 8% during this run, which was also the longest duration of oxygen production ever achieved on any of the MOXIE systems; the iASR increased more sharply at lower pressures than at high pressures. Due to the rising iASR, an optimization study was required to determine the combined quantitative effect of the iASR and increased Nernst potential margin, which are opposing forces driving the utilization that the system can achieve, on the achievable oxygen production rate. This study found that, while the iASR did reduce the maximum utilization that could be achieved at low pressures, the optimal pressure to maximize oxygen production was still at the lowest pressure reached in this test, 92 mbar. This indicates that at the pressures examined in this experiment, the increased margin in the voltage that the cells can operate at has a stronger effect than the corresponding increase in iASR as cathode pressure is decreased. Therefore, from an electrolysis perspective, future Martian oxygen production systems should operate at as low of a pressure as possible, as these operating conditions will maximize the oxygen production rate that can be achieved for a given inlet mass flow rate.

Chapter 3

FlatSat Compressor Power Characterization

3.1 Motivation

As FM energy usage on Mars is limited by the Mars 2020 mission constraints, predicting the power draw of all MOXIE components is a critical step in optimizing planned operations on Mars. The Multi-Mission Radioisotope Thermoelectric Generator (MMRTG) onboard the Perseverance Rover generates about 110 W of electric power, and the rover batteries can store up to approximately 1000 W-hrs. As the desired battery charge level is between 40% and 80%, and the MMRTG continues to generate power during MOXIE's operations, energy usage on the FM is limited to approximately 1000 W-hrs. This includes power consumed by the Primary Bus MAIN, which powers all electronics, sensors, and the compressor, as well as power provided to the rover to support its battle short configuration, and the Primary Bus SOXE, which drives the SOXE Heaters and Electrolysis Stack (Hecht et al., 2021). Therefore, in order to maximize the available power for electrolysis and oxygen generation, it is desirable to both minimize the compressor power dissipation (assuming a fixed power draw for electronics) as well as accurately predict compressor power so that all remaining energy can be used for electrolysis. The below figures show the various power draws and energy usages for MOXIE's eleventh oxygen-producing run

(FM OC19) on Mars - data is smoothed using a moving average filter with a span of 10 seconds to eliminate noise in the signals (MOXIE Team, 2022b).

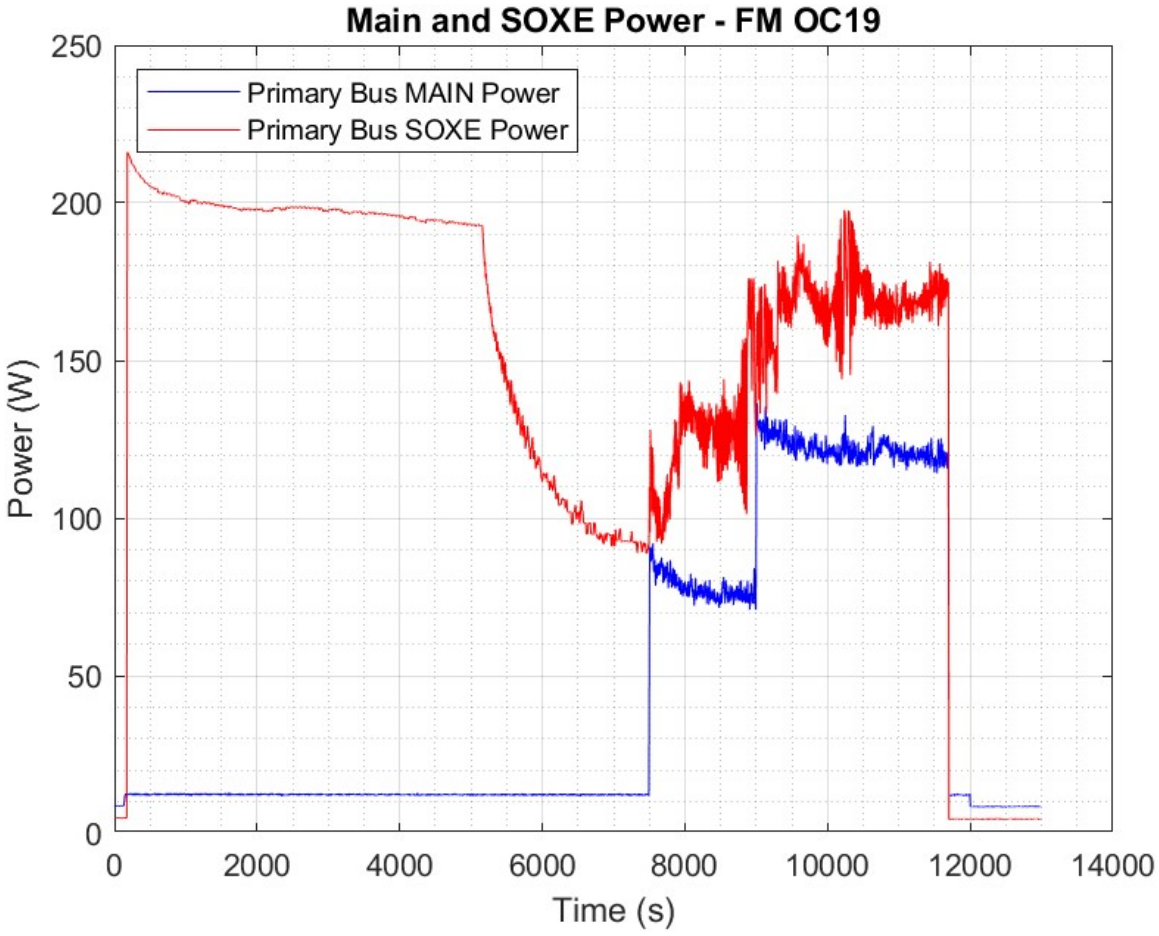

Figure 3-1: FM OC19 Primary Bus MAIN and Primary Bus SOXE Power.

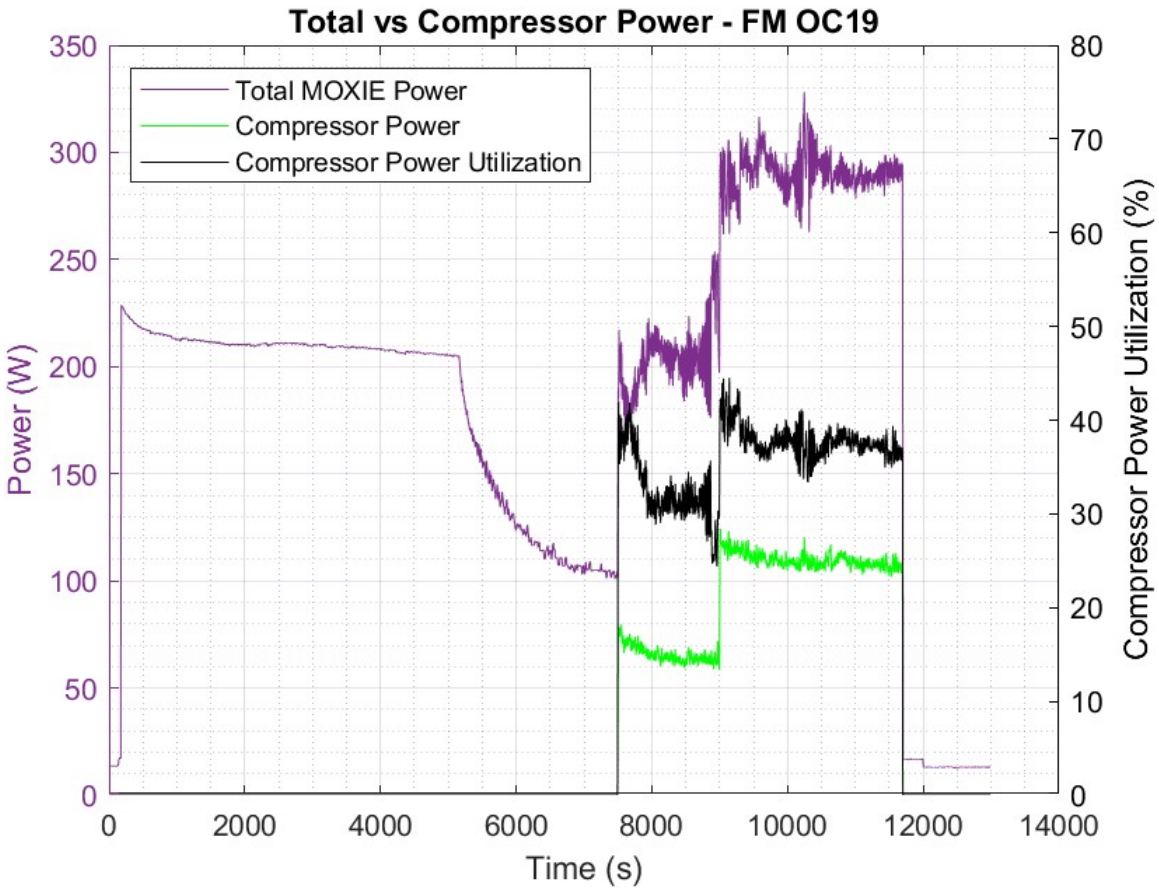

Figure 3-2: FM OC19 Total vs. Compressor Instantaneous Power.

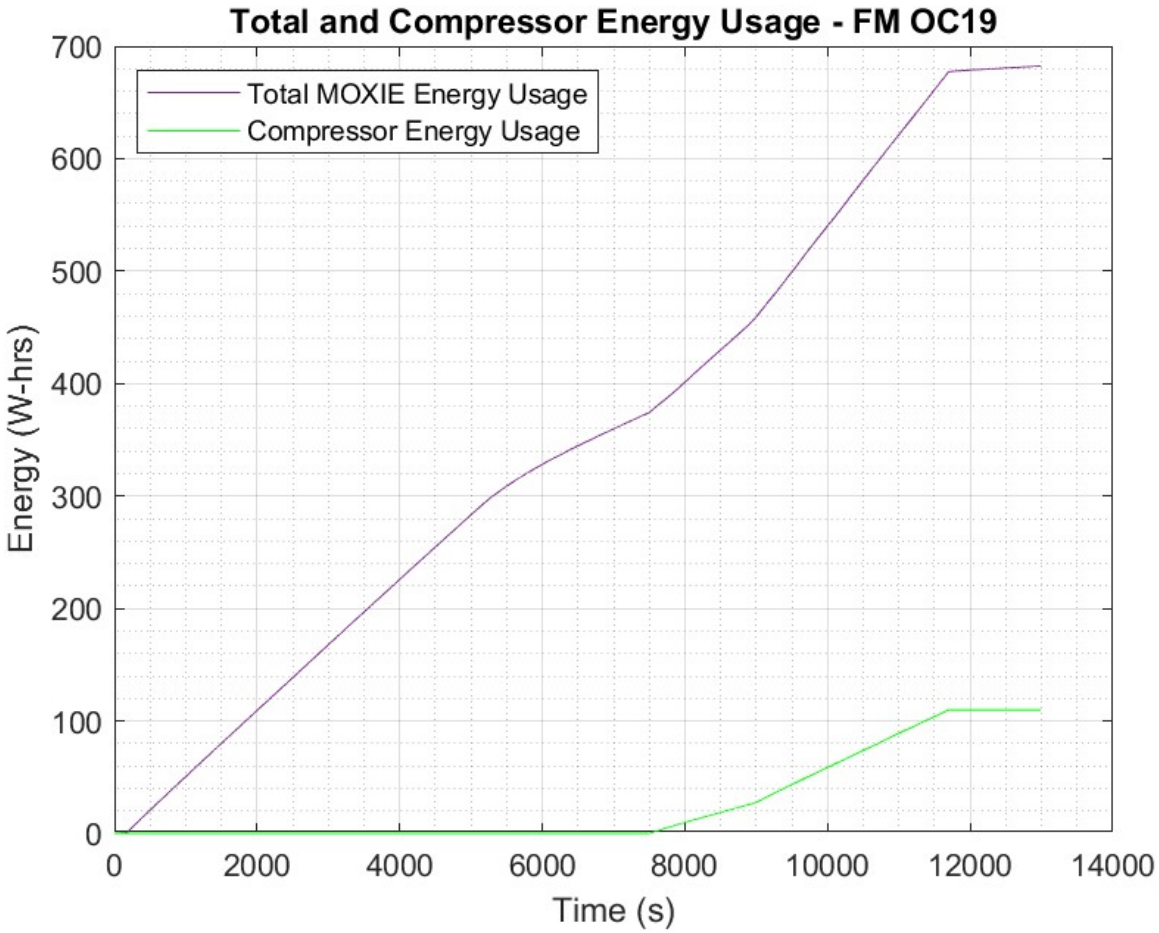

Figure 3-3: FM OC19 Total vs. Compressor Energy Usage.

As seen when comparing Figure 3-1 and Figure 3-2, the bulk of the Primary Bus MAIN Power is required for the compressor, which turns on approximately 7500 seconds into the run. The Primary Bus SOXE Power is greater for the duration of the run due to the power required to operate the SOXE Heaters. For approximately the first 7500 seconds of the run, only the SOXE Heaters and various MOXIE electronics were powered. However, once the compressor turns on, it is responsible for upwards of 40% of the instantaneous power draw of the FM, which is seen in Figure 3-2. Ultimately, for a standard MOXIE run such as FM OC19, over 15% of the total energy usage is due to the operation of the compressor, which is shown in Figure 3-3 - this is a significant amount of energy that is not being used for electrolysis, so developing

accurate predictions of this energy usage and determining how to minimize it is important for MOXIE operations. Prior work done by a member of the MOXIE team identified that a scroll compressor, similar to the type used on MOXIE, would be the best carbon dioxide acquisition system for a full-scale equivalent oxygen production plant, due to its high adiabatic efficiency, demonstrated performance, and simple design, which reduces cost and increases reliability (Hinterman, 2022). Although design modifications such as staging compressors, which would increase the compression ratio achieved within the compressor scrolls themselves, would reduce the energy usage seen in MOXIE operations, empirically determining operating conditions to minimize compression power and energy usage is critical for a full-scale system, where maximizing electrolysis power is desired.

The stepped power draw seen at approximately 9000 seconds in Figure 3-2 is due to an increase in the compressor rotational speed - this, along with other factors discussed below, drive the compressor power dissipation. As discussed in Chapter 1, the compressors used on all MOXIE models are scroll compressors, which take in a fixed volume of gas, 30.1 cm^3, with each rotation and compress it to a smaller fixed volume, 5.19 cm^3. The compressed gas is then fed into a downstream plenum of a fixed size. The energy cost of this compression is proportional to the ΔP between the compressor inlet and outlet, which is in turn dependent on the density of the gas entering the compressor, the compressor rotation rate, and the flow resistance of the downstream plenum (Hecht et al., 2021).Therefore, as discussed briefly in Chapter 2, operating at a low cathode pressure would greatly reduce the thermodynamic power needed for compression, without requiring a decrease in the rotational speed and therefore mass flow rate into the system. The total power dissipated by the compressor is greater than just the thermodynamic power needed for compression - the remainder of the compressor power usage can be attributed to tip and bearing friction, as well as losses through the controller and compressor motor. As wear on the compressor tip seals would decrease friction and the resulting frictional power dissipation, extended operation of the scroll compressors may further decrease compressor power at the expense of decreased gas flow for a given compressor speed.

Therefore, characterizing compressor power dissipation as a function of inlet conditions, outlet conditions, and rotational speed will inform the planning of MOXIE runs on Mars in terms of energy usage, as well as identify operating conditions that would minimize compression thermodynamic power for a full-scale oxygen production plant on Mars. However, as described in Section 1.3, the FlatSat Qual compressor differs from the FM compressor - the differences between the two compressors have not been extensively quantified, so it remains uncertain how applicable the FlatSat compressor data is to the FM compressor. Characterizing the power dissipation of the FlatSat Qual compressor and comparing it to data from the FM will further increase the MOXIE team's understanding of the differences between the two units, and inform the applicability of FlatSat compressor data to the FM compressor. In addition, by examining the FM compressor power across completed runs on Mars, the decrease in power due to tip seal wear can be quantified and applied to understand component-level degradation for MOXIE, as well as to analyze and model long-duration operation of a future system.

3.2 Prior Work

The same supplier, Air Squared (AS), manufactured the compressors used on the FM, EM, and FlatSat, as well as a Flight Spare unit. Prior to delivery of the compressor units to the MOXIE team, AS conducted acceptance tests in 2018 in order to measure the power dissipation of the FM, EM, and Flight Spare units under various operating conditions. Documentation of these acceptance tests is sparse, and no such acceptance tests were conducted on the FlatSat Qual compressor. This necessitates the need for independent, controlled experimentation on the FlatSat compressor, which can be used with prior work as well as FM and EM run data in order to compare the compressors.

The AS acceptance tests consisted of the compressor being placed in a vacuum chamber under Mars pressure (several Torr) - gas from the chamber directly entered the inlet of the compressor. The exhaust from the compressor was fed to a Viscous

Flow Control Device (VFCD) with a flow resistance of 5,000 Lohms, which is a unit of fluid resistance invented by the Lee Company, who were responsible for manufacturing the orifices onboard the various MOXIE models (Rapp, 2022a). The below equation, used for Lohm flow resistance calculations, is defined such that 1 Lohm will flow 100 gallons per minute of water with a pressure drop of 25 psi at a temperature of 80°F (The Lee Company, 2022).

$$Lohms = \frac{100}{flow(gal/min\ H_2O\ @\ 25\ psid)} \tag{3.1}$$

The vacuum chamber could be set to any temperature between -55°C and 70°C. A high-level schematic of the AS acceptance test is shown below.

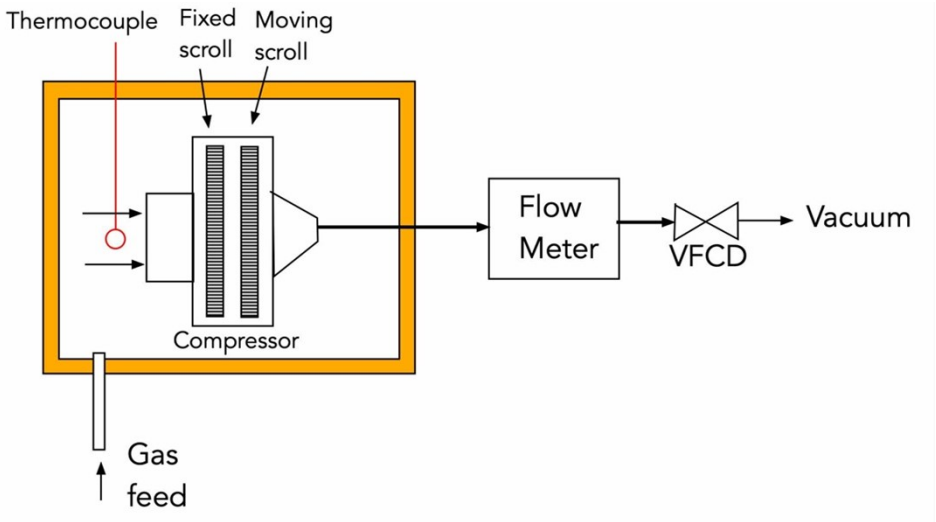

Figure 3-4: AS Acceptance Test Schematic (Rapp, 2022a).

The acceptance test setup seen in Figure 3-4 differs from the gas flow path on all MOXIE models, as the VFCDs on MOXIE result in a net flow resistance of 3,767 Lohms, compared to the 5,000 Lohms used by AS. In addition, the MOXIE system has additional internal flow resistances, as shown below in Figure 3-5.

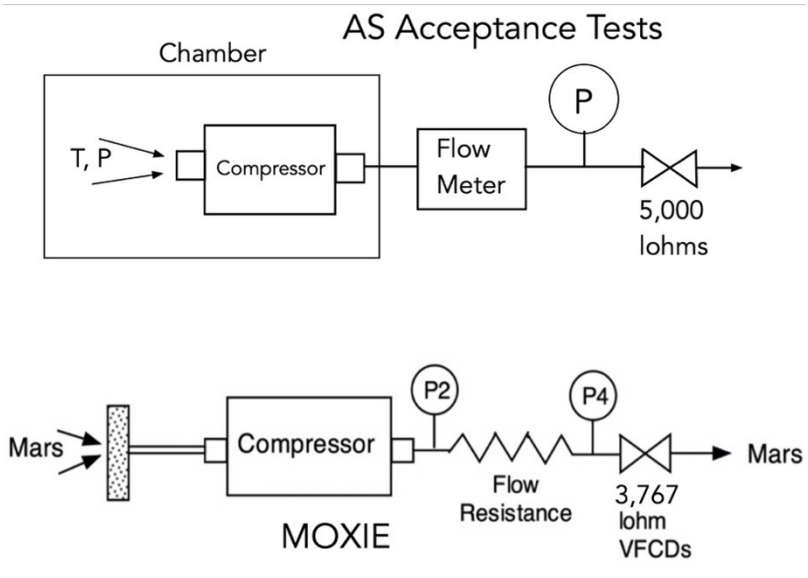

Figure 3-5: AS Acceptance Test vs. MOXIE Compressor Flow Path (Rapp, 2022a).

This results in a different exhaust pressure for MOXIE compressors vs. the AS compressor - as mentioned above, modifying the exhaust pressure affects the power required for thermodynamic compression, so the power measured in the AS acceptance tests is not directly applicable for a prediction of MOXIE compressor power. Nonetheless, AS conducted the following tests as a part of the acceptance test procedure (Rapp, 2022a):

1. "Nominal": These runs were conducted with inlet (chamber pressure) at 5 Torr and chamber temperature of 20°C, at three values of RPM: 2,500, 3,000 and 3,500. For the FM and FlatSat each run was repeated three times, while for the EM only a single run was conducted at each RPM.

2. "S-S Thermal": Two runs were conducted with inlet (chamber pressure) at 5 Torr, at 3,500 RPM. In one run, the chamber was at -55°C, and the other had a chamber temperature of 70°C.

3. "P-Sweep": Four runs were completed at 3,000 RPM and a chamber temperature of 20°C, with inlet pressure stepped at 4, 5, 6 and 7 Torr. This was repeated at 3,500 RPM, for a total of 8 runs.

4. “Extended”: Three runs were repeated at 3,500 RPM, with 5 Torr inlet pressure and 55°C inlet temperature.

5. “Thermal Cycle”: Four runs were completed at 3,500 RPM and an inlet pressure of 5 Torr, at inlet temperatures of 20, 55, -45 and then 20°C respectively.

For each run, a fixed voltage of 30.0 V was supplied to the compressor motor, and the current through the motor coils was measured in order to calculate the compressor power. As the AS test setup had a fixed flow resistance on the compressor exhaust, which resulted in an exhaust pressure proportional to the inlet gas density and compressor rotational speed, the power was instead plotted as a function of mass flow rate and compressor speed. By tracking the compressor power as a function of mass flow rate, the changes in inlet pressure and their resulting effect on power are accounted for; likewise, tracking the rotational speed accounts for the dependence of exhaust pressure on RPM. As discussed previously, both the mass flow and compressor rotational speed affect the energy usage by the compressor. An increased mass flow for a given rotational speed, i.e. when the inlet pressure is increased, requires greater power for thermodynamic compression. On the other hand, an increased rotational speed for a given mass flow, i.e. when the inlet pressure is decreased, results in a greater energy loss to friction. Therefore, plotting the compressor power as a function of both the mass flow and compressor speed allows for an analysis of compressor power usage due to both the thermodynamic compression power and losses due to friction. The results for the acceptance tests are shown below for the FM, EM, and Flight Spare compressors.

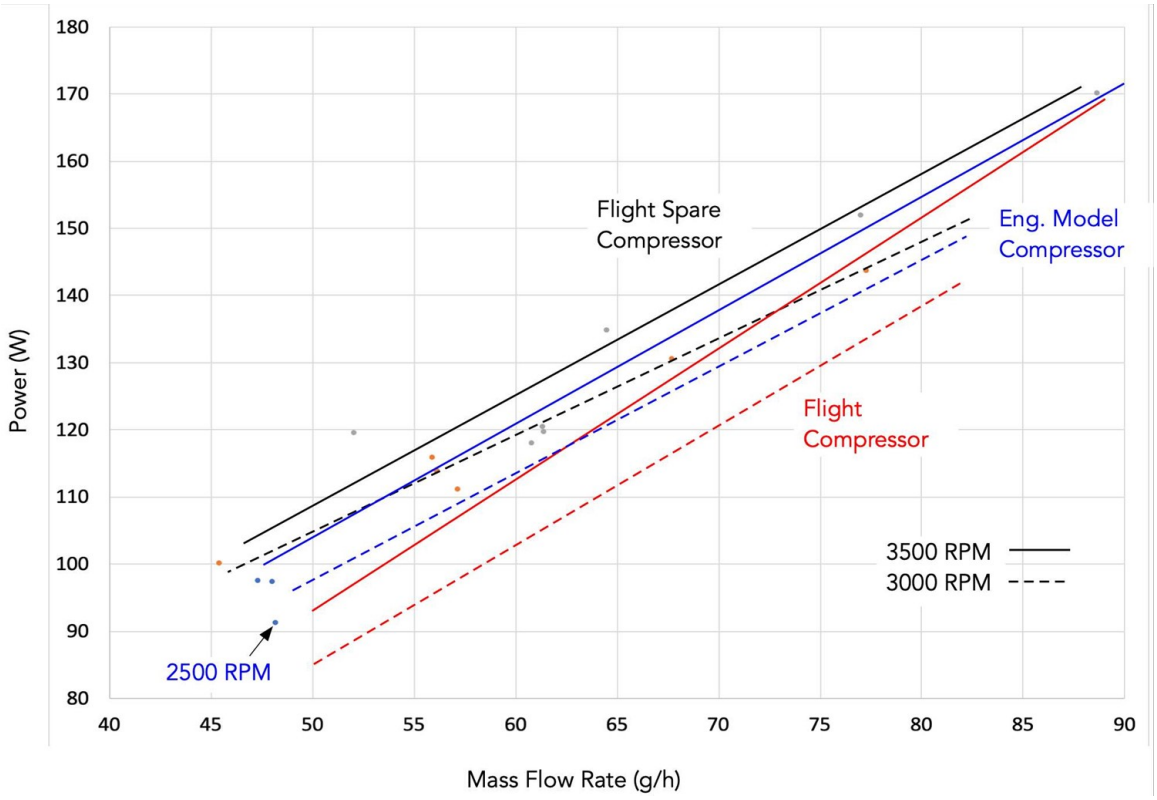

Figure 3-6: AS Acceptance Test Compressor Power vs. RPM and Mass Flow Rate (Rapp, 2022a).

As seen in Figure 3-6, the compressor power dissipation appears to scale with the mass flow rate and compressor rotational speed; however, the limited number of data points prohibits the determination of a numerical relationship from this data alone. For example, there are some data points for the Flight Compressor at 2,500 RPM that show a higher power than runs at 3,000 and 3,500 RPM, which does not match the observed increase in power from 3,000 RPM to 3,500 RPM. As there were few tests at this low rotational speed, it cannot be determined from this data alone if those data points are outliers. In addition, as the inlet and exhaust pressures are implicit in these measurements, the specific contributions of each to the compressor thermodynamic power cannot be quantified. It can also be seen that power dissipation differed across the three compressor units: this is likely due to differences in tip seal friction across the models. It was also observed in the AS acceptance tests that repeating the same

tests resulted in decreased power dissipation for all three models of up to 10% - this suggests decreasing power as wear on the tip seals increases. No prior analysis has been completed on the FM data to identify if the decreasing power seen in the AS acceptance tests has been observed with continued operations on Mars; therefore, this investigation into compressor power dissipation will also determine if this behavior remains true for post-acceptance test operation of the compressor units.

However, due to the large differences between the measured power for all compressor models, and the coupled nature of the test variables, additional experimentation was necessary to quantify the contributions of inlet and exhaust conditions on compressor power, as well as identify the changes in power dissipation as the tip seals degrade further. As the FlatSat is readily available for experimentation when compared to the EM and FM, a dedicated set of experiments was planned for the FlatSat to further explore MOXIE compressor power dissipation. This data was then be compared to FM data in order to identify common trends as well as differences between compressor units. These experiments are detailed in the following section.

3.3 Experimental Methods

The experiment to characterize compressor power dissipation included a single test to measure the power consumption of the compressor at various inlet, outlet, and rotational rate conditions. This was designed to to allow for characterization of compressor power under various operating conditions, for comparison to the FM compressor and to inform the optimal operating conditions for the compressor of a full-scale Martian oxygen production plant.

There was one direct objective for this experiment:

1. Measure compressor power at a range of inlet gas pressures, outlet pressures, and compressor rotational speeds that correspond to the operation of MOXIE as well as the range of likely operating conditions for a next-generation atmospheric Martian oxygen production plant.

The indirect objectives of this experiment were as follows:

1. Determine the FlatSat compressor power consumption at above operating conditions and determine extensibility of power relationship to FM compressor for use in FM run planning.

2. Determine operating conditions that minimize compressor power consumption, to inform design of a full-scale scroll compressor.

3. Quantify differences in power consumption between FlatSat Qual Compressor and FM Compressor.

The laboratory configuration and data acquisition methods used in this test are summarized below in Table 3.1. The temperature sensors T1, T3, and T4 refer to the temperature at the FlatSat sensor panel, the temperature at the compressor housing, and the temperature at the compressor motor housing respectively (Morris, 2018).

Table 3.1: Compressor Power Characterization Methods

Overview	This test involves measuring compressor mass flow and power as a function of inlet pressure, outlet pressure and RPM. The outlet pressure was intentionally varied over a range using a variable impedance needle valve. The compressor RPM was set via standard MOXIE run control table.
Compressor I/O	**Inlet**: Vacuum chamber at pressures of 6, 7.5, 9, and 10.5 mbar. These pressures, along with gas at approximately 20°C, represent the typical density range of gas entering the FM compressor on Mars, which differs from Martian atmospheric density due to warming in the MOXIE inlet tube (Rapp, 2022a). **Outlet**: Alicat PC–Series Pressure Controller, which maintained outlet pressure setpoints of 100, 200, 300, 400, 500, 600, 700, 800, 900, and 1000 mbar, vacuum pump at 0 torr.
Environment composition	Chamber total pressure p[CO_2] = 6, 7.5, 9, 10.5 mbar

Compressor configuration	Compressor outlet connected to three-way solenoid-controlled manifold. Flow configured for chamber recirculation or exhausted through Drivac BH2-60HD vacuum pump (see Figure 3-7)
Vacuum pump configuration	**Before starting compressor**: Drivac BH2-60HD on, solenoid-controlled manifold set to recirculation. **While compressor is running**: Drivac BH2-60HD on, solenoid-controlled manifold set to exhaust.
SOXE configuration	No flow through SOXE. Compressor outlet directly plumbed to three-way solenoid-controlled manifold.
RPM range	1000 to 4000 with 500 RPM steps.
RPM step duration	180 seconds at 1000 RPM, and 120 seconds at other RPM steps. The extended dwell at 1000 RPM allowed the vacuum chamber pressure to stabilize, as it takes approximately 60 seconds for the chamber pressure control loop to restore the pressure setpoint after large RPM step changes.
Temperature Measurements	Standard FlatSat temperature measurements to be taken (T1, T3, T4 in telemetry data). Gas temperature measured in three additional locations: **Gas in chamber**: Infrared camera and Kapton film. **Compressor inlet**: Honeywell Thin Film Platinum Resistance Temperature Detector. **Compressor outlet**: Alicat Whisper MW–Series Low Pressure Drop 2 SLPM Flow Meter.

Data acquisition	All non-standard MOXIE measurements (flow meter, pressure measurements) made with 16bit 0-5 VDC analog inputs read via a LabJack T7. Compressor mass flow measured using an Alicat Whisper MW–Series Low Pressure Drop 2 SLPM Flow Meter. Compressor outlet pressure measured using both an Alicat PC-Series Pressure Controller and an MKS 902B pressure gauge for redundancy. Compressor RPM setpoint, measured RPM, and chamber and compressor temperatures (T1, T3, T4) observed by MOXIE FlatSat electronics and rover emulator data module. Compressor power calculated using V28VM (MAIN Voltage) and I28VM (MAIN Current) readings from MOXIE FlatSat electronics and rover emulator data module.
Data format	All data saved in a .xlsx file in calibrated units.

The experimental setup is shown below in Figure 3-7.

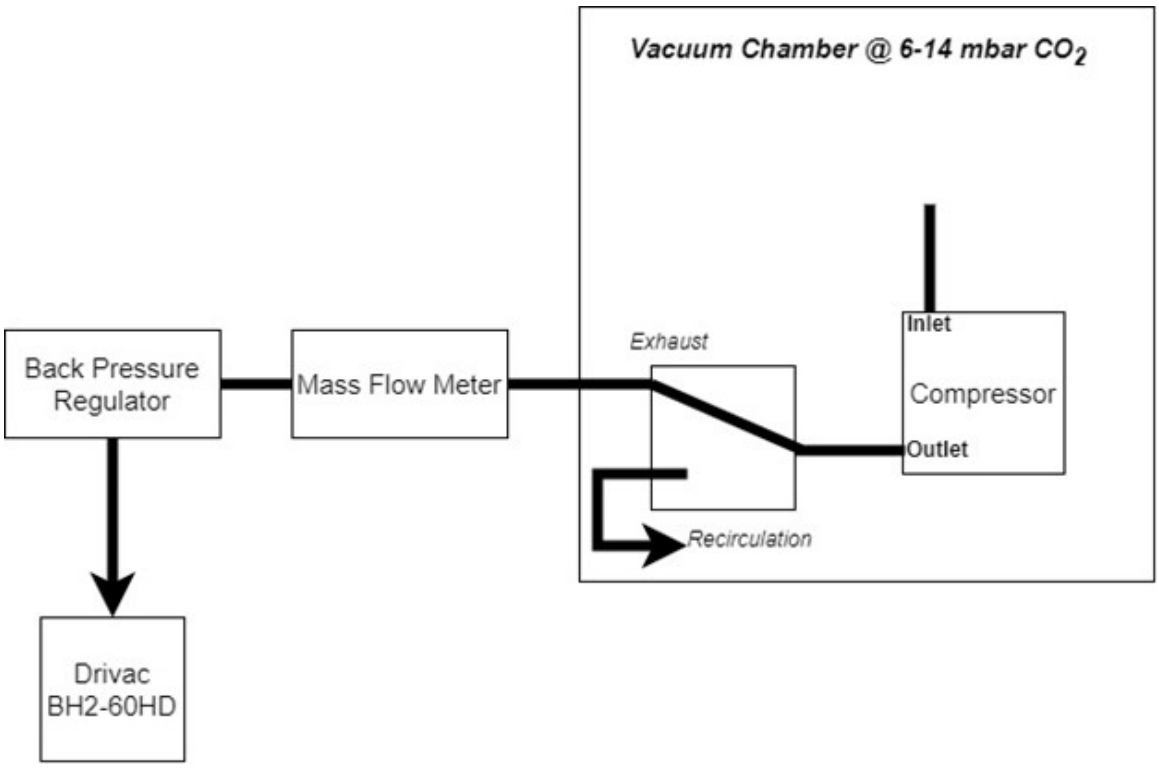

Figure 3-7: FlatSat compressor power characterization experimental setup.

Figure 3-8, Figure 3-9, and Figure 3-10 below show the planned inlet pressures, outlet pressures, and compressor RPM setpoints for the duration of the test. The inlet pressures were selected to cover both the range of expected gas densities on Mars, as well as the densities of gas entering the MOXIE compressor, as warming in the inlet tube leading to the MOXIE compressor results in a pressure decrease and temperature increase for the entering gas (Hecht et al., 2021). The outlet pressures were chosen to cover both low and high solid oxide electrolysis operating pressures, as previous work discussed in Chapter 2 outlines the benefits of operating the electrolysis stack at a low cathode pressure. The RPM setpoints were chosen to cover the range of operation for the FM compressor, which ensures that the data collected in this experiment remains relevant for comparison to FM data.

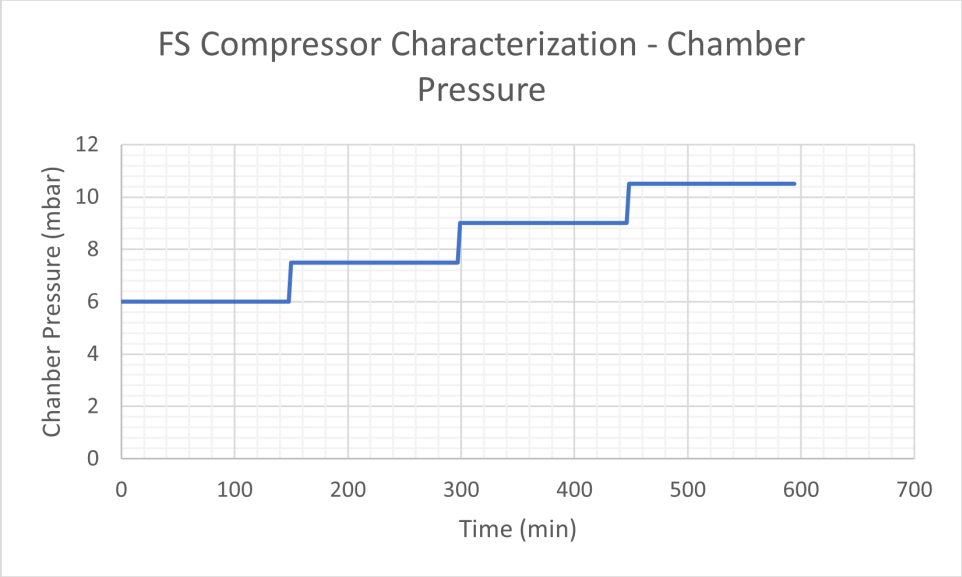

Figure 3-8: FlatSat compressor power characterization chamber pressure.

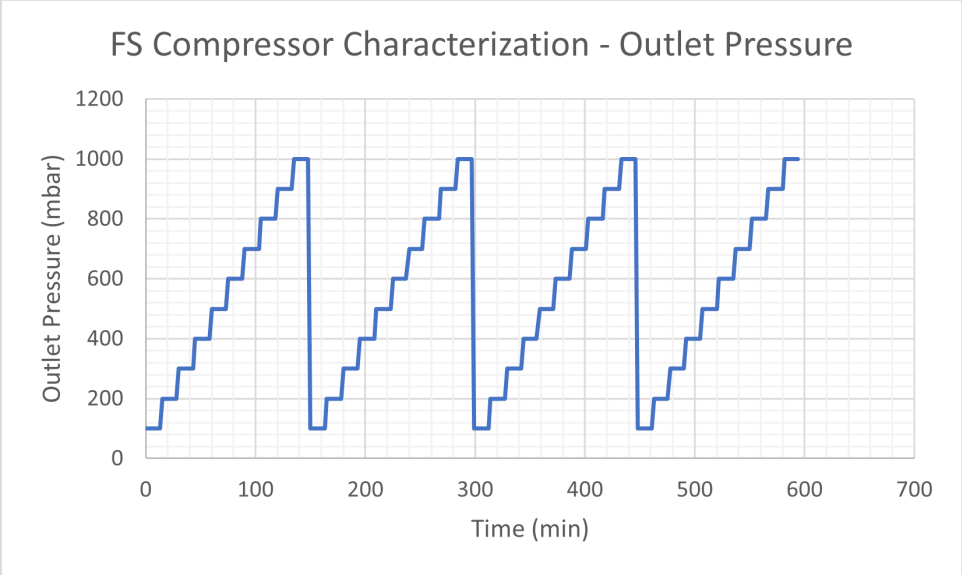

Figure 3-9: FlatSat compressor power characterization outlet pressure.

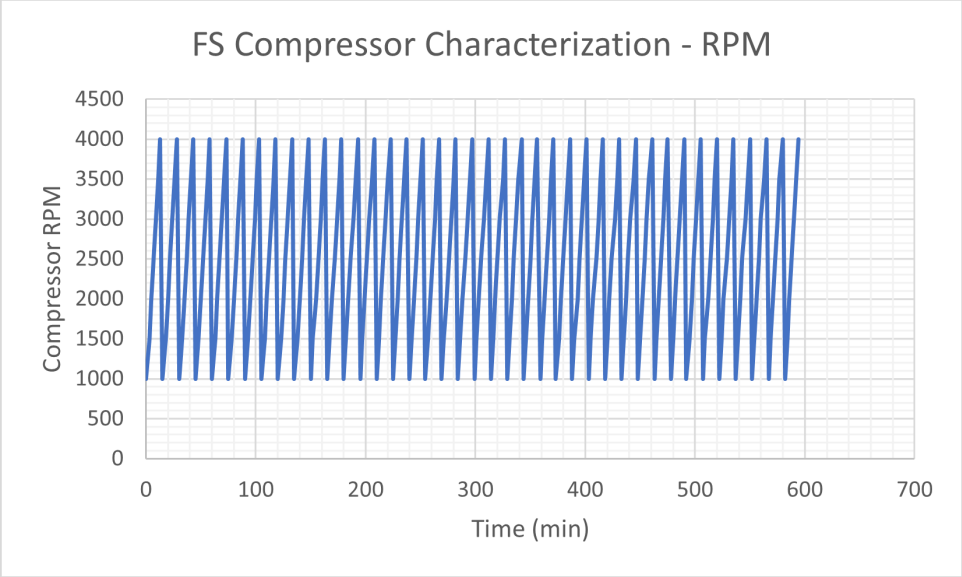

Figure 3-10: FlatSat compressor power characterization, compressor rotational speed.

The results and conclusions from the above experiment are discussed in the following section.

3.4 Results and Analysis

The experiment to characterize FlatSat compressor power was completed over two days with no anomalies, with the run segments at chamber pressures of 6 mbar and 7.5 mbar completed on the first day and the segments at chamber pressures of 9 mbar and 10.5 mbar completed on the second day. The following sections describe the collected data and the resulting findings, as well as how they relate to the FM and future Martian oxygen production systems.

3.4.1 Compressor Power Experiment Data

As mentioned in the previous section, the compressor power was calculated using the MAIN bus power, which in turn was calculated using the V28VM (MAIN voltage) and I28VM (MAIN current) readings from the FlatSat telemetry (Morris, 2018). The average MAIN power when the compressor was off, which is the power provided to

electronics and the battle short configuration, was subtracted from the MAIN power to isolate the compressor power.

The data was then filtered using the following criteria:

1. The compressor is on, indicated by a measured rotational speed greater than 0 RPM.

2. The compressor outlet pressure measured by the MKS 902B pressure gauge is within 5 mbar of the pressure setpoint input to the Alicat PC-Series Pressure Controller. At the lowest mass flows, i.e. at low chamber pressure and compressor rotational speed, and high outlet pressure setpoints, the back pressure regulator was unable to maintain the outlet pressure due to a lack of sufficient flow. This resulted in a discrepancy between the commanded outlet pressure and the achieved outlet pressure. Therefore, these data points were removed prior to analysis.

3. The compressor outlet mass flow measured by the Alicat Whisper Mass Flow Meter is less than 2 SLPM, which is the range of the flow meter. At the highest mass flows, i.e. at high chamber pressure and compressor rotational speed, and low outlet pressure setpoints, the volumetric flow through the flow meter exceeded its maximum rated value. This caused an error in the flow meter, which reported non-physical mass flow values above the meter's operating range. Therefore, these data points were removed prior to analysis.

For the remaining data, the power dissipation at each run step was averaged, resulting in a single power data point for each combination of chamber pressure, outlet pressure, and compressor rotational speed. The resulting filtered and averaged compressor power is shown below in Figure 3-11, plotted as a function of the compressor outlet pressure. The data is colored by the compressor rotational speed, and the plot markers indicate the chamber pressure at those data points - this is captured in the figure legend.

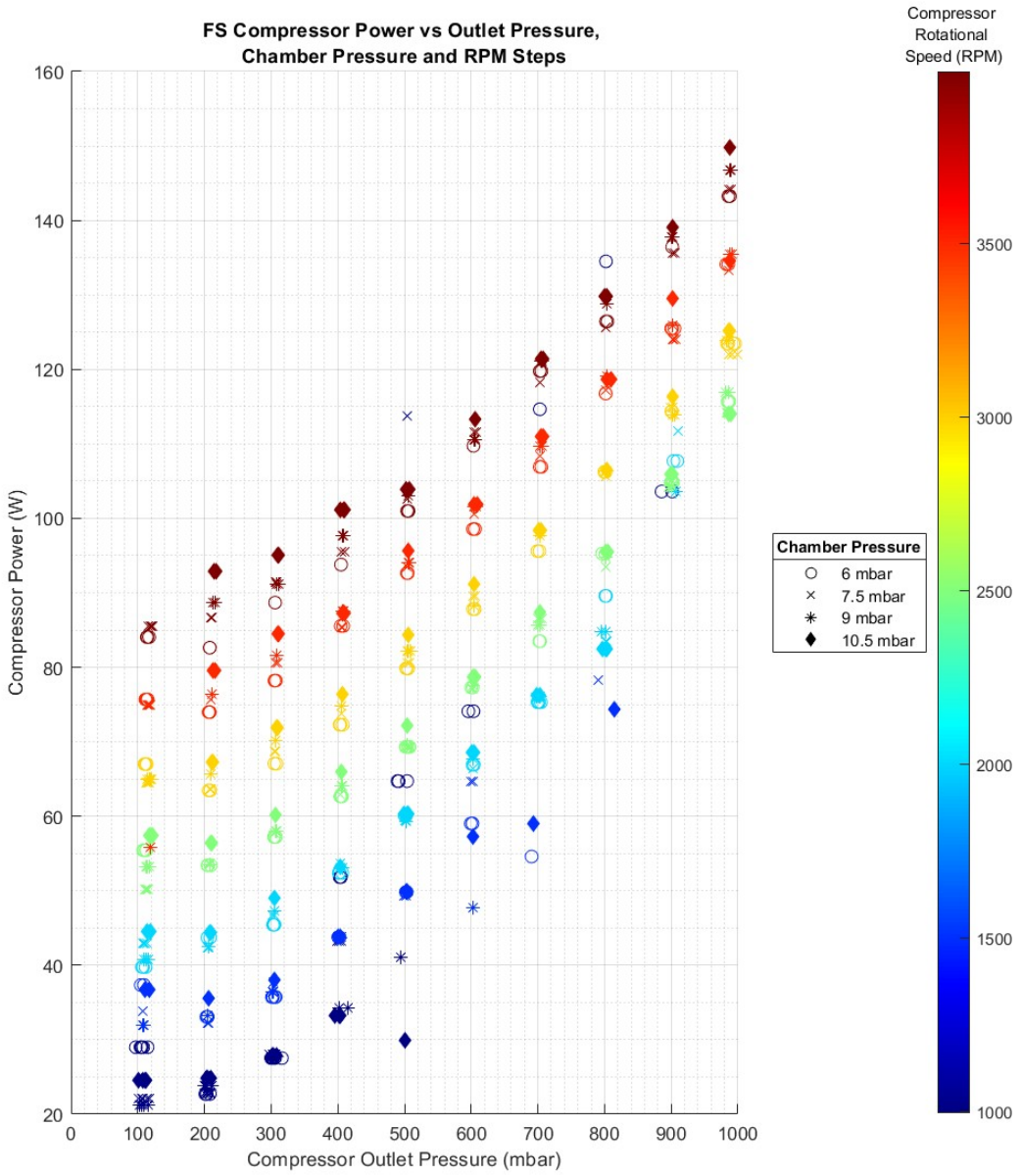

Figure 3-11: FlatSat compressor power as a function of outlet pressure, with marker colors corresponding to compressor rotational speed and shapes corresponding to vacuum chamber pressure.

As seen in Figure 3-11, the compressor power is dependent on all three of the independent variables. Specifically, an exponential relationship is observed between

the compressor outlet pressure and power - as discussed in Section 3.1, a lower compressor outlet pressure requires a lower compression energy cost. Therefore, it was expected that the compressor outlet and power are positively correlated. In addition, the power appears to scale linearly with rotational speed, which also matches the expected positive correlation, as operating the compressor at higher rotational speeds requires greater energy than operating it at lower rotational speeds. Lastly, a weak linear relationship is observed between the chamber pressure (and therefore density) and compressor power - however, the chamber density has a much smaller effect on compressor power than the outlet pressure and rotational speed. With these qualitative observations, it became possible to fit the compressor power as a function of the three independent variables: chamber density, rotational speed, and outlet pressure.

3.4.2 Fitting Compressor Power

Using the observations discussed in the previous section, a fit of the form in Equation (3.2) was implemented, where P_C is the compressor power in W, P_{outlet} is the outlet pressure in mbar, ω is the compressor rotational speed in RPM, ρ is the inlet gas density in kg/m^3, and A through G are constants.

$$P_C = (Ae^{BP_{outlet}} + C)(D\omega + E) + (F\rho + G) \tag{3.2}$$

The above form captures the exponential dependence of compressor power on outlet pressure, the direct proportionality between rotational speed and power, and the weak linear dependence of power on inlet gas density. The fit coefficients and the resulting fitted data are shown below, in Table 3.2 and Figure 3-12 respectively..

Table 3.2: FlatSat Compressor Power Fit Coefficients

Constant	Value
A	1.646
B	0.001314
C	65.82
D	0.0003124
E	14.37
F	271.1
G	-978.8

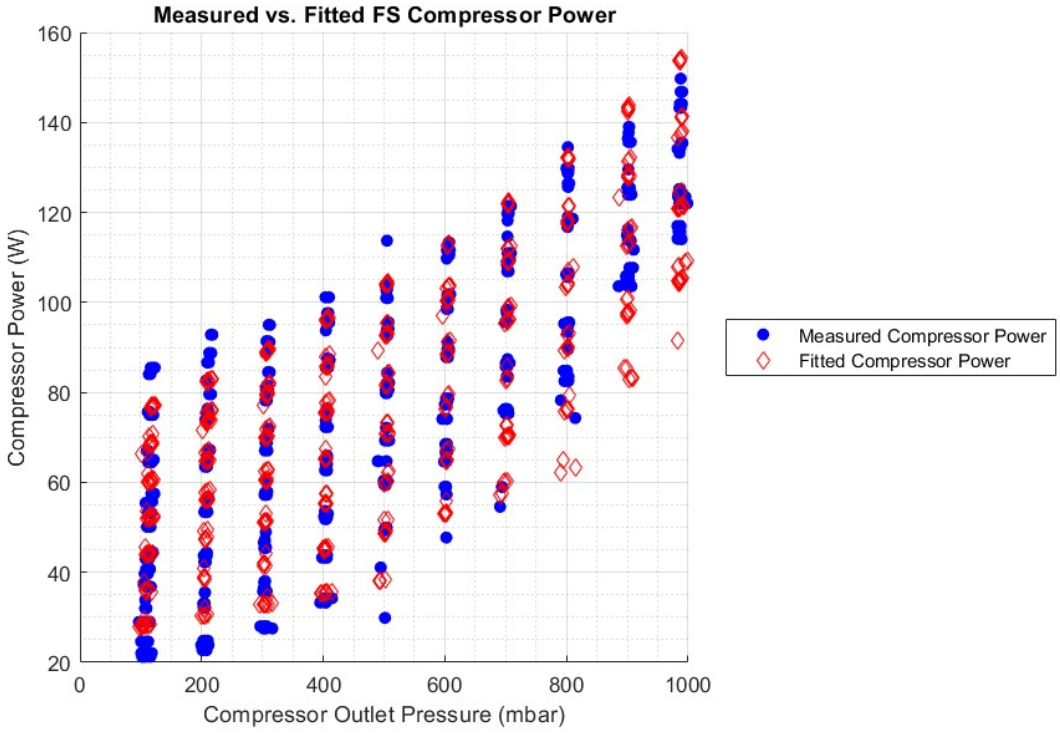

Figure 3-12: Fitted FlatSat compressor power compared to measured power.

As seen in Figure 3-12, the fitted data is within 0.5% of the measured experimental data for a majority of data points, excluding outliers. This indicates that the fit form in Equation (3.2) accurately captures the effects of changes in inlet gas density,

compressor rotational speed, and compressor outlet pressure on compressor power. However, it then became necessary to verify the fit coefficients in Table 3.2 using an independent FlatSat operational cycle, in order to ensure that the predictive equation for FlatSat compressor power translates to normal operations, where the compressor outlet is controlled to a VFCD and the outlet pressure is no longer independently controlled.

3.4.3 Verification of Fitted Power

To verify the FlatSat compressor power fit from Section 3.4.2, the data from a previously completed FlatSat run was used. This run, named FS OC05 to indicate that it was the fifth operational cycle of the electrolysis stack on the FlatSat, was intended to verify a planned FM operational cycle on Mars - as the run was of an extended duration compared to previous FM runs, it was first tested on the FlatSat to ensure that no faults were tripped during the FM run.

FS OC05, unlike the FlatSat compressor power experiment, used the FlatSat in its normal configuration, with the compressor drawing pure CO_2 from the vacuum chamber, but then exhausting this gas to the flowmeter VFCD and through the rest of the traditional flow path, compared to the pressure regulator exhaust used in the compressor characterization experiments. Therefore, the compressor outlet pressure was dependent on the compressor rotational speed and chamber gas density, rather than an independent variable. This run consisted of two rotational speed setpoints: 2403 RPM and 4000 RPM, with the chamber pressure held constant at 8.3 mbar - therefore, any changes in the inlet gas density are due to changes in temperature within the vacuum chamber. As the run used a chamber density typical of FlatSat operations, as well as rotational speed setpoints both on the low and high ends of compressor operation, it was considered an appropriate verification case for the FlatSat compressor power equation.

The compressor power for FS OC05 was isolated from the FlatSat telemetry data using the same methods described in Section 3.4.1. To calculate the fitted power, the inlet gas density was calculated using the measured chamber pressure and tempera-

ture, and the compressor rotational speed and outlet pressure were extracted directly from the FlatSat telemetry using the variables RPMM1 and P2 respectively (Morris, 2018). The outlet pressure was smoothed using a moving average filter to remove compressor rotation-induced oscillations in the P2 pressure reading. The resulting data was then fitted using Equation (3.2) and the coefficients in Table 3.2. The measured and fitted data are plotted below in Figure 3-13.

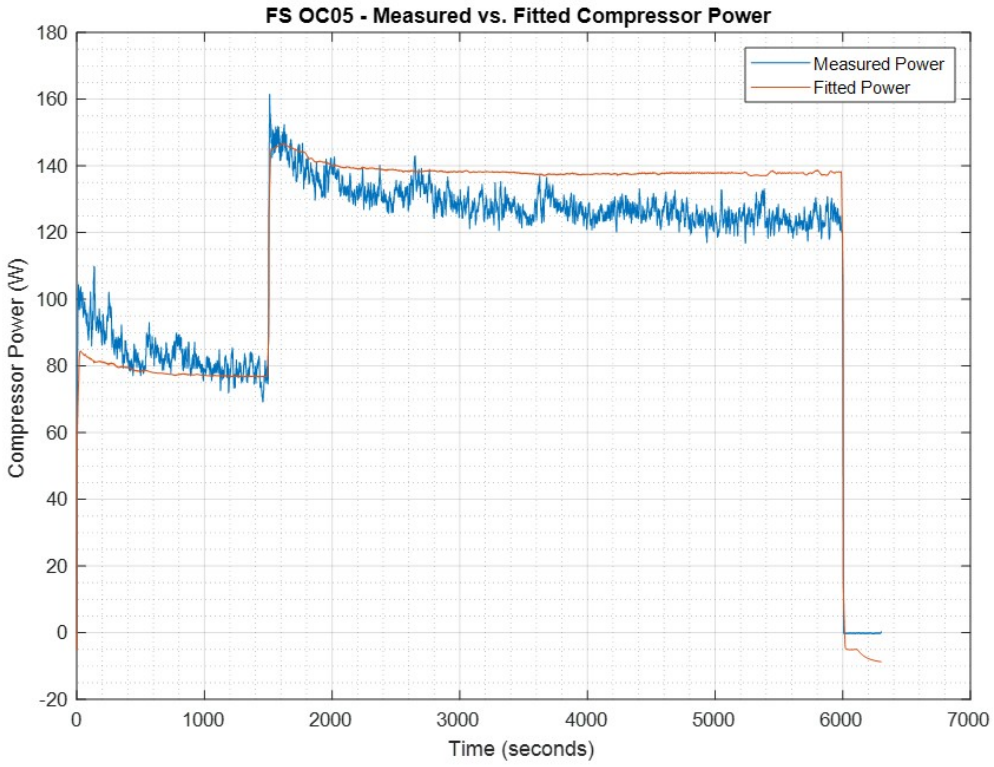

Figure 3-13: Comparison of measured and fitted power for FS OC05.

As seen in Figure 3-12, the fitted data tracks the measured compressor power for both rotational speed setpoints, and captures the increase in power when both rotational speed and outlet pressure are increased. However, especially for the extended duration run step at 4000 RPM, which is from approximately 1500 to 6000 seconds in the above figure, it can be seen that the measured power decreases more than the predicted power, resulting in approximately a 10% difference between the two. This can

be explained by several potential factors. First, the power prediction assumes that the density of gas entering the compressor is equal to the density of gas in the vacuum chamber. However, during extended duration steps at a high rotational speed, like the one seen in FS OC05, the gas temperature may increase within the compressor itself, as the compressor motor and housing are at significantly higher temperatures than the ambient chamber environment, on the order of 70 °C compared to 20 °C. This would result in a lower gas density through the compressor than predicted, resulting in a lower power dissipation than the fit predicts, as the results of the dedicated power-fitting experiment indicate that compressor power is proportional to inlet gas density. However, as the fit derived in Section 3.4.2 indicates only a small dependence on inlet gas density, a 50 °C increase in gas temperature would only account for an approximately 0.5% decrease in compressor power, so this hypothesis alone is not sufficient to explain the approximately 10% decrease in compressor power. A more likely cause for the observed decrease in compressor power is the tip seal friction within the compressor. As the compressor operates for an extended duration at a higher rotational speed, the tip seals may wear slightly, decreasing frictional energy losses. This would result in a lower power dissipation over continued operations when compared to the initial operating period at this rotational speed, where frictional losses would be greater. As the experimental steps used in developing the predictive fit for power were of a shorter duration than this extended run step, this decrease in power dissipation would not be captured, which may explain the difference between the predicted and measured compressor power.

However, this verification test demonstrates that the variables that affect FlatSat compressor power as well as their relative effects on power have been accurately captured in the developed fit.

3.4.4 Comparison to FM Data

After the FlatSat compressor power fit was developed and verified, the same methodologies were then implemented to develop a fit of the FM compressor power. As some of the goals in analyzing FlatSat compressor power were to understand unit-to-unit

differences between the MOXIE compressors, therefore allowing the MOXIE team to determine the extensibility of the FlatSat as a testbed and run verification platform for the FM, directly comparing compressor power dissipation for the two units was crucial.

To complete this, FM run data from nine operating cycles on Mars were analyzed: FM OC09, FM OC10, FM OC11, FM OC12, FM OC13, FM OC14, FM OC15, FM OC16, and FM OC18. These runs span nearly the entire Martian year as well as both day and night, capturing the diurnal and seasonal changes in Mars atmospheric density (Hoffman et al., 2022). In addition, the runs include a large variety in compressor rotational speed and therefore outlet pressure, as the two are coupled on the FM due to the presence of the VFCD downstream of the compressor. The compressor power from the FM data was isolated and filtered using the same methods discussed in Section 3.4.1.

The Mars pressure at the time of each run was extracted using data from Mars Environmental Dynamics Analyzer (MEDA), which is an additional payload onboard the Perseverance rover (Sotomayor, 2022). Inlet gas temperature was assumed using prior analysis that determined that the temperature is approximately 270 K during daytime runs, and 265 K during nighttime runs, as the inlet gas temperature is strongly influenced by warming due to the greater temperature of the Rover Avionics Mounting Panel (RAMP) onboard the rover (Rapp, 2022a) compared to the atmospheric temperature. This allowed for approximation of the inlet gas density, which cannot be measured directly using the sensors on the FM.

Prior to developing a fit for the FM compressor power, the power data was compared for each run, to determine if there was any decrease in power over continued operation. This was done to determine if the decrease in power seen in the AS acceptance tests, as discussed in Section 3.2, was also observed during continued operations, which would be indicative of continuing tip seal wear within the FM compressor. The FM compressor power is plotted below, compared to both compressor rotational speed and inlet gas density for the cumulative duration of the nine examined runs. Each run is demarcated by a dashed black line.

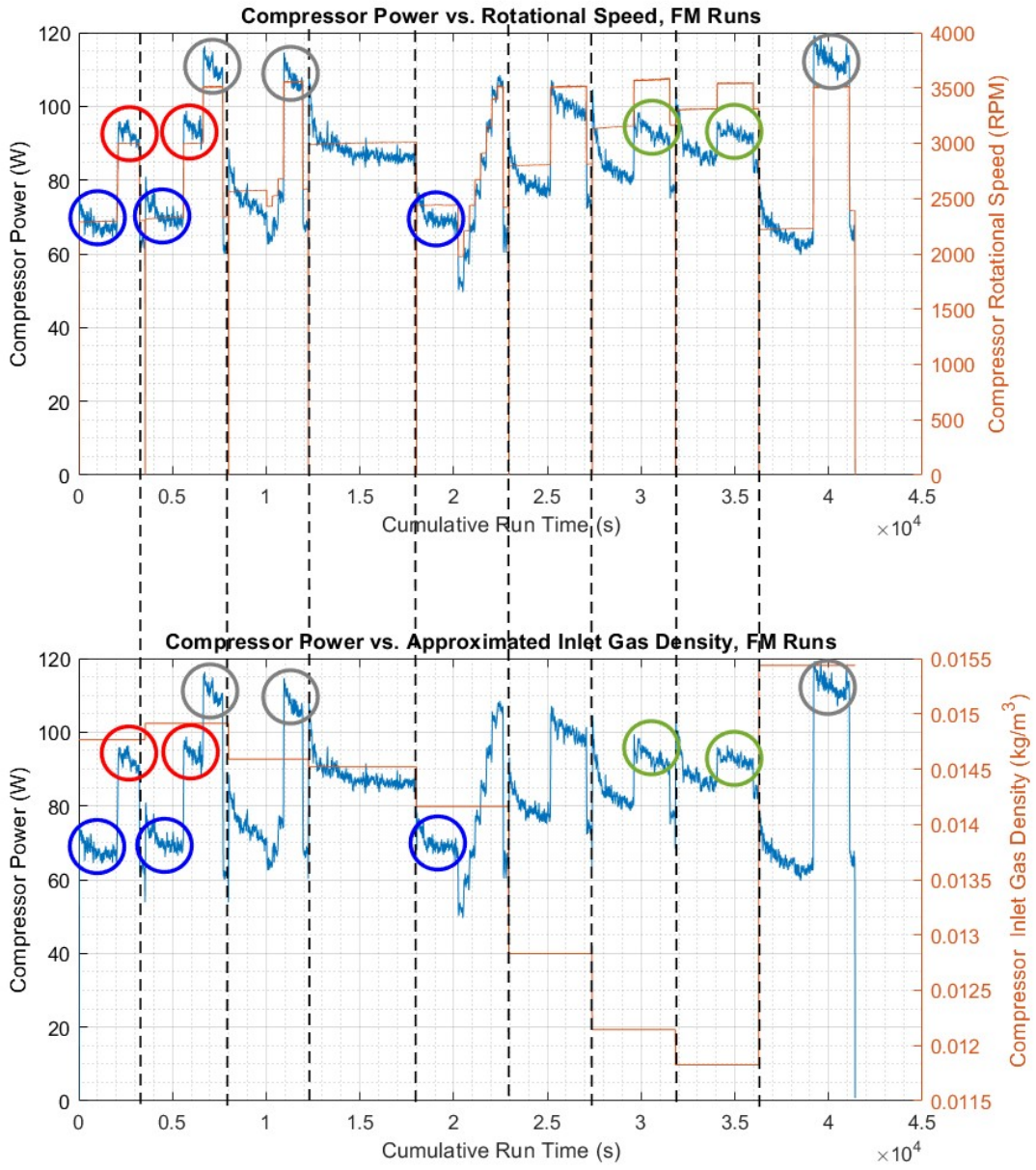

Figure 3-14: FM Compressor power (left axis) over nine examined runs, compared to compressor rotational speed (top, right axis) and inlet gas density (bottom, right axis).

As seen in Figure 3-14, the FM compressor power does not appear to decrease over

continued operation - run segments of similar compressor rotational speeds and inlet gas density, indicated by the various sets of colored ovals in the figure, have approximately the same compressor power dissipation. If there was continued tip seal wear on the FM compressor, the power would decrease, as seen in the AS acceptance tests. Therefore, the FM data suggests that while there was likely a period of initial wear during acceptance testing, the compressor units reach a steady-state power dissipation for a given set of operating conditions - in addition, the lack of degradation seen when operating on Mars indicates that the compressors have a significant operating lifetime, as no changes in the power dissipation were observed across over 10 operating cycles. Although there may be temporary tip seal wear during run steps, as seen through the decrease in power during FM run steps as well as the FS run examined in Section 3.4.3, this appears to be temporary, rather than permanent degradation of the compressors. As the FlatSat compressor, while a different unit, is of the same design as the FM compressor, it can therefore be inferred that the measured and fitted compressor power dissipation from this experiment will apply to subsequent operational cycles on the FlatSat. It can also be seen in Figure 3-14 that for each run segment, the compressor power decreases throughout the duration of the segment. As the time scale of these segments is significantly shorter than the diurnal variations on Mars, this is not likely to be due to changes in the atmospheric density; rather, this suggests that gas entering the compressor inlet warms during compressor operations, decreasing the gas density and therefore power. This is the same behavior observed during the extended duration segment of FS OC05, discussed in Section 3.4.3, which indicates that a common physical phenomenon is causing the power decrease in both cases.

Next, the approximated FM inlet density was used along with the compressor outlet pressure and rotational speed from the FM telemetry to create a fit of the same form as the FlatSat compressor power, Equation (3.2), for direct comparison between the two units. The FM fit coefficients are tabulated below in Table 3.3, alongside the FlatSat fit coefficients for comparison.

Table 3.3: FM and FlatSat Compressor Power Fit Coefficients

Constant	FlatSat Value	FM Value
A	1.646	1.302
B	0.001314	0.001423
C	65.82	84.16
D	0.0003124	0.0001748
E	14.37	18.25
F	271.1	-85.81
G	-978.8	-1558

As the fit equation is of a complex form, direct comparison of the coefficients does not allow for a straightforward comparison between FlatSat and FM compressor power dissipation. Therefore, the inlet density, outlet pressure, and compressor rotational speed for the FM were used as inputs with both the fitted FlatSat coefficients and FM coefficients. These two fits, along with the actual measured FM compressor power, are plotted below in Figure 3-15.

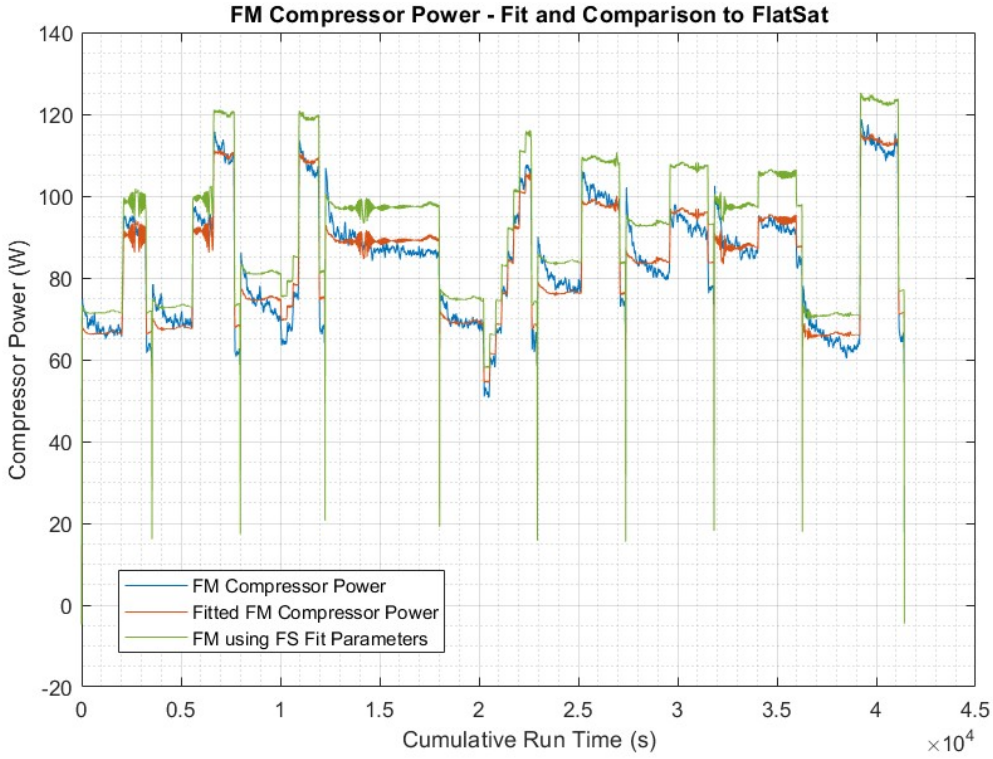

Figure 3-15: Comparison of FM compressor power to fits using FlatSat (labeled as FS) coefficients and FM coefficients.

As seen in Figure 3-15, the fitted FM compressor power, shown in orange, tracks the measured power, shown in blue, across all examined run segments, and therefore accurately captures the effects of changes in inlet density, compressor rotational speed, and the resulting change in compressor outlet pressure. The fitted data assumes a constant inlet gas density, which is why the decrease in power as the gas likely heats up during extended operations is not captured in the fit; however, this is less than a 5% difference at all run segments. It can also be seen that the fitted data using the FlatSat coefficients, shown in yellow, is significantly higher than the measured FM compressor power, by approximately 10 % across all run segments. Although the FlatSat fit follows approximately the same form as the FM fit, the predicted power dissipation is significantly higher using the FlatSat coefficients, which indicates that

the FlatSat compressor has a larger power draw than the FM by about 10% on average for a given set of operating conditions.

As a critical objective of the FS is to validate FM runs and predict FM run performance, the above methods were then applied to demonstrate the prediction of FM compressor power using FS compressor data, as well as to further highlight the differences between the FM and FS compressor power fit parameters. This is shown below in Figure 3-16.

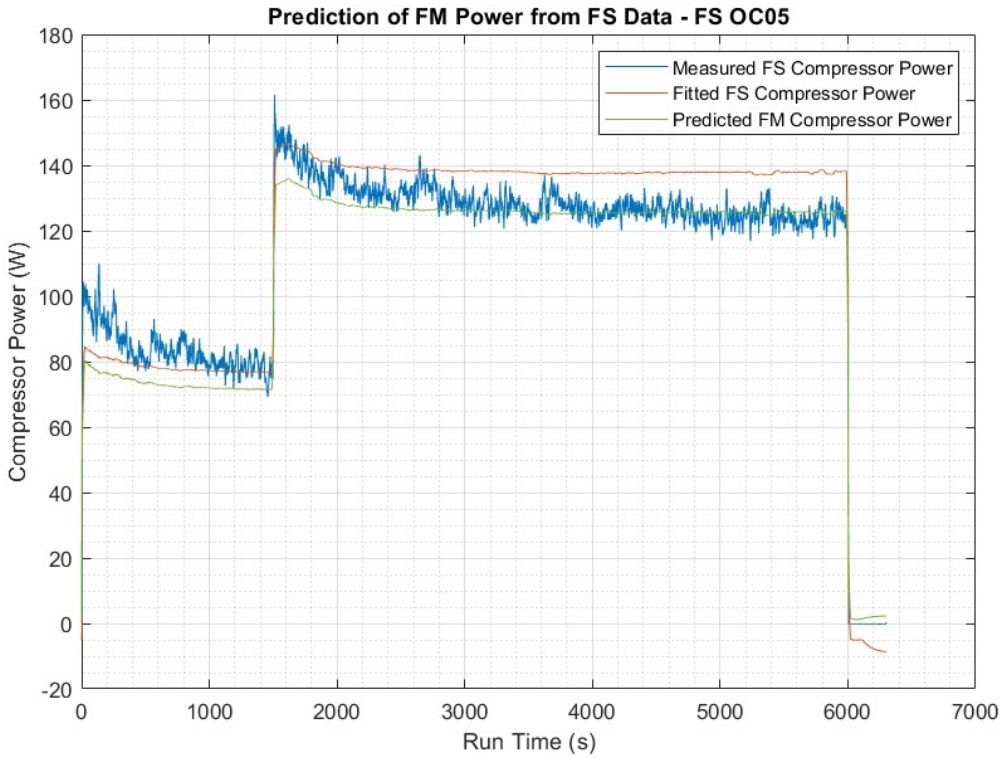

Figure 3-16: Comparison of FS compressor power to fits using FlatSat (labeled as FS) coefficients and FM coefficients.

As seen in Figure 4-8, the predicted steady-state FM compressor power would be slightly lower than the measured FS compressor power for the FS OC05 inlet conditions and run set points, which would result in a lower FM energy usage than the FlatSat for the given run and environmental conditions. Therefore, if the FS

run met mission energy usage constraints, it could be determined that the FM run would also meet the same constraints, as the FM compressor would use less power and therefore energy for the same run.

As the outlet pressure is dependent on the inlet density and rotational speed on the FM, the power fit using Equation (3.2) truly only contains two independent variables. However, the MOXIE Dynamic Model, which is used for FM run verification and energy prediction, contains a power prediction built into Simulink, and can therefore use all three parameters when estimating the energy that will be used for a given run (Hinterman, 2018). Therefore, the power fit developed in this analysis will be implemented into the MOXIE Dynamic Model for FM energy usage prediction for runs moving forward.

3.5 Compressor Power Conclusions

The power dissipation of the MOXIE compressor, which may require over 40 % of the total power used by the instrument as well as use upwards of 15 % of the total energy during a MOXIE run, is a critical component of the MOXIE system that required additional characterization. As the compressor onboard the FlatSat testbed, while identical in design to the FM compressor, did not go through the same acceptance testing as the FM compressor, a dedicated experiment measuring power dissipation of the FlatSat compressor was needed to quantify the effects of different operating conditions on compressor power. This also allowed for direct comparison between the two compressor units to further quantify the differences between the FlatSat and FM, which is essential when using the FlatSat as a verification platform for FM runs.

The results of this investigation demonstrate that as expected, compressor outlet pressure is the largest driver of compressor power onboard both the FlatSat and FM. This demonstrates that on FM runs where minimizing energy consumption is key, such as those that are designed with an extended oxygen production segment, running the compressor at lower rotational speeds and during the day, where the inlet gas density is lower, would minimize energy usage, at the expense of a lower flow rate.

In addition, this experiment demonstrates one of the benefits of operating at a low cathode pressure - decreased power and energy. Therefore, for a next-generation Mars oxygen production plant, operating at a lower compressor outlet pressure would be a method of saving energy and reducing the total power required for the system to operate.

When comparing the FlatSat and FM compressor power, it was also seen that the FM compressor uses on average 10% less power than the FlatSat unit for a given set of operating conditions. This is not an unexpected result - as adiabatic power is only approximately 25 % of the total compressor power, and the remainder is due to friction losses, unit-to-unit power differences can differ greatly with different levels of tip seal wear. However, as total energy is one of the constraints for operating the FM on Mars, this allows the FlatSat to be used as a conservative testbed for FM runs. When operating a planned FM run on the FlatSat, the total energy usage will be greater than it would be on the FM due to the larger FlatSat compressor power draw - this results in a conservative prediction of energy usage. If the FlatSat energy usage is less than the constrained limit of 1000 W-hrs, it can be assumed that the FM will use less energy than that limit as well, as the FlatSat compressor will have used more energy than the FM compressor would. This assumes an equivalent energy consumption for the heaters and electrolysis stack, which is outside of the scope of this investigation.

Lastly, this analysis demonstrated that during continued operations on Mars, no additional drop in compressor power dissipation was seen, unlike what was observed in the AS Acceptance tests. Therefore, the MOXIE team can use the predictive power fits developed for both the FlatSat and FM, without including additional considerations for changes in compressor power over time.

Chapter 4

FlatSat Compressor Volumetric Efficiency Characterization

4.1 Motivation

The volumetric efficiency (VE) of the MOXIE compressors is the ratio of actual flow rate through the compressor to the theoretical flow rate; as discussed in Chapter 3, the scroll compressors take in a fixed volume of gas with each rotation, which determines the theoretical flow. However, backflow of gas through the compressor to the low-pressure Martian atmosphere results in an actual flow rate that is lower than the theoretical flow (Hecht et al., 2021). Equation (4.1) defines the VE η, where F_S is the actual flow rate to the SOXE, ρ_i is the inlet gas density, ω is the commanded compressor rotation speed, and V_0 is the sealed volume per rotation, 30.1 cm^3.

$$\eta = \frac{F_S}{(\rho_i)(\omega)(V_0)} \tag{4.1}$$

The VE is a critical parameter in planning MOXIE runs, as it is necessary to calculate the actual mass flow to the SOXE for a given set of inlet conditions and compressor speed. The safe operating regime for MOXIE is where the operating voltage is above the Nernst voltage for oxygen production, and below the Nernst voltage for carbon formation; this was discussed previously in Chapter 2, t. As seen

in Equation (2.1), the Nernst voltage for oxygen formation drops as the flow of CO_2 increases, while the Nernst voltage for carbon formation in Equation (2.2) does not change. This means that at higher mass flow rates, there is a larger safe margin of operation for a given oxygen production rate; conversely, in conditions where there is low flow (such as when the Martian atmospheric density is low), this margin is smaller. This is seen below in Figure 4-1, where the Nernst voltages for O_2 and C formation are plotted as a function of mass flow rate.

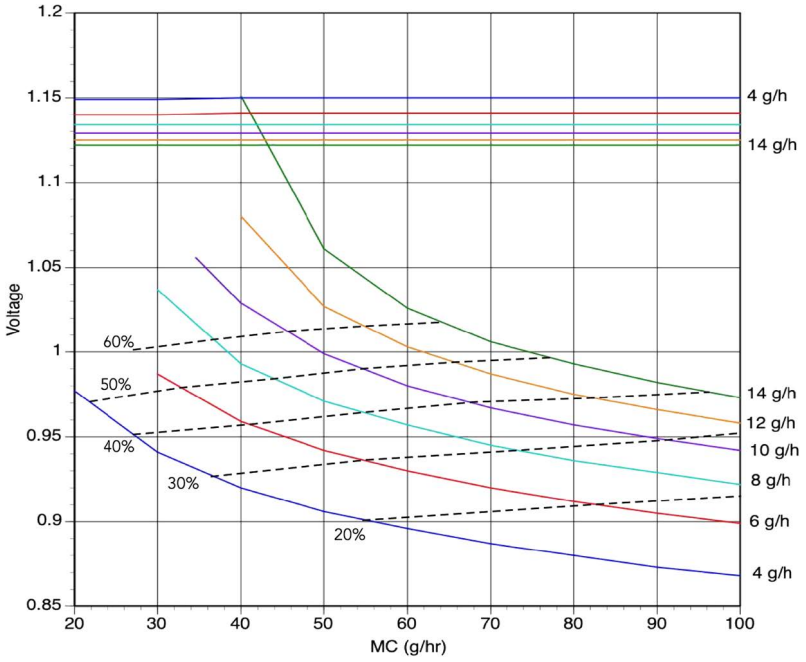

Figure 4-1: $V_N(O_2)$ vs. F_S (labeled as MC) for various oxygen production rates. Upper horizontal lines indicate $V_N(C)$, and dotted lines indicate constant values of the utilization factor u (Hecht et al., 2021).

When planning MOXIE's operations on Mars, the compressor rotational speed is set based on the desired oxygen production rate and predicted Mars atmospheric density at the time of the run, in order to ensure that MOXIE is operating at a sufficient mass flow to avoid carbon deposition for given atmospheric conditions. Therefore, in order to accurately set compressor rotational speed to achieve the target inlet mass flow rate, the VE must be understood. In addition, conducting experimentation to characterize VE on the FlatSat EDU compressor will allow for comparison to data

points from FM runs on Mars - by quantifying unit-to-unit differences in compressor VE, FM runs can accurately be modified for testing on the FlatSat, and dedicated FlatSat runs can be planned with higher fidelity.

4.2 Prior Work

The AS acceptance tests discussed in Section 3.2 were also used to characterize volumetric efficiency for the FM, EM, and Flight Spare compressors. For each test, the measured mass flow was compared to the theoretical mass flow to calculate the compressor volumetric efficiency. As discussed above, it was expected that volumetric efficiency would show a strong inversely proportional relationship with exhaust pressure, as a higher exhaust pressure would result in greater backflow through the compressor. However, while a weak correlation was observed for all three compressor units under test, as shown in Figure 4-2, there is a significant amount of scatter and a limited amount of data points to quantify this relationship precisely.

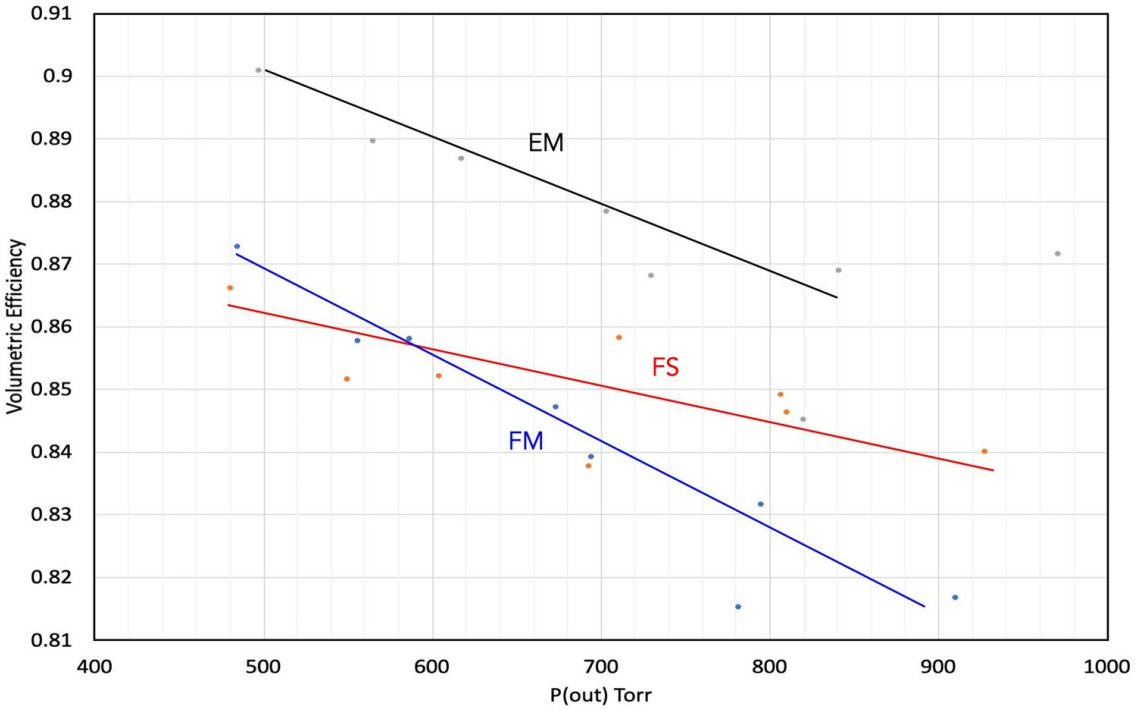

Figure 4-2: VE vs. exhaust pressure, AS acceptance test "P-Sweep runs (Rapp, 2022a).

Due to these problems, as well as the differences in the AS test setup when compared to the MOXIE flow path, additional experiments were conducted to quantify the dependence of the FlatSat compressor on inlet and outlet conditions, as well as the compressor rotational speed. This data will be compared to FM data to determine the unit-to-unit variations between the compressors, and if a common trend exists across the units.

4.3 Experimental Methods

The experiment to characterize compressor volumetric efficiency included a single test to measure the mass flow rate through the compressor at various inlet, outlet, and rotational rate conditions. The data from this test allowed for characterization of compressor VE for various operating conditions, for comparison to the FM compressor

and to inform the design of runs for both the FM and FlatSat moving forward.

There was one direct objective for this experiment:

1. Measure the FlatSat compressor mass flow rate at a range of inlet gas pressures, outlet pressures, and compressor rotational speeds that correspond to the operation of MOXIE.

The indirect objectives of this experiment were as follows:

1. Determine compressor volumetric efficiency at above operating conditions and quantify effect of inlet conditions, outlet conditions, and compressor rotational speed on compressor VE.

2. Quantify the differences between FlatSat and FM compressor VE in order to develop a prediction of FM compressor VE at FM operating conditions.

3. Quantify differences in power consumption between FlatSat EDU Compressor and FM Compressor.

These objectives could be accomplished with the same experimental setup, data acquisition systems, and procedure detailed in Section 3.3. The collected data on the mass flow rate through the compressor as well as the RPM setpoints and inlet/outlet conditions were then used to determine the numerical relationships governing compressor volumetric efficiency. The results and conclusions from this experiment are discussed in the following section.

4.4 Results and Analysis

The experiment to characterize FlatSat compressor VE was completed successfully over two days, with the run segments at chamber pressures of 6 mbar and 7.5 mbar completed on the first day and the segments at chamber pressures of 9 mbar and 10.5 mbar completed on the second day. The following sections describe the collected data and the resulting findings, as well as how they relate to the FM and future Martian oxygen production systems.

4.4.1 Compressor Volumetric Efficiency Experiment Data

As mentioned in Section 3.3, the mass flow rate through the FlatSat compressor was measured directly using a mass flow meter connected to the compressor outlet. The mass flow was measured in standard liters per minute (SLPM), which uses a reference temperature of 298.15 K and reference pressure of 1013 mbar to calculate the molar volume of a gas through the meter. The below equations were used to convert the measured volumetric flow in SLPM to the mass flow in grams per hour. Equation (4.2) was used to calculate the molar volume of the gas, CO_2 in this case, which was then used to calculate molar flow rate using Equation (4.3). The mass flow rate was then calculated using Equation (4.4).

$$F_S(L/mol) = \bar{R}\frac{(298K)}{(1013mbar)} \tag{4.2}$$

$$F_S(mol/min) = \frac{F_S(SLPM)}{F_S(L/mol)} \tag{4.3}$$

$$F_S(g/hr) = (F_S(mol/min))(MW_{CO_2})(\frac{60min}{1hr}) \tag{4.4}$$

The volumetric efficiency was then calculated using Equation (4.1), and filtered using the same criteria listed in Section 3.4.1:

For the remaining data, the VE at each run step was averaged, resulting in a single VE data point for each combination of chamber pressure, outlet pressure, and compressor rotational speed. The resulting filtered and averaged compressor VE is shown below in Figure 4-3, plotted as a function of the compressor outlet pressure. The data is colored by the compressor rotational speed, and the plot markers indicate the chamber pressure at those data points - this is captured in the figure legend.

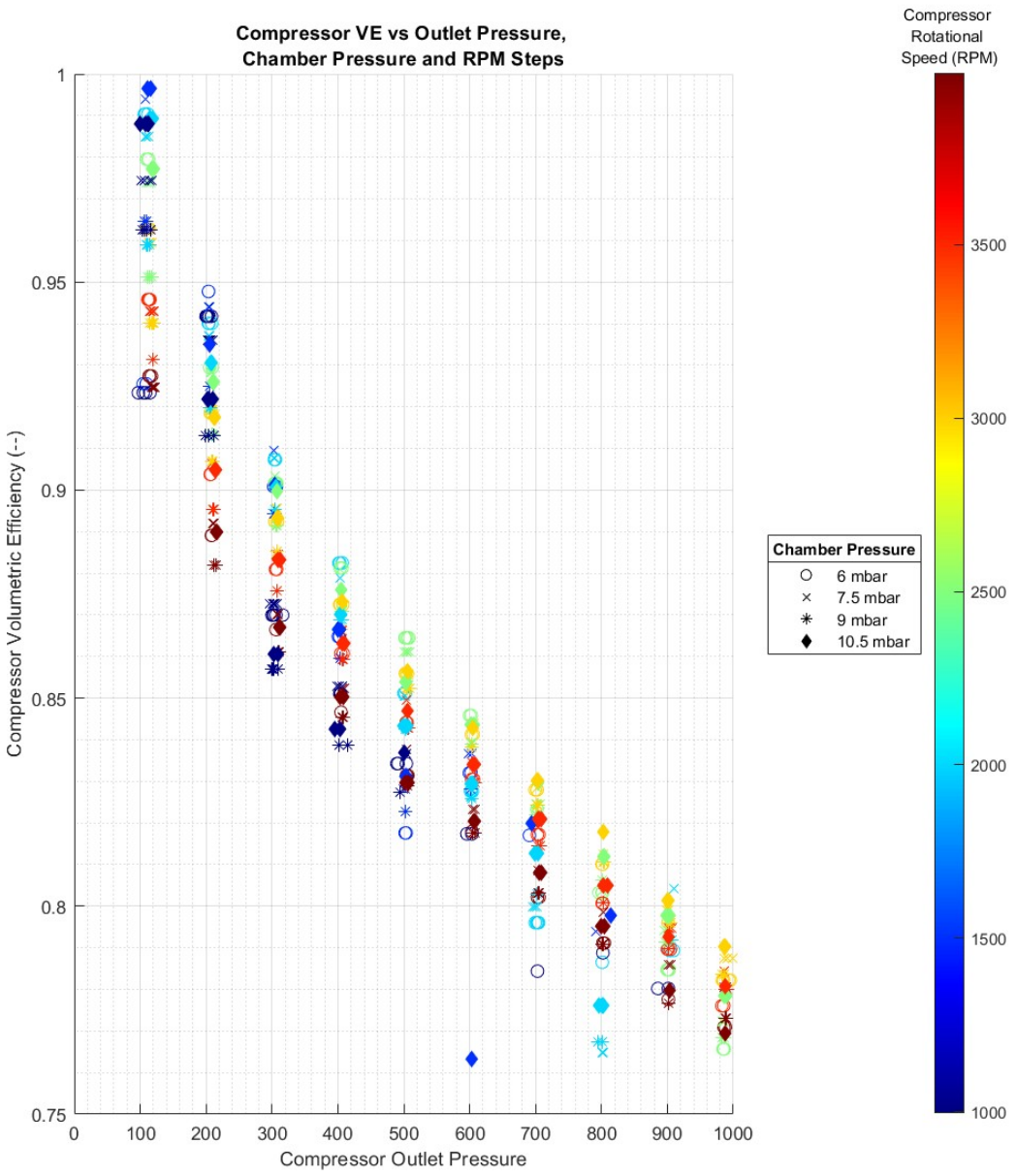

Figure 4-3: FlatSat compressor VE as a function of outlet pressure, with marker colors corresponding to compressor rotational speed and shapes corresponding to vacuum chamber pressure.

As seen in Figure 4-3, the compressor VE is dependent on all three of the independent variables, albeit in a different way than the compressor power as discussed in

Section 3.4.1. Specifically, a negative exponential relationship is observed between the compressor outlet pressure and VE. In addition, the volumetric efficiency appears to decrease as compressor rotational speed is increased, although there are several outliers that do not fit this trend. Lastly, a weak linear relationship is observed between the chamber pressure (and therefore density) and compressor VE - however, similar to the behavior seen in the analysis of compressor power, the chamber density has a much smaller effect on compressor VE than the outlet pressure and rotational speed. With these qualitative observations, it became possible to fit the compressor VE as a function of the three independent variables: chamber density, rotational speed, and outlet pressure.

4.4.2 Fitting Compressor Volumetric Efficiency

Using the observations discussed in the previous section, a fit of the form in Equation (4.5) was implemented, where VE_C is the unitless compressor volumetric efficiency, P_{outlet} is the outlet pressure in mbar, ω is the compressor rotational speed in RPM, ρ is the inlet gas density in kg/m^3, and A through G are constants. This is the same form used for the fit of compressor power, although the magnitudes and signs of the constants will differ due to the different type of dependency on the independent variables.

$$VE_C = (Ae^{BP_{outlet}} + C)(D\omega + E) + (F\rho + G) \tag{4.5}$$

The above form captures the exponential dependence of compressor VE on outlet pressure, the direct proportionality between rotational speed and VE, and the weak linear dependence of VE on inlet gas density. The fit coefficients and the resulting fitted data are shown below, in Table 4.1 and Figure 4-4 respectively..

Table 4.1: FlatSat Compressor VE Fit Coefficients

Constant	Value
A	0.4625
B	-0.001897
C	-0.1527
D	-5.958e-5
E	0.7363
F	-0.3168
G	0.833

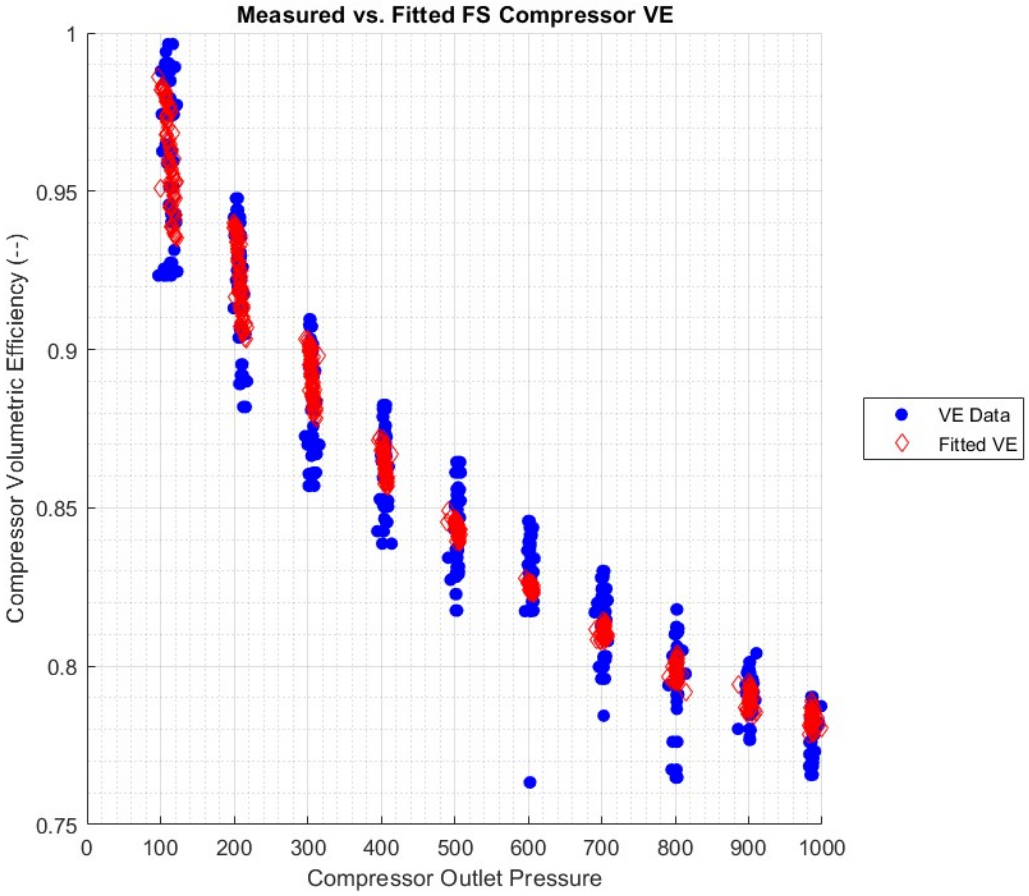

Figure 4-4: Fitted FlatSat compressor volumetric efficiency compared to measured volumetric efficiency.

As seen in Figure 4-4, the fitted data tracks the measured data, although with less scatter above and below the median of the measured data. Even with filtering and averaging of the compressor mass flow rate, the measured mass flow rate data still had noise from compressor-induced oscillations of the gas flowing through it, which resulted in significant scatter, particularly at low outlet pressures. Therefore, the fitted data has less deviation from the median of the measured data, as the high and low data points from these oscillations offset in the fitted data. The accuracy of the fitted data indicates that the fit form in Equation (4.5) captures the effects of changes in inlet gas density, compressor rotational speed, and compressor outlet

pressure on compressor VE. However, it was necessary to verify the fit coefficients in Table 4.1 using an independent FlatSat operational cycle, in order to ensure that the predictive equation for FlatSat compressor VE translates to normal operations, where the compressor outlet is controlled to a VFCD and the outlet pressure is no longer independently controlled.

4.4.3 Verification of Fitted VE

To verify the FlatSat compressor VE fit from Section 4.4.2, the data from FS OC05 was used, which was the same FlatSat run discussed in Section 3.4.3. To determine the measured mass flow from the compressor, the following equations were used, which use the VFCD flow resistances and gas properties to calculate the total mass flow (MOXIE Team, 2022a). In the below equations, K_t is a VFCD temperature correction factor, F_O2_I_G_HR is the oxygen production rate derived using the SOXE current, and F_S_P4_G_HR is the total SOXE inlet mass flow rate calculated using the cathode VFCD flow resistance and oxygen production rate. As mass flow is conserved in the system, combining the oxygen flow with the cathode exhaust flow yields the total mass flow through the system, and therefore the output mass flow of the compressor. These equations also include the contribution of recirculation flow from the cathode. Temperature readings T16 and T18 are in °C, IT and IB are measured currents in A, and P4 is the SOXE cathode pressure in bar.

$$K_t = \sqrt{\frac{530}{1.8(\frac{T16+T18}{2}) + 492}} \tag{4.6}$$

$$F\_O2\_I\_G\_HR = \frac{1}{0.335}(\frac{IT + IB}{2}) \tag{4.7}$$

$$F\_S\_P4\_G\_HR = 0.129K_t(750P4) + F\_O2\_I\_G\_HR \tag{4.8}$$

Using Equation (4.8), the actual flow rate from the compressor was calculated, which was then compared to the predicted mass flow using Equation (4.1) to calcu-

late the volumetric efficiency. The independent variables to fit the measured VE were isolated from the FlatSat telemetry as discussed in Section 3.4.3, with the same moving average applied to the outlet pressure (P2) data to remove compressor rotation-induced oscillations in the pressure reading. The resulting data was then fitted using Equation (4.5) and the coefficients in Table 4.1. The measured and fitted data are plotted below in Figure 4-5.

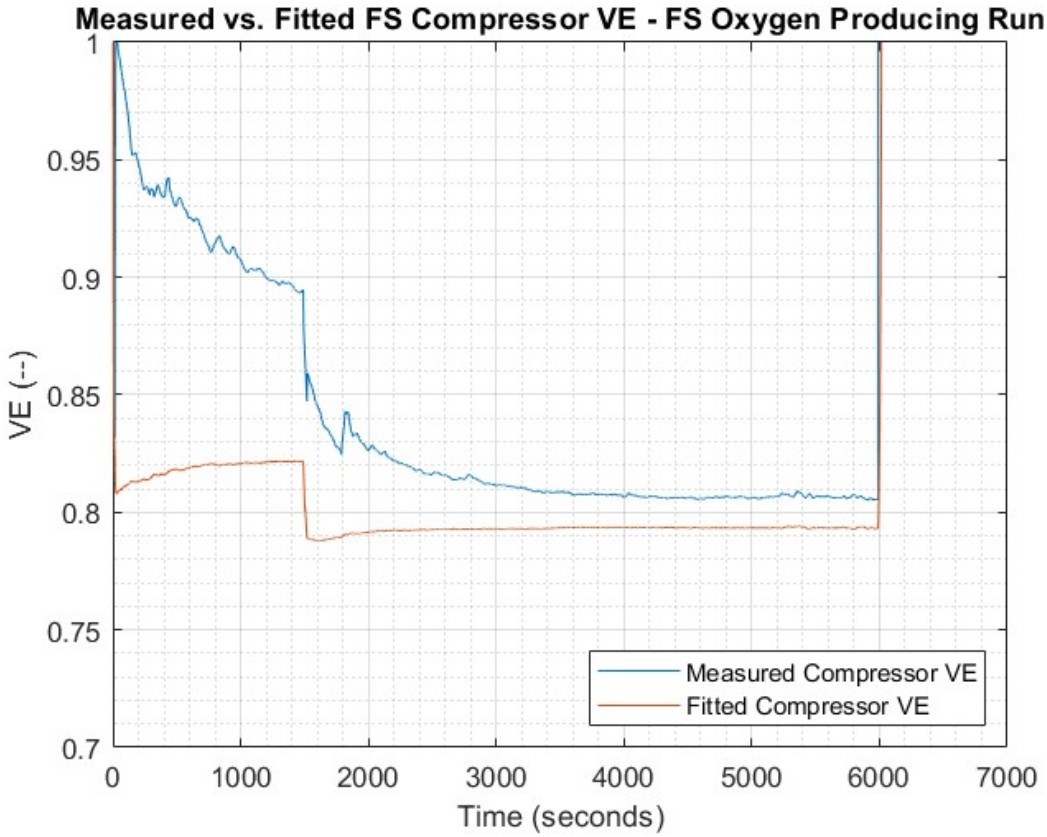

Figure 4-5: Comparison of measured and fitted VE for FS OC05.

As seen in Figure 4-5, the fitted data differs significantly from the measured VE during the initial 1600 seconds of the run, but is within 2% of the measured VE during the last 2000 seconds of the run, where the compressor was set to a high rotational speed for an extended duration. These observations can be explained by several potential factors. First, as seen in Equation (4.8) and Equation (4.7), the calculated

mass flow used to determine the measured volumetric efficiency using Equation (4.1) assumes that the oxygen production is proportional to current. However, while true, the numerical terms in those equations assume steady-state SOXE operations, which require thermal equilibration within the system. For approximately the first 20 minutes of SOXE operations (Rapp, 2022b), thermal equilibration within the stack has not yet been reached, resulting in a lower oxygen production rate than would be predicted using Equation (4.7). This results in a calculated mass flow greater than the actual mass flow, therefore resulting in a higher measured VE than the physical VE during that time frame. As the equilibration period proceeds, the electrolysis process approaches its steady-state performance, which is why the VE gradually decreases across this segment. The fitted VE, on the other hand, shows the effect of an increasing chamber gas temperature and therefore decreasing inlet gas density density during the initial run segment. As seen in the fit derived in Section 4.4.2, the FS compressor VE has an inverse relationship with inlet gas density; as the chamber warms and the density decreases, the predicted VE using the fit increases. This equilibration also occurs, albeit with a smaller time scale, when the SOXE current is changed, which is why from approximately 2000 to 3000 seconds, another gradual decrease in the calculated mass flow (and therefore VE) is seen. When the stack is at thermal equilibrium, such as the segment between 4000 and 6000 seconds, the discrepancy between the calculated and actual mass flow is no longer present. For this run segment, the fitted VE very closely matches the measured VE, demonstrating that the fit is an accurate predictor of FlatSat compressor VE during steady-state operations.

In addition, small errors in calibration for the outlet pressure reading used in fitting the FS OC05 compressor VE may contribute to the difference between measured and predicted VE - as compressor outlet pressure is the largest contributor to compressor VE, a pressure reading that is calibrated slightly high would result in a lower predicted VE due to the negative exponential nature of the relationship between outlet pressure and VE.

Overall, this verification test demonstrates that the variables that affect FlatSat VE as well as their relative effects on VE have been accurately captured in the devel-

oped fit. However, it was also seen that the developed fit is only directly applicable to the FlatSat VE at steady-state conditions, and may differ from the actual VE during dynamic run segments. However, as MOXIE runs are designed with steady-state flow rate targets, the developed predictive fit for VE can be used in FlatSat run planning.

4.4.4 Comparison to FM Data

After the FlatSat compressor VE fit was developed and verified, the same methodologies were then implemented to develop a fit of the FM compressor VE - the rationale for FM and FlatSat compressor comparison was discussed in detail in Section 3.4.4. The FM runs and MEDA data used for the compressor power comparison were also used for analysis of the VE, and the FM compressor VE was calculated using the methods discussed in Section 4.4.3.

Prior to developing a fit for the FM compressor VE, the calculated volumetric efficiencies were compared for each run, to determine if there was any decrease in VE over continued operation. This was conducted to determine if any component-level degradation, such as wear resulting in reduced efficiency, was observed during continued operation. The FM compressor VE is plotted below, compared to both compressor rotational speed and inlet gas density for the cumulative duration of the nine examined runs.

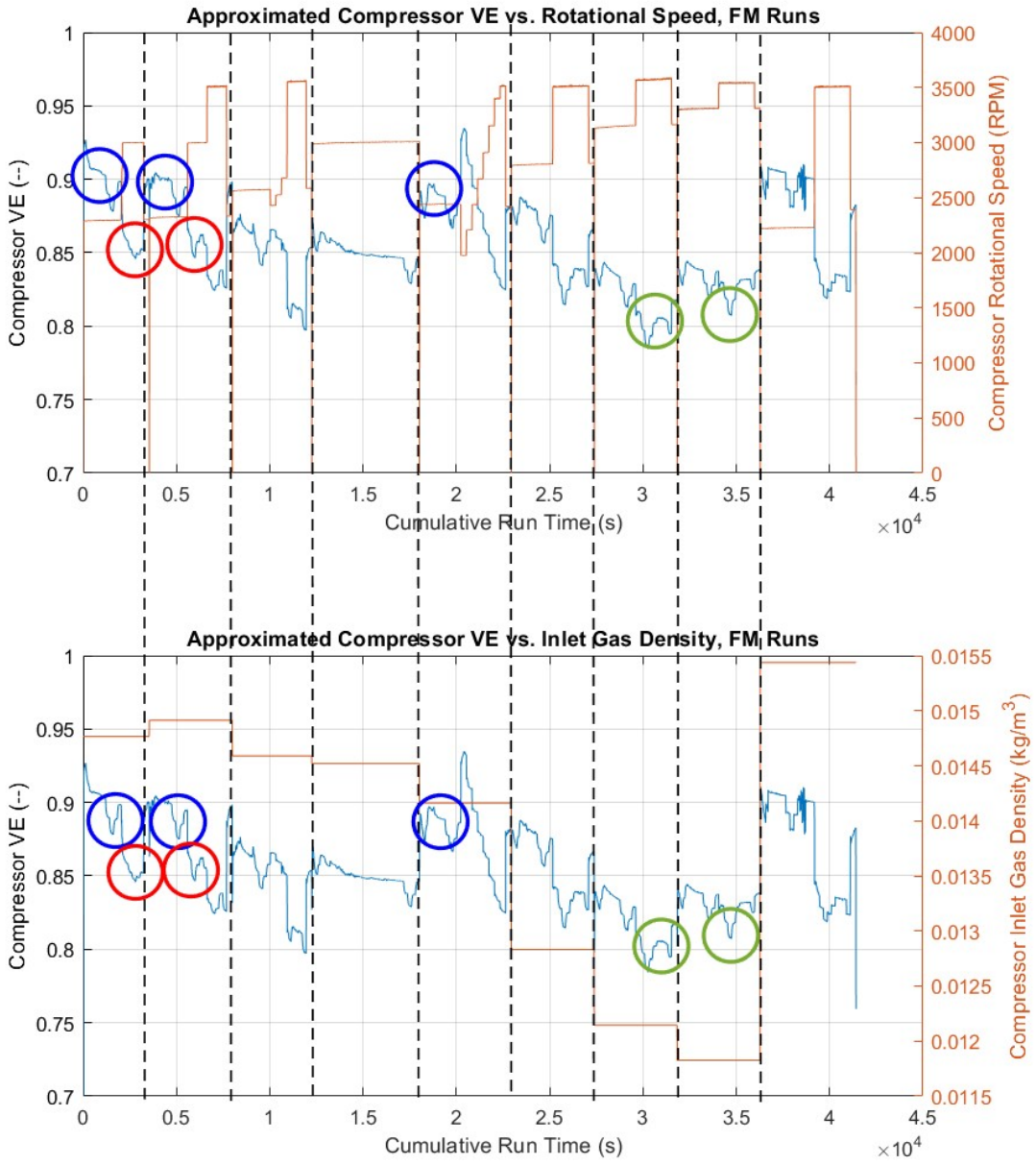

Figure 4-6: FM Compressor volumetric efficiency (left axis) over nine examined runs, compared to compressor rotational speed (top, right axis) and inlet gas density (bottom, right axis).

As seen in Figure 4-6, the FM compressor VE does not appear to change sig-

nificantly over continued operation - run segments of similar compressor rotational speeds and inlet gas density, indicated by the various sets of colored ovals in the figure, have approximately the same compressor VE, similar to the observations made with compressor power in Section 3.4.4. Therefore, the FM data suggests that while there was likely a period of initial wear during acceptance testing, the compressor units reach a steady-state volumetric efficiency for a given set of operating conditions - in addition, the lack of degradation seen when operating on Mars indicates that the compressors have a significant operating lifetime without a change in performance, as no changes in the volumetric efficiency were observed across over 10 operating cycles. As the FlatSat compressor, while a different unit, is of the same design as the FM compressor, it can therefore be inferred that the measured and fitted compressor VE from this experiment will apply to subsequent operational cycles on the FlatSat. It can also be seen in Figure 4-6 that for each run segment, the compressor VE changes as the current through the SOXE changes - this is the same behavior observed in FS OC05, which as discussed in Section 4.4.3 is due to equilibration in the electrolysis stack. In addition, it can be seen in Figure 4-6 that increases in compressor rotational speed correspond to a decrease in VE, particularly around 20,000 seconds in the top plot. This aligns with the negative correlation between compressor rotational speed and VE identified in Section 4.4.2.

Next, the approximated FM inlet density was used along with the compressor outlet pressure and rotational speed from the FM telemetry to create a fit of the same form as the FlatSat compressor VE, Equation (4.5), for direct comparison between the two units. The FM fit coefficients are tabulated below in Table 4.2, alongside the FlatSat fit coefficients for comparison.

Table 4.2: FM and FlatSat Compressor Volumetric Efficiency Fit Coefficients

Constant	FlatSat Value	FM Value
A	0.4625	1.439
B	-0.001897	-0.006481
C	-0.1527	-0.1523
D	-5.958e-5	0.0003387
E	0.7363	-0.4483
F	-0.3168	4.337
G	0.833	0.8675

As the fit equation is of a complex form, direct comparison of the coefficients does not allow for a straightforward comparison between FlatSat and FM compressor volumetric efficiencies. Therefore, the inlet density, outlet pressure, and compressor rotational speed for the FM were used as inputs with both the fitted FlatSat coefficients and FM coefficients. These two fits, along with the actual measured FM compressor VE, are plotted below in Figure 4-7.

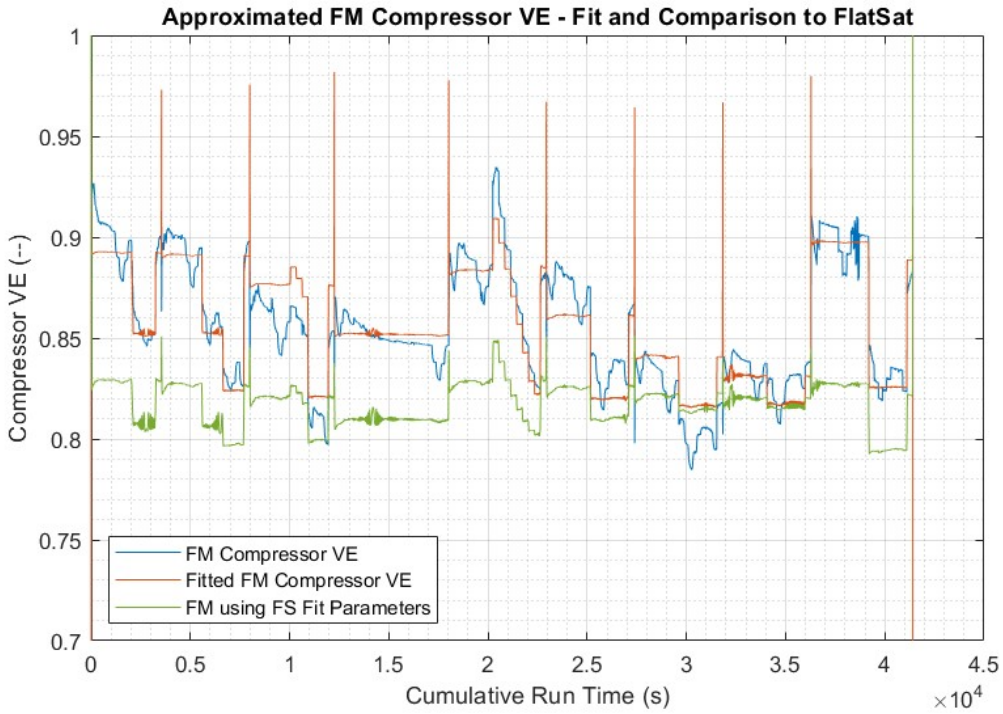

Figure 4-7: Comparison of FM compressor volumetric efficiency to fits using FlatSat (labeled as FS) coefficients and FM coefficients.

As seen in Figure 4-7, the fitted FM compressor VE, shown in orange, generally tracks the measured VE, shown in blue, across all examined run segments, and therefore accurately captures the effects of changes in inlet density, compressor rotational speed, and the resulting change in compressor outlet pressure. The predicted VE does differ from the measured data on a run-by-run basis; as discussed in Section 3.4.4, the inlet gas density was approximated for each run using MEDA and RAMP data. Therefore, the actual inlet gas density differs from the assumed value by a different magnitude for each run, which results in predicted VE data that is slightly high or low for certain runs. However, the predicted VE is within 5% of the measured VE for a majority of the examined run segments, so the fit is considered an accurate predictive method for FM compressor volumetric efficiency. It can also be seen that the fitted data using the FlatSat coefficients, shown in yellow, is significantly lower than the measured FM compressor VE, by approximately 0.04 for a majority of the run

segments. This can also be seen through the value of the "G" coefficient in Table 4.2, which is the constant offset term. Although the FlatSat fit follows approximately the same form as the FM fit, the predicted VE is significantly lower using the FlatSat coefficients for all run segments, which indicates that the FlatSat compressor has a lower volumetric efficiency than the FM for a given set of operating conditions. Due to this, when running FM runs on the FlatSat for validation prior to running on Mars, the chamber density will need to be greater than the inlet gas density on Mars, as a lower VE on the FlatSat indicates that for a given inlet gas density and compressor rotational speed, the output mass flow of the FlatSat compressor will be lower than that of the FM. As the purpose of FM run validation on the FlatSat is to use the same Run Control Table (Morris, 2018) and flow rates as the FM, increasing the chamber gas density will ensure that the same target flow rate will be reached without changing the commanded compressor rotational speed setpoints. This method has not yet been implemented on FM validation runs on the FS, but will be tested during the next such validation run. A method for calculating the necessary chamber gas density is discussed in Section 4.4.4. In addition, it can be seen in Figure 4-7 that the FlatSat compressor VE has a lower range of values than the FM compressor - the FlatSat compressor VE is "flatter" than the FM, and differs by smaller amounts than the FM compressor VE when the inlet gas density or compressor rotational speed are changed.

To further demonstrate the differences between the FM and FS compressor VE fit parameters, as well as how the FS data can be used as a predictive method for FM run planning, the FS data from FS OC05 was then fitted using the FM fit parameters. This is shown below in Figure 4-8.

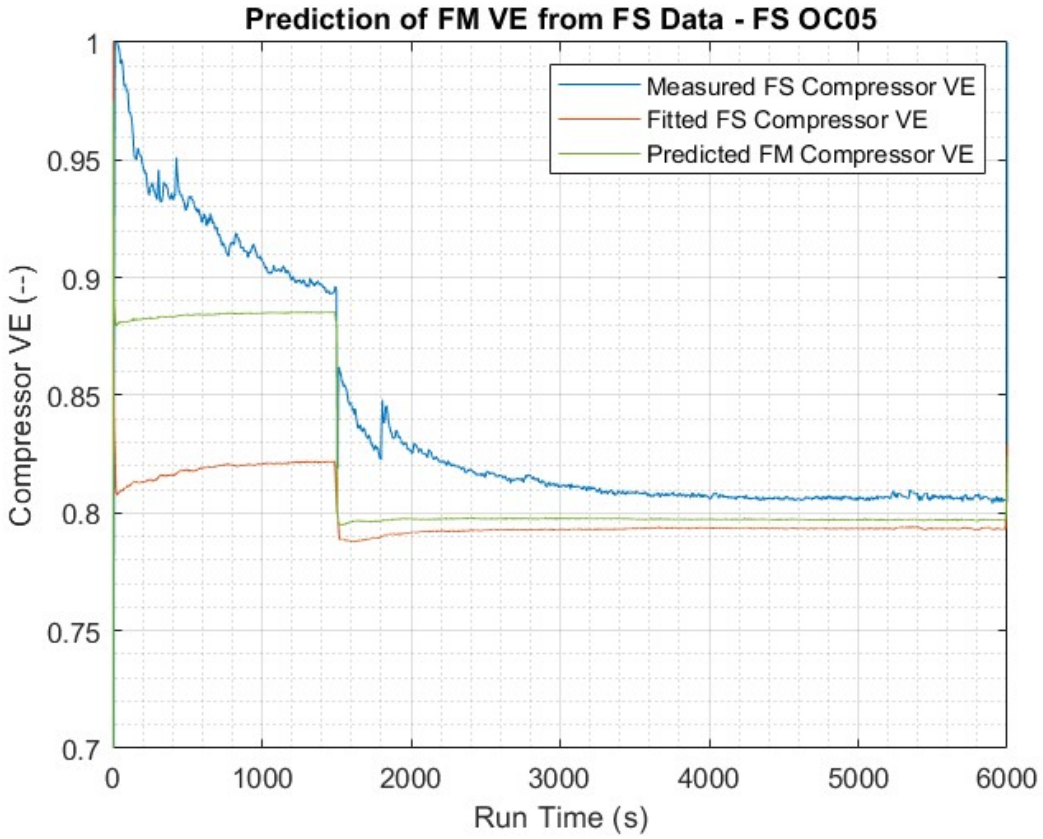

Figure 4-8: Comparison of FS compressor volumetric efficiency to fits using FlatSat (labeled as FS) coefficients and FM coefficients.

Due to the limited number of FS VE data points in a compressor-driven configuration, the contrast between FM and FS compressor VE is not as pronounced as that seen in Figure 4-7. Specifically, there is a single run segment not including the equilibration period discussed in Section 4.4.3, during which the measured FS compressor VE, fitted FS compressor VE, and predicted FM compressor VE are all within 2% of each other. However, as seen in Figure 4-8, the predicted steady-state FM compressor VE (excluding the equilibration period discussed in Section 4.4.3) would be slightly higher than the predicted FS compressor VE for the FS OC05 inlet conditions, which would result in a higher mass flow through the FM compressor for the same conditions. Therefore, to match the desired flow rate from the FM compressor for a given

run, the inlet gas density would have to be modified as discussed earlier - this would result in the FS flow rate matching the desired FM flow rate. If the anticipated FM compressor inlet conditions were instead used on the FS, flow through the FS would be lower than desired for the given run, and the FS run would not adequately validate the planned FM run.

As the outlet pressure is dependent on the inlet density and rotational speed on both the FM as well as the FlatSat in its standard configuration, the VE fit using Equation (4.5) truly only contains two independent variables during normal operations. Unlike the compressor power and energy usage, which is predicted using the MOXIE Dynamic Model after a run is already designed, the volumetric efficiency is a required input when selecting compressor rotational speed setpoints for a desired flow rate and given atmospheric density. Therefore, it was necessary to transform Equation (4.5) and the resulting coefficients in Table 4.2 into a form using only the two independent variables: inlet gas density and compressor rotational speed. Transforming the equation into this form will allow the MOXIE team to design both FM and FlatSat runs without requiring independent knowledge of the compressor outlet pressure, as well as allow calculation of the necessary FlatSat chamber gas density to match target FM mass flow rates. This is discussed in greater detail in the following section.

As mentioned above, the compressor outlet pressure is not an independently controllable variable on the FlatSat and FM, and is instead dependent on the inlet gas density and compressor rotational speed. This is because the compressor outlet VFCD has a fixed flow resistance, unlike the back pressure regulators used in the FlatSat compressor characterization experiments that allow independent control of outlet pressure through variation of the flow resistance. Therefore, in order to predict the compressor-driven mass flow rate on the FlatSat and FM using the fits developed in Section 4.4.2 and Section 4.4.4, it was necessary to eliminate the outlet pressure term and replace it with a different term capturing the dependence of outlet pressure on inlet gas density and compressor rotational speed. This allows a prediction of the compressor VE and therefore mass flow rate using only the inlet gas density and

compressor rotational speed, which are known parameters during run planning and operation.

4.4.5 Transformed FlatSat Volumetric Efficiency Fit

On both the FlatSat and FM, the compressor outlet pressure is measured using the P2 pressure sensor. To transform the developed FlatSat compressor VE from the form in Equation (4.5) to one where the compressor outlet pressure is implicit, the P2 reading was fit as a function of inlet gas density and compressor rotational speed. The fit form is shown below in Equation (4.9), where ρ is the inlet gas density in kg/m^3 and ω is the compressor rotational speed in RPM.

$$P2 = (A\rho + B) + (C\omega + D) \tag{4.9}$$

The P2 reading from FS OC05, which is the same FlatSat run used for verification of the compressor power and VE fits, was fit to the form in Equation (4.9). The resulting fit coefficients are tabulated in Table 4.3, with the measured and fitted data plotted in Figure 4-9.

Table 4.3: FlatSat P2 Fit Coefficients

Constant	Value
A	0.1904
B	-29.49
C	14945.3
D	-29.39

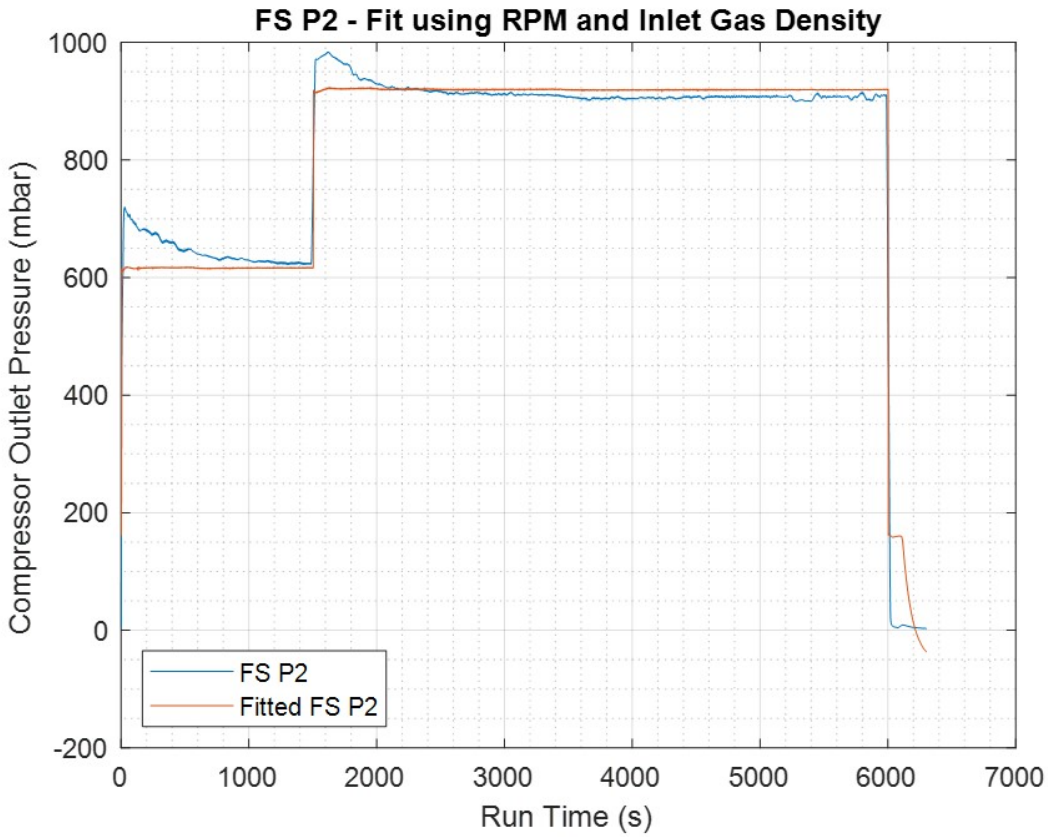

Figure 4-9: Measured and Fitted FlatSat P2 reading for FS OC05.

After verifying visually through Figure 4-9 that the relative contributions of inlet gas density and compressor rotational speed to compressor outlet pressure were correctly identified, the fit form in Equation (4.5) was then modified. The term for compressor outlet pressure, P_{outlet}, was replaced with the form shown in Equation (4.9), and simplified using the numerical coefficients in Table 4.1 and Table 4.3. The resulting equation, shown below in Equation (4.10), predicts the FlatSat compressor volumetric efficiency as a function of the compressor rotational speed in RPM and and inlet gas density in kg/m^3.

$$VE_{FS} = 0.833 - ((5.958e{-}5)\omega - 0.7363)(0.4625e^{0.1117 - 28.35\rho - 0.0003612\omega} - 0.1527) - 0.3168\rho \tag{4.10}$$

The equation in the form in Equation (4.10) contains the compressor outlet pressure implicitly. Therefore, it captures the results of the FlatSat compressor VE characterization experiment in a form that can be used in FlatSat run planning, where the compressor rotational speed and inlet gas density are design variables.

4.4.6 Transformed FM Volumetric Efficiency Fit

The same transformation of the VE fit completed for the FlatSat compressor was then completed for the FM compressor, using the fit developed in Figure 4-7 and the P2 data from the FM runs analyzed in the same section. Using the form in Equation (4.9), the fit coefficients for the FM compressor are tabulated below in Table 4.4, followed by the measured and fitted P2 data plotted in Figure 4-10.

Table 4.4: FM P2 Fit Coefficients

Constant	Value
A	0.1954
B	-302.11
C	5103.0
D	-302.01

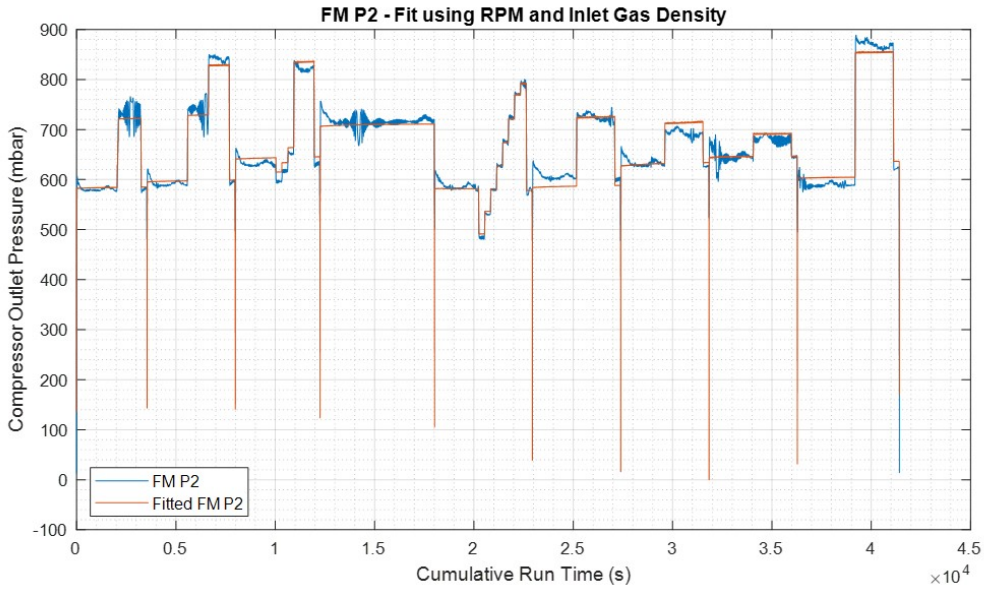

Figure 4-10: Measured and Fitted FM P2 reading for examined runs.

After verifying visually through Figure 4-10 that the relative contributions of inlet gas density and compressor rotational speed to compressor outlet pressure were correctly identified, the fit form in Equation (4.5) was then modified to match the format discussed in Section 4.4.5 The resulting equation, shown below in Equation (4.11), predicts the FlatSat compressor volumetric efficiency as a function of the compressor rotational speed in RPM and and inlet gas density in kg/m^3.

$$VE_{FM} = 0.8675 + ((0.0003387)\omega - 0.4483)(1.4393e^{3.9153 - 330.7\rho - 0.001266\omega} - 0.1523) + 4.3367\rho \tag{4.11}$$

The equation in the form in Equation (4.11) contains the compressor outlet pressure implicitly. Therefore, it captures the results of the FM compressor VE characterization experiment in a form that can be used in FM run planning. As inlet gas density is approximated based on the time of the planned run, and each run segment is planned with a target flow rate, the VE form in Equation (4.11) can be used to predict the FM compressor flow rate for a given compressor rotational speed, or solved

for the compressor rotational speed using Equation (4.1). The equation in this form is compatible with current tools used by the MOXIE team for run design, and can replace existing VE predictive methods of a lower fidelity.

4.5 Compressor VE Conclusions

The volumetric efficiency of the MOXIE compressor determines the actual flow rate through the system for a given set of inlet gas densities and compressor rotational speeds - due to backflow through the compressor, this value is always less than one. As MOXIE experiments are planned with a specific target flow rate for each segment, characterizing the VE for all compressor units with a high fidelity is important, as this shapes the design of run segments as well as the vacuum chamber conditions for FlatSat runs. As there was limited existing data on the volumetric efficiency of the FlatSat compressor, a dedicated experiment was planned to quantify the effects of inlet conditions, outlet conditions, and rotational speed on the compressor VE. This also allowed for direct comparison between the two compressor units to further quantify the differences between the FlatSat and FM, which is essential when using the FlatSat as a verification platform for FM runs.

The results of this investigation demonstrate that as expected, compressor outlet pressure is the largest driver of compressor VE onboard both the FlatSat and FM. However, the FlatSat has a lower VE on average than the FM, and would therefore require a higher inlet gas density or higher compressor rotational speed in order to match the flow rate through the FM compressor. As FM verification runs on the FlatSat are designed to use the same Run Control Table, and therefore the same compressor rotational speeds as FM segments, the chamber gas density must be increased to match FM target flow rates on the FlatSat. In addition, the FlatSat compressor volumetric efficiency is less affected by changes in the inlet gas density and compressor rotational speed when compared to that of the FM compressor. Therefore, the FlatSat compressor is less sensitive to small changes in chamber gas density, such as the decrease in density when the chamber temperature increases during extended

operations - this demonstrates robustness, as the flow rate is less likely to change significantly during a given run segment due to changes in the VE.

The predictive methods for calculating VE were also transformed to a usable form by the MOXIE operations team for both the FlatSat and FM compressors, by replacing the dependency on compressor outlet pressure with an implicit relationship using only the inlet gas density and compressor rotational speed. These variables, which are both already inputs when planning MOXIE runs, allow the high-fidelity fit for compressor VE developed during this experiment to be used with existing run-planning tools and processes.

Lastly, this analysis demonstrated that during continued operations on Mars, no additional drop in compressor volumetric dissipation was seen, which indicates that no significant compressor-level degradation has occurred during these extended operations. Therefore, the MOXIE team can use the predictive VE fits developed for both the FlatSat and FM, without including additional considerations for changes in compressor VE over time.

Chapter 5

Next Steps

The experiments discussed in this thesis demonstrate the capability of the FlatSat testbed to aid in characterizing the performance of MOXIE on Mars, as well as the broader performance of critical subsystems that will be present in a next-generation Mars ISRU system. With the increased understanding of both SOE operations and the FlatSat that is now present after the completion of the aforementioned experiments, there are several additional experimental investigations that can be conducted to build upon the research in this thesis.

It is likely that a next-generation Mars ISRU system will have a multi-stage compressor, as this would decrease the power requirements for a given compression ratio when compared to a single-stage compressor like that on the FM and FlatSat (Hinterman, 2022). With the modular capabilities of the FlatSat, a multi-stage compressor can be designed and installed without reconfiguring the remainder of the FlatSat flow path. This would enable the repetition of the power and VE studies discussed in this thesis, in order to quantify the improvements in power dissipation and efficiency that could be enabled by increasing the number of compressor stages. In addition, while the analysis of FM compressor power and VE discussed in this thesis demonstrated that there is no significant variability in these parameters over the lifetime of the FM compressor, the experiments discussed in Chapter 3 and Chapter 4 could be repeated on the FlatSat in order to ensure that these parameters are also relatively stable across multiple FlatSat runs.

In addition, the experiments conducted to characterize low pressure operations could be extended to lower cathode pressures with the replacement of the existing FlatSat SOXE assembly with a modified SOXE with a larger-diameter exit plenum - this would reduce the pressure drop across the SOXE, enabling lower cathode pressures than those achievable in the experiments conducted in this thesis.

Lastly, while this thesis only discussed selected ISRU characterization activities enabled by the FlatSat, there are several other experiments that could be conducted to better inform design of a next-generation Mars ISRU system. For example, lifetime tests could be conducted for both the compressor and SOXE. In these tests, the system would operate continuously for several weeks or months. This would better characterize system degradation in operating conditions similar to those that a next-generation system would be operating under, as a full-scale system would likely be operating continuously with high levels of autonomy to maximize oxygen production. As both the FM and FlatSat have only been operated for hours at a time, rather than months, there is currently limited experimental data on the lifetime of such components. As the FlatSat is modular, components can be tested until failure and then replaced with spares, therefore enabling the identification of possible life-limiting subsystems in a full-scale system.

Chapter 6

Conclusions

The experiments conducted on the FlatSat to characterize both low pressure operations as well as compressor operations at varying conditions demonstrate the versatility of the FlatSat testbed in extending ISRU characterization efforts beyond what is possible on the MOXIE FM. As predicted, operating the SOXE at a low cathode pressure is advantageous for MOXIE operations for various reasons. As demonstrated through the compressor characterization experiments, both the compressor power and volumetric efficiency are driven mostly by compressor outlet pressure, with a minimized power and maximized volumetric efficiency at the lowest tested compressor outlet pressures. The inlet pressure has the smallest effect on both power and volumetric efficiency, likely due to induced sonic flow downstream of the compressor that is independent of upstream conditions. Therefore, for a desired inlet mass flow rate on a next-generation system, operating at a low SOXE pressure and therefore compressor outlet pressure will maximize volumetric efficiency (reducing the required compressor rotational speed) and minimize compressor energy usage.

In addition, the results of FS OC07 demonstrate that the SOXE can be operated as pressures as low as 92 mbar, albeit with an increase in iASR of approximately 8% as the cathode pressure was decreased from 900 mbar. However, the higher safe utilization of CO_2 that is achievable at these low pressures compensates for the increased iASR, allowing for a maximum achievable oxygen production rate at the minimum pressure of 92 mbar. It was also observed that the achievable cathode

pressure was limited by pressure drops throughout the SOXE caused by the small diameter exit plenum and heat exchanger channels - even with an independently controllable cathode outlet pressure, a large pressure drop was observed across the SOXE. Therefore, a full-scale system should be designed to eliminate as many areas of flow restriction as possible, so that the cathode pressure can be decreased further.

Lastly, the successful experiments completed on the FlatSat showcase its utility as a standalone ISRU testbed - the ability to remove and replace components that are unchangeable on the FM, as well as the independently controllable environmental conditions, greatly enhance the ISRU characterization activities that can be conducted without the limitations of a flight system. Therefore, it may be beneficial for a similar ground-based testbed to be designed concurrently with or prior to implementation of a next-generation Mars-based system, as this would allow the design team to further characterize optimal design and operating conditions at a lower cost and increased cadence.

Bibliography

Drake, B. G. and Watts, K. D. (2009). *Human Exploration of Mars Design Reference Architecture 5.0*. NASA Johnson Space Center, Houston, Texas.

Hecht, M., Hoffman, J., Rapp, D., McClean, J., SooHoo, J., Schaefer, R., Aboobaker, A., Mellstrom, J., Hartvigsen, J., Meyen, F., Hinterman, E., Voecks, G., Liu, A., Nasr, M., Lewis, J., Johnson, J., Guernsey, C., Swoboda, J., Eckert, C., Alcalde, C., Poirier, M., Khopkar, P., Elangovan, S., Madsen, M., Smith, P., Graves, C., Sanders, G., Araghi, K., de la Torre Juarez, M., Larsen, D., Agui, J., Burns, A., Lackner, K., Nielsen, R., Pike, T., Tata, B., Wilson, K., Brown, T., Disarro, T., Morris, R., Schaefer, R., Steinkraus, R., Surampudi, R., Werne, T., and Ponce, A. (2021). Mars Oxygen ISRU Experiment (MOXIE). *Space Science Reviews*, 217(1).

Hinterman, E. (2022). *Multi-Objective System Optimization of a Mars Atmospheric ISRU Plant*. Doctoral thesis, Massachusetts Institute of Technology.

Hinterman, E. D. (2018). *System Modeling, Graphical User Interface Development, and Sensors Testing for the Mars Oxygen In-Situ Resource Utilization Experiment (MOXIE)*. Master's thesis, Massachusetts Institute of Technology.

Hoffman, J. A., Hecht, M. H., Rapp, D., Hartvigsen, J. J., SooHoo, J. G., Aboobaker, A. M., McClean, J. B., Liu, A. M., Hinterman, E. D., Nasr, M., Hariharan, S., Horn, K. J., Meyen, F. E., Okkels, H., Steen, P., Elangovan, S., Graves, C. R., Khopkar, P., Madsen, M. B., Voecks, G. E., Smith, P. H., Skafte, T. L., Araghi, K. R., and Eisenman, D. J. (2022). Mars Oxygen ISRU Experiment (MOXIE)-Preparing for human Mars exploration. *Science Advances*, 8(35):1–7.

Kaplan, D. I., Ratliff, J. E., Baird, R. S., Sanders, G. B., Johnson, K. R., Karlmann, P. B., Baraona, C. R., Landis, G. A., Jenkins, P. P., and Scheiman, D. A. (2001). THE MARS IN-SITU-PROPELLANT-PRODUCTION PRECURSOR (MIP) FLIGHT DEMONSTRATION. *Workshop on Mars 2001*, pages 1–3.

Masson, P. (2005). The History of Mars Exploration. In *1st Mars Express Science Conference*.

Morris, R. (2018). Mars Oxygen ISRU Experiment (MOXIE) Command and Telemetry Dictionary (C&TD). *Internal MOXIE Documentation*, Rev. B.

MOXIE Team (2022a). MOXIE Data Product SIS v4.0. *NASA Planetary Data System*.

MOXIE Team (2022b). NASA Planetary Data System - MOXIE Bundle. https://pds-atmospheres.nmsu.edu/PDS/data/PDS4/Mars2020/moxie_bundle/.

National Aeronautics and Space Administration (NASA) (2020). Mars Oxygen In-Situ Resource Utilization Experiment (MOXIE). https://mars.nasa.gov/mars2020/spacecraft/instruments/moxie/.

Rapp, D. (2013). *Use of Extraterrestrial Resources for Human Space Missions to Moon or Mars*.

Rapp, D. (2022a). MOXIE Handbook Volume 1A - Basics. *Internal MOXIE Documentation*, 1A(3).

Rapp, D. (2022b). MOXIE Handbook Volume 1B - Basics. *Internal MOXIE Documentation*, 1B(4).

Sotomayor, L. M. (2022). NASA Planetary Data System - MEDA Bundle. https://pds-atmospheres.nmsu.edu/PDS/data/PDS4/Mars2020/mars2020_meda/.

The Lee Company (2022). THE LEE COMPANY'S LOHM LAWS. https://www.theleeco.com/lohm-calculator/.